GIANT DINOSAUR (THEROPOD) EGGS OF THE OOGENUS MACROELONGATOOLITHUS (ELONGATOOLITHIDAE) FROM SOUTHEASTERN IDAHO: TAXONOMIC, PALEOBIOGEOGRAPHIC, AND REPRODUCTIVE IMPLICATIONS

by

Danielle Jade Simon

A thesis submitted in partial fulfillment
of the requirements for the degree

of

Master of Science

in

Earth Sciences

MONTANA STATE UNIVERSITY
Bozeman, Montana

May 2014

ACKNOWLEDGEMENTS

I would like to thank my committee members Dave Varricchio, Frankie Jackson, and Jack Horner for their encouragement and assistance throughout this project. Research was funded by National Science Foundation grant #0847777 (EAR) to D. Varricchio and additional support was provided by National Geographic Grant 8752-10 to D. Varricchio. Travel to present research at the Society of Vertebrate Paleontology 72nd Annual Meeting was provided by the College of Letters and Science Student Research Grant. Jamie Fearon and Ashley Poust assisted with stratigraphic section work in the Wayan Formation. Laurie Spicher, Takuya Imai, and Michael Holland assisted with preparation of Wayan specimens. Imaging and analysis were possible thanks to help from staff at the Imaging and Chemical Analysis Laboratory at Montana State University. Dave Mogk provided crucial assistance with X-ray Diffraction techniques and analysis. Ellen Lamm and Jack Horner at the Museum of the Rockies Paleontology lab provided access to equipment and expertise in analytical techniques critical to this study. Frankie Jackson contributed vital assistance with eggshell microstructural analysis and use of equipment in both the Traphagen Petrographic Analysis lab and the Museum of the Rockies Paleontology lab. The Idaho Museum of Natural History graciously provided extended access to Wayan Formation egg material, while Xingsheng Jin and Zhejiang Museum of Natural History staff provided access to Liangtoutang specimens and assistance with specimen photography. Xingsheng Jin, Wenjie Zheng, Xiuti Li, and Shengxiao Gu provided assistance during travel to Hangzhou. Sara Oser and Daniel Barta contributed valuable discussion and insight involved in every aspect of this project.

TABLE OF CONTENTS

TABLE OF CONTENTS CONTINUED

TABLE OF CONTENTS CONTINUED

LIST OF TABLES

Table Page

LIST OF TABLES CONTINUED

Table Page

LIST OF FIGURES

Figure Page

LIST OF FIGURES CONTINUED

Figure Page

ABSTRACT

Macroelongatoolithus eggs are best known for their gigantic size and elongate shape, ranging from 34 – 61 cm in length with an elongation index of 2-3.1. Ootaxonomic placement of this oogenus, and the oospecies within it, has varied widely among authors, necessitating a re-evaluation of the group. This study represents the first comprehensive comparison of gross morphology, microstructural variation, and gas conductance within a *Macroelongatoolithus* oospecies. Four specimens, egg pair IMNH 2428\49608 and additional eggshell from the Albian-Cenomanian Wayan Formation of Idaho, eggshell fragment ES305 from the Albian-Cenomanian Blackleaf Formation of Montana, eggshell fragment thinsections ES301 and ES305-306 from the early Late Cretaceous Thomas Fork Formation of Wyoming, and egg pair ZMNH M8705 from the Cenomanian-Turonian Liangtoutang Formation of China, are examined, described, and assigned to the oospecies *Macroelongatoolithus carlylei*. Eggs are 39.8 – 41.65 cm long and 10.8 – 14.28 cm wide, with an eggshell thickness ranges from 1.01 – 2.17 mm, and CL:ML ratio ranging from 2.05:1 – 7.68:1. Eggshell consists of two structural layers of calcite separated by a distinct, undulating boundary. Gas conductance of IMNH 2428\49608-2 and ZMNH M8705-1 is 1119 – 1597 mg H2O torr-1 day-1, 2.9 – 5.6 times higher than values predicted for open nest mass-equivalent eggs. These values suggest a humid or enclosed nesting environment. The lower value calculated for the Liangtoutang Formation specimen (ZMNH M8705-1) may reflect differences in nesting environment between the semi-arid floodplain mudstones of the Wayan Formation in Idaho and the shallow laucustrine red siltstones and sandstones of the Liangtoutang Formation of Zhejiang, China. The observed microstructural variation within and between IMNH 2428/49608 and ZMNH M86705 expands the range of expected variation for an oospecies, and calls into question the over splitting of ootaxa on the basis of traits that may reflect individual variation or growth stage of the laying animal. The discovery and description of an intact *M. carlylei* specimen from North American confirms the synonymy of *M. xixiaensis* into the previously named *M. carlylei* suggested by Zelenitsky et al. 2000, and expands the geographic and temporal distribution of the oogenus and parent animal to include the Albian – Cenomanian of North America.

CHAPTER 1

INTRODUCTION

Fossil eggs are classified on the basis of gross morphological features combined with microstructural characteristics and organized into oofamilies, oogenera, and oospecies (Mikhailov 1991; Zelenitsky and Hirsch 1997). Eggs of the oogenus *Macroelongatoolithus,* oofamily Elongatoolithidae, have been described from complete eggs and partial to complete clutches from mid Cretaceous formations in the Henan and Zhejiang Provinces of Southern China (Li et al. 1995; Fang et al. 2000; Jin et al. 2007) and the Goseong Basin of South Korea (Kim, Huh et al. 2011; Kim, Yang et al. 2011; Huh et al. 2014). Zelenitsky (2000) was the first to recognize *Macroelongatoolithus* material from North America, re-identifying isolated eggshells of the mid Cretaceous of Utah to this ootaxon. New Idaho material with intact and partial eggs in situ provides the opportunity to more fully examine this ootaxon in North America.

First collected in Mongolia by Henry Osborn and the American Museum of Natural History, Elongatoolithid eggs were described at a macroscopic level and named *Oolithes elongatus* by VanStraelen in 1925 and later by Young in 1954. Zhao 1975 established a formal parataxonomic system and reassigned many ootaxa previously termed *Oolithes* into various oogenera based comparisons of egg size and shape, ornamentation, eggshell thickness, and pore system. Fossils previously termed *Oolithes* were thus reassigned to newly erected oogenera and oospecies. Eggs of the oofamily Elongatoolithidae, established by Zhao 1975, are characterized by elongate shape and distinct microstructure consisting of two structural layers of calcite separated by a distinct

boundary, a pore system defined by narrow, straight pores, and variable ornamentation ranging from nodes to linear ridges (Mikhailov 1997, Carpenter 1999). These eggs have been attributed to oviraptorosaur dinosaurs based on embryonic remains and association of adult oviraptorosaurs with egg clutches (Clark et al. 1999; Dong and Currie 1996; Norell et al. 1994, 2001; Weishampel et al. 2008; Fanti et al. 2012).

Macroelongatoolithus eggs are best known for their gigantic size and elongate shape, ranging from 34 – 61 cm in length with an elongation index of 2-3.1. Ootaxonomic placement of this oogenus, and the oospecies within it, has varied widely from author to author, necessitating a re-evaluation of the group. Microstructure has typically been defined by examination of only a few isolated fragments, rather than by zonal sampling along a longitudinal profile of intact specimens. Additionally, though published reports of this egg type are common, gas conductance studies have been largely neglected. Interpretations of nesting mode and reproductive biology of the *Macroelongatoolithus* egg-laying animal have been the subject of much speculation and study, however detailed gas conductance and variability in egg morphology and microstructure has been neglected. The discovery and examination of an intact *Macroelongatoolithus* egg from the Wayan Formation of Idaho, combined with detailed examination and comparison to an intact egg of the same oospecies from the Liangtoutang Formation of China provides an excellent opportunity to explore potential inter and intra variation in egg morphology, microstructure, and gas conductance, and the reproductive biology of the large oviraptorids that likely laid eggs of this type.

Macroelongatoolithus eggs consistently occur in pairs and within ring-shaped, single-horizon clutches of anywhere between twelve and twenty-four eggs. The single

layer contrasts with clutches of other Elongatoolithid eggs, which may have up to three stacked layers of eggs in a clutch (Dong and Currie 1996; Clark et al. 1999; Zhao 2000). *Macroelongatoolithus* eggs are typically inclined toward the center of the clutch at a low angle with the slightly more blunt end of the eggs facing inward (Zhao 2000; Grellet-Tinner et al. 2006). Described microstructural features of *Macroelongatoolithus* include linear ridge and nodular ornamentation with a high variability along each egg, eggshell composed of two structural layers, an undulating boundary between these layers, fairly straight and narrow pores, and a high overall pore density (Fang et al. 2000; Zhao 2000; Grellet-Tinner et al. 2006; Jin et al. 2007).

Pairing in all Elongatoolithid eggs has been hypothesized to indicate the presence of two functioning oviducts in theropods in contrast to the one functioning oviduct in modern birds (Varricchio et al. 1997; Larson 1998; Zhao 2000; Sato et al. 2005; Grellet-Tinner et al. 2006; Jin et al. 2007). Combined with the circular clutch arrangement, pairing is also used to argue that these theropods developed their entire egg clutch at once and then laid the paired eggs in a short time span by squatting and rotating about the center of the clutch (Larson 1998; Zhao 2000). In contrast, Varricchio et al. (1997) used pairing to argue for iterative laying in troodontids and oviraptors, a position supported in oviraptorosaurs by the presence of an adult with two eggs preserved in the pelvic region (Sato et al. 2005). Additionally, Varricchio et al. (2008) argue that clutch size compared to adult body size is particular high in oviraptors and troodontids, and more akin to the paternal care model seen in extant avian theropods in which multiple females contribute eggs to a shared nest incubated or cared for by a single male. Mass egg laying over a short time frame is a reproductive feature seen in crocodilians, whereas birds develop and

lay one egg at a time over several days until the entire nest is laid. Larson (1998) suggested that *Macroelongatoolithus* eggs were pushed into a pre-loosened sediment mound by the force of a muscular oviduct. Retention of the paired arrangement in combination with the presence of multi-tiered clutches of Elongatoolithid eggs indicates a lack of egg rotation among theropods, which also implies the lack of chalazae in these eggs (Varricchio et al. 1997).

Studies comparing porosity of various oogenera with both extant avian and reptilian eggs have established a link between porosity and gas conductance and nesting mode (Ar et al. 1974; Seymour 1979; Sabath 1991; Deeming 2006; Jackson et al. 2008). Deeming (2006) calculated a gas conductance value for *Macroelongatoolithus* eggs based on isolated eggshell fragments. This value, 600 mg H2O $torr^{-1}$ day^{-1}, was used to suggest that *Macroelongatoolithus* eggs were either buried in sediments or covered with a mound as high conductance indicates a humid environment. The inclination of eggs observed in *Macroelongatoolithus* ring clutches is also used to argue the presence of a substrate mound which the eggs were laid on, imparting a tilted orientation prior to further burial of the eggs by the parent (Zhao 2000).

Macroelongatoolithus eggs have been attributed to tyrannosaurs, therizinosaurs, and giant oviraptorids based on their extremely large size (Mikhailov 1994a; Zelenitsky et al. 2000; Grellet-Tinner et al. 2006; Jin et al. 2010). The therizinosaur hypothesis can likely be disregarded as embryonic remains of those specialized theropods have been found in eggs of a drastically different microstructure and morphology from the Elongatoolithidae (Kundrat et al. 2007). No microstructural or skeletal evidence has been found to support the tyrannosaur origin of *Macroelongatoolithus*. Multiple eggs and

clutches of Elongatoolithid eggs demonstrate a strong link between this egg type and oviraptorids via embryological remains and association with adult skeletons (Norell et al. 1994; Dong and Currie 1996; Clark et al 1999; Norell et al. 2001; Sato et al. 2005; Cheng et al. 2008; Weishampel et al. 2008). Additionally, a single Chinese specimen of *Macroelongatoolithus* with associated embryonic remains has been reported as containing an edentulous premaxillary, a trait associated with oviraptorosaurs (Grellet-Tinner 2005; Grellet-Tinner and Makovicky 2006). From evidence listed above, the most likely affinity of all known elongatoolithid eggs is within Oviraptorosauria.

Four specimens are examined and described in this study: An egg pair IMNH 2428\49608 and additional eggshell from the Albian-Cenomanian Wayan Formation of Idaho, eggshell fragment ES305 from the Albian-Cenomanian Blackleaf Formation of Montana, eggshell fragment thinsections ES301 and ES305-306 from the early Late Cretaceous Thomas Fork Formation of Wyoming, and an egg pair ZMNH M8705 from the Cenomanian-Turonian Liangtoutang Formation of China.

Stratigraphic sections of the quarried areas in conjunction with microscopic analysis of the lithology allow for a reconstruction of the egg-bearing unit, which represents the environment chosen as a nesting ground by the *Macroelongatoolithus* egg-laying animals. Microscopic examination of the Wayan eggs and associated mudstones, combined with study of paired eggs and clutches from China are used here to determine geographic distribution, environmental context, and reproductive biology of these animals. Gross morphology and microstructure are used to assign the material to an oospecies. Comparisons of examined material with previously established oospecies are also used to re-evaluate the validity of oospecies within the *Macroelongatoolithus*

oogenus. Microstructural variation and gas conductance is examined along intact specimens from early Late Cretaceous localities of North America and China, using a zonal sampling method to increase understanding of variation within a single specimen and among specimens of similar lithologic age between North America and China. Given the established linked between gas conductance and nest humidity, nesting mode of the egg-laying animal is evaluated through comparisons of total gas conductance to values expected for avian eggs of equivalent mass, and through comparisons of conductance across individual zones of each egg.

CHAPTER 2

LITERATURE REVIEW

Description and Occurrence of Elongatoolithidae

Elongatoolithid eggs are commonly documented from the Upper and Lower Cretaceous of China and Mongolia (Mikhailov 1994a; Carpenter 1999), but have also been recognized from South Korea (Kim et al. 2011; Huh et al. 2014), Kazakhstan (Mikhailov 1994a), India (Mohabey 1998), the US (Jensen 1970; Zelenitsky et al. 2000), Spain (Amo et al. 2000; Canudo et al. 2010) and Argentina (Salgado et al. 2007). Until this study, North American elongatoolithid material was restricted to accumulations of eggshell fragments (Bray 1998; Dorr 1985; Jensen 1970; Zelenitsky et al. 2000). Paleocene eggs from Spain and France have also been designated as belonging within Elongatoolithidae (Donaire and Lopez-Martinez 2009).

Elongatoolithus, the type oogenera within Elongatoolithidae, has been extensively discussed in egg literature. First described as "*Protoceratops*" eggs by VanStraelen (1925) and others, *Elongatoolithus* eggs containing oviraptorid embryos were described by Norell et al. (1994), thus up-ending the longstanding impression of oviraptorosaurs as egg-stealers preying upon *Protoceratops* nests.

Elongatoolithidae is defined by eggs consisting of two distinct structural layers with a clear boundary, mammillae consisting of radiating calcite crystals, and a squamatic texture in the upper layer (Zhao 1975; Mikhailov 1994a; Mikhailov 1997). Elongatoolithidae eggs typically lack well-defined shell units in the second structural

layer, possibly because they are obscured by proteinaceous material within the eggshell matrix. Because of this, the second structural layer is referred to as the cryptoprismatic or continuous layer.

Elongatoolithid eggs typically have an angusticanaliculate pore system – with straight, narrow pores- and dispersituberculate to lineartuberculate ornamentation, though rimocanalicuate, i.e., fan shaped, pores have also been described. A wavy or undulating contact between the mammillary layer and cryptoprismatic layer and accretion lines throughout both layers also characterize this oofamily. Known clutches are composed of paired eggs arranged in concentric circles of up to three superimposed layers and are typically inwardly inclined, but are preserved in a horizontal orientation in some cases.

Ten oogenera have been described within Elongatoolithidae to date. Occurrence and description of each follows.

Nanhsiungoolithus Zhao 1975

This oogenera includes one oospecies, *Nanshiungoolithus chuetiensis* (Zhao 1975). Found in Upper Cretaceous strata of China and Mongolia, these eggs are among the smaller elongatoolithid oogenera, described as having a maximum size of 14.5 cm, and have been described as nearly smooth. Ornamentation of *Nanshiungoolithus* has been characterized as very faint, in some cases absent (Carpenter 1999; Mikhailov 1997).

Elongatoolithus Zhao 1975

Though mainly described from Upper Cretaceous rocks of China and Mongolia, this oogenera has also been described, in limited number, from Kazakhstan and South America (Carpenter 1999; Mikhailov 1997; Nessov 1995; Salgado et al. 2007).

Elongatoolithus is defined by eggs up to 17 cm long and 8 cm wide, with an elongation index of 2- 2.2, ornamentation grading from fine ramotuberculate – lineartuberculate, an abrupt boundary between the CL and ML, and a CL:ML ratio range of 2:1 to 6:1 (Carpenter 1999).

Several oospecies have been described that mainly vary in eggshell thickness, mammillary to continuous layer ratio, and overall size (Table 2.1). These oospecies include: *E. elongatus* (Young 1954), *E. andrewsi* (Zhao 1975), *E. magnus* (Zeng and Zhang 1979), *E. excellens* (Mikhailov 1994), *E. frustrabilis* (Mikhailov 1994), *E. sigillarius* (Mikhailov 1994), *E. subtitectorius* (Mikhailov 1994), and *E. tiantaiensis* (Fang et al. 2000), *E. chichengshanensis* (Fang et al. 2003), and *E. laijiaensis* (Fang et al. 2003). Distribution of *Elongatoolithus* eggs spans multiple formations from the Late Cretaceous of China and Mongolia (Table 2.2).

Table 2.1 Comparison of *Elongatoolithus* Oospecies. 1) Carpenter 1999, 2) Fang et al. 2000, 3) Fang et al. 2003, 4) Mikhailov 1994, 5) Young 1954, 6) Zeng and Zhang 1979, 7) Zhao 1975.

Oospecies	Egg L x W cm	Elongation Index	Ornamentation	Shell Thickness mm	CL:ML ratio	Reference
E. elongatus	14-15 x 6.1-6.7	2.25	-	0.7-1.1	5:1	1, 5
E. andrewsi	13.8-15.1 x 5.5-7.7	2-2.75	-	1.1-1.5	4:1	1, 7
E. magnus	16.2-17.2 x 6.3-8.2	2.1-2.6*	-	0.6-0.9	6:1	1, 6
E. frustrabilis	15-17 x 6-7	2.5	Linear	0.8-1.5	-	1, 4
E. subtitectorius	-	-	Nodose-Linear	0.7-0.8	-	1, 4
E. sigillarius	15-17 x 6-7	2.5	Dispers-Linear	0.3-1.1	-	1, 4
E. excellens	9-11 x 4	2.25-2.7	Linear-Anast	0.3-0.9	-	1, 4
E. tiantaiensis	11 x 2-5	2.2-5.5	-	0.8	1:1	2
E. chichengshanensis	7 x 1.5-3.5	2-4.7*	-	1.2-1.5	-	3
E. laijiaensis	8 x 3-3.8	2.1-2.7	-	0.3	-	3
***Elongatoolithus* Summary**	**7-17.2 x 1.5-8.2**	**2-5.5**	**Variable**	**0.3-1.5**	**1:1-6:1**	

Table 2.2 Distribution of *Elongatoolithus* Oospecies. 1) Chow 1954, 2) Dauphin 1994, 3) Dong 1979, 4) Dong 1980, 5) Fang et al. 1998, 6) Fang et al. 2000, 7) Fang et al. 2003, 8) Fang et al. 2005, 9) Fang et al. 2009, 10) Liang et al. 2009, 11) Mikhailov 1994, 12) Qian et al. 2007, 13) Young 1954, 14) Yu et al. 2010, 15) Zeng and Zhang 1979, 16) Zhang and Li 1998, 17) Zhao and Jiang 1974, 18) Zhao 1975, 19) Zhao 1979a, 20) Zhao 1994.

Oospecies	Age	Formation	Province/State	Country	Reference
E. elongatus	Late Cretaceous	Wangshi Group	Shandong	China	1, 3-5, 13, 19-20
	Late Cretaceous	Nanxiong	Guangdong	China	3, 9, 18-19
	Cretaceous	Dongyuan/Xiantang/Geling	Guangdong	China	8
	Late Cretaceous	Yuanpu/Pingling	Guangdong	China	20
	Late Cretaceous	Siguou/Luyemiao/Hugang	Henan	China	10, 19
	Late Cretaceous	Djadokhta		Mongolia	11
E. andrewsi	Late Cretaceous	Wangshi Group	Shandong	China	19
	Late Cretaceous	Nanxiong	Guangdong	China	2, 5, 9, 19
	Late Cretaceous	Siguou/Luyemiao/Hugang	Henan	China	10
	Late Cretaceous	Hugang	Henan	China	19
	Late Cretaceous	Yuanpu/Pingling	Guangdong	China	19
	Late Cretaceous	Djadokhta		Mongolia	11
	Late Cretaceous	Nemegt		Mongolia	11
E. magnus	Late Cretaceous	Shulao	Hunan/Ghangde	China	4, 15-16
E. frustrabilis	Late Cretaceous	Djadokhta		Mongolia	11
E. subtitectorius	Late Cretaceous	Djadokhta		Mongolia	11
E. sigillarius	Late Cretaceous	Nemegt		Mongolia	11
E. excellens	Late Cretaceous	Nemegt		Mongolia	11
E. tiantaiensis	Late Cretaceous	Chichengshan	Zhejiang	China	6, 12, 14
E. chichengshanensis	Late Cretaceous	Chichengshan	Zhejiang	China	7
E. laijiaensis	Late Cretaceous	Laija	Zhejiang	China	7
	Late Cretaceous	Liangtoutang	Zhejiang	China	14

Macroolithus Zhao 1975

Originally described as *Oolithes rugustus* by Young 1965, this oogenera includes five oospecies: *Macroolithus rugustus* (Zhao 1975), *M. yaotunensis* (Zhao 1975), *M. mutabilis* (Mikhailov 1994), *M. lashuyuanensis* (Fang et al. 2009), and *Macroolithus turolensis* (Amo et al. 2000) (Table 2.3). Distribution of this oogenus includes Early-Late Cretaceous strata of China, Mongolia, Kazakhstan, and Spain (Table 2.4).

Larger than most elongatoolithid eggs, *Macroolithus* range from 16 to 21 cm in length and have a range of ornamentation from coarse lineartuberculate to dispersituberculate (Young 1965; Mikhailov 1994). Eggshell thickness ranges from 0.55 – 2.7 mm and is thinnest in *M. turolensis* (Mikhailov 1994; Amo et al. 2000; Liang et al.

2009). Unfortunately *Macroolithus* microstructure is not well defined and is discussed in only a few publications. Where described, continuous layer to mammillary layer ratio varies from 2:1 to 3:1 and the CL – ML boundary is unclear. Pore system varies between angusticanaliculate (straight, narrow pore shape), oblicucanuliculate (diagonally oriented narrow pore shape) and rimocanalicuate (fan shaped pores that open at the eggshell surface as linear slits) (Mikhailov 1994; Amo et al. 2000; Liang et al. 2009). The extensive variation in the pore system of *Macroolithus* eggs may be related to nesting mode, as the size and shape of pores has an affect on gas conductance. Clutches of *Macroolithus* contain up to twenty eggs and are arranged in a circular manner of two or more superimposed layers (Mikhailov 1994; Nessov 1995; Young 1965).

Table 2.3 Comparison of *Macroolithus* Oospecies. 1) Amo et al. 2000, 2) Canudo et al. 2010, 3) Carpenter 1999, 4) Fang et al. 2009, 5) Mikhailov 1994, 6) Young 1965, 7) Zhao 1975, 8) Zhao 1979a.

Oospecies	Egg L x W cm	Elongation Index	Ornamentation	Shell Thickness mm	CL:ML ratio	Reference
M. rugustus	16.5-18 x 7.5-8.5	1.75-2.2	Ramo-Pitted	0.8-1.7	-	3, 6, 8
M. yaotunensis	17.5-21 x 6.7-9.4	2.2-2.5	-	1.4-1.9	-	3, 7-8
M. mutabilis	-	-	Dispers-Linear	1.3-2	-	3, 5
M. turolensis	-	-	Nodose-Linear	0.45-1.35	2:1	1-2
M. lashuyuanensis	-	-	-	2.3-2.7	1.5:1-2:1	4
***Macroolithus* Summary**	**16.5-21 x 6.7-9.4**	**1.75-2.5**	**Variable**	**0.45-2.7**	**1.5:1-2:1**	

Table 2.4 Distribution of *Macroolithus* Oospecies. 1) Amo et al. 2000, 2) Canudo et al. 2010, 3) Carpenter 1999, 4) Cheng et al. 2008, 5) Dauphin 1994, 6) Dong 1979, 7) Fang et al. 1998, 8) Fang et al. 2005, 9) Fang et al. 2009, 10) Liang et al. 2009, 11) Mikhailov 1994, 12) Ruiz-Omenaca et al. 2004, 13) Sato et al. 2005, 14) Young 1965, 15) Zhao 1975, 16) Zhao 1979a, 17) Zhao 1994, 18) Zhou et al. 1993.

Oospecies	Age	Formation	Province/State	Country	Reference
M. rugustus	Late Cretaceous	Nanxiong	Guangdong	China	3, 5-7, 9, 14-16
	Late Cretaceous	Yuanpu	Guangdong	China	3, 17
	Maastrichtian	Pingling		China	3, 11
	Maastrichtian	Manrak		Kazakhstan	3, 11
	Late Cretaceous	Nemegt		Mongolia	3, 11
	Late Cretaceous	Barun-Goyot		Mongolia	3, 11
M. yaotunensis	Late Cretaceous	Dongyuan	Guangdong	China	8
	Late Cretaceous	Nanxiong	Guangdong	China	5, 7, 9, 15-16
	Late Cretaceous	Nanxiong	Jiangxi	China	13
	Late Cretaceous	Nanxiong	Jiangxi	China	4
	Late Cretaceous	Siguou/Luyemiao	Henan	China	10
	Late Cretaceous	Hugang	Henan	China	2, 16
	Late Cretaceous	Yuanpu/Pingling	Guangdong	China	3, 17-18
M. mutabilis	Late Cretaceous	Barun-Goyot		Mongolia	3, 11
M. turolensis	Lower Barremian	Castellar		Spain	1, 12
	Hauterivian-Barremian	Blesa	Teruel	Spain	2
M. lashuyuanensis	Cretaceous		Guangdong	China	9

<u>*Macroelongatoolithus* Li, Yin, and Liu 1995</u>

Macroelongatoolithus eggs are unique in their large size and elongation, ranging from 34 to 61 cm long with an elongation index of 1.6 to 3.2 (Jin et al. 2007; Wang, Zhao et al. 2010; Kim et al. 2011; Huh et al. 2014). Ornamentation on these eggs is extremely variable, often gradational between lineartuberculate, ramotuberculate, and dispersituberculate. Clutches of *Macroelongatoolithus* contain up to 26 eggs arranged in pairs forming a ring-shaped single horizon clutch that may be 2.1 – 3.3 m in external diameter (Li et al. 1995; Wang and Zhou 1995; Currie 1996; Carpenter 1999; Grellet-Tinner 2005; Kim et al. 2011).

Macroelongatoolithus eggs were first described the Henan Province of China. While initially named as an oogenus within Elongatoolithidae, this group has been the subject of much controversy since its establishment. The first oospecies,

Macroelongatoolithus xixiaensis, was named by Li et al. 1995 and placed within Elongatoolithidae. Later in the same year Wang and Zhou name *Longiteresoolithus xixiaensis*, with a description that compares favorably to the already established *Macroelongatoolithus xixiaensis* specimens. Wang and Zhou erected a new oofamily, Macroelongatoolithidae, to include *Longiteresoolithus*, rather than placing the oogenus within Elongatoolithidae, as done for *Macroelongatoolithus xixiaensis* in Li et al. 1995. As the Li et al. 1995 paper was published first, *Macroelongatoolithus xixiaensis* has priority and *Longiteresoolithus* is considered a synonym of *Macroelongatoolithus*. Subsequent publications typically retain the position of *Macroelongatoolithus* within the oofamily Elongatoolithidae, however occasionally Macroelongatoolithidae and *Longiteresoolithus* still crop up in published literature (Liang et al. 2009). Though typically disregarded, the oofamily Macroelongatoolithidae was re-established in Wang, Zhao et al. 2010, in a revision of *Macroelongatoolithus* specimens. In that publication Wang et al. split *Macroelongatoolithus* into two oogenera – *Macroelongatoolithus* and *Megafusoolithus*- and argue for the use of Macroelongatoolithidae due to the large size (and subsequently large eggshell thickness and clutch size) of these specimens.

Macroelongatoolithus specimens have previously been reported from China, South Korea and North America (Li et al. 1995; Wang and Zhou 1995; Zelenitsky et al. 2000; Grellet-Tinner et al. 2006; Jin et al. 2007; Wang, Zhao et al. 2010; Kim, Yang et al. 2011; Huh et al. 2014). The occurrence of elongatoolithid eggs over 40 cm in length indicates the presence of *Macroelongatoolithus* in Mongolia as well (Watabe 1997), however a more detailed description of Mongolian material is not available.

Oospecies include: *Macroelongatoolithus carlylei* (Jensen 1970), *Macroelongatoolithus xixiaensis* (Li et al. 1995), *Macroelongatoolithus zhangi* (Fang, Wang, Jiang 2000), *Megafusoolithus qiaoxiaensis* (Wang et al. 2010), and *Macroelongatoolithus goseongensis* (Kim et al. 2011). According to Wang et al. (2010), *Macroelongatoolithus zhangi* should be regarded as a junior synonym of *Macroelongatoolithus xixiaensis*.

Table 2.5 Comparison of *Macroelongatoolithus* Oospecies. 1) Bray 1998, 2) Fang et al. 1998, 3) Fang et al 2000, 4) Grellet-Tinner 2005, 5) Huh et al. 2014, 6) Jensen 1970, 7) Jin et al. 2007, 8) Kim et al. 2011, 9) Li et al. 1995, 10) Liang et al. 2009, 11) Wang and Zhou 1995, 12) Wang, Zhao et al. 2010, 13) Zelenitsky et al. 2000.

Oospecies	Egg L x W cm	Elongation Index	Ornamentation	Shell Thickness mm	CL:ML ratio	Reference
Macroelongatoolithus carlyei	-	-	Dispers-Linear	1.5-3	2:1-4:1	1, 6, 13
Macroelongatoolithus xixiaensis	34-61 x 13-17.9	2-3.6	Dispers-Linear	1.2-4.75	1.6:1-8:1	2, 4-5, 7, 9-12
Macroelongatoolithus zhangi	45^{+} x 15	3	"Vermicular"	2	1.5:1	3. 12
Megafusoolithus qiaoxiaensis	40 x 13	3	Linear	1.45-1.6*	3:1	12
Macroelongatoolithus goseongensis	39 x 11.4	3.4	Linear	2.3-3.1	-	8
***Macroelongatoolithus* Summary**	**34-61 x 11.4-17.9**	**2-3.6**	**Variable**	**1.45-4.75**	**1.5:1-8:1**	

Table 2.6 Distribution of *Macroelongatoolithus* Oospecies. 1) Carpenter 1999, 2) Fang et al. 1998, 3) Fang et al. 2000, 4) Grellet-Tinner et al. 2006, 5) Jensen 1970, 6) Jin et al. 2007, 7) Kim et al. 2011, 8) Li et al. 1995, 9) Wang, Zhao et al. 2010, 10) Wang et al. 2012, 11) Yu et al. 2010, 12) Yu et al. 2012, 13) Zhou et al. 1999.

Oospecies	Age	Formation	Province/State	Country	Reference
Macroelongatoolithus carlylei	Early Cretaceous	Cedar Mt/Kelvin	Utah	US	5
Macroelongatoolithus xixiaensis	Early Cretaceous	Liangtoutang	Zhejiang	China	6
	Late Cretaceous	Liangtoutang	Zhejiang	China	11
	Late Cretaceous	Chichengshan	Zhejiang	China	9
	Late Cretaceous	Zhaoying	Henan	China	10
	Late Cretaceous	Sigou/Zoumagang	Henan	China	1-2, 8
	Maastrichtian	Zoumagang	Henan, Sanlimiao	China	4
	Late Cretaceous	Gaogou/Majiacun	Henan	China	13
Macroelongatoolithus zhangi	Late Cretaceous	Chichengshan	Zhejiang	China	3
Megafusoolithus qiaoxiaensis	Late Cretaceous	Chichengshan	Zhejiang	China	9, 12
Macroelongatoolithus goseongensis	Late Cretaceous	Goseong		South Korea	7

Macroelongatoolithus carlylei (Jensen 1970) is described on the basis of eggshell fragments from the Cedar Mountain and Dakota Formations of Emery County, Utah. Eggshell thickness varies from 1.5 – 3 mm, CL:ML ratio is 2:1 – 4:1, and the CL-ML boundary is abrupt and undulating (Zelenitsky et al. 2000). Ornamentation is dispersituberculate to lineartuberculate. In some thin sections the CL-ML boundary is obscured due to alteration (Zelenitsky et al. 2000).

Macroelongatoolithus xixiaensis (Li et al. 1995, within Elongatoolithidae), from Henan province of China, are 39.3 – 51.6 cm long and 13 – 17.9 cm wide. Shell thickness ranges from 2 – 3.2 mm and the CL:ML ratio varies from 7:1 to 8:1. Later descriptions of *M. xixiaensis* (Wang and Zhou 1995; Liang et al. 2009; Fang et al. 1998; Grellet-Tinner 2005; Jin et al. 2007; Huh et al. 2014) eggs broaden the definition of the oospecies to include eggs 34 – 61 cm long by 13 – 17.9 cm wide with an elongation index of 2 – 3.63. Ornamentation grades from dispersituberculate and ramotuberculate at poles to lineartuberculate at the midpoint of eggs. Some specimens have ramotuberculate ornamentation between the poles and midpoint as well, and occasionally have smooth poles. Eggshell varies from 1.2 – 4.75 mm thick, with a CL:ML ration ranging from 1.62:1 – 8:1. The boundary between the CL and ML is typically clear and undulating, but may be obscured by alteration and appear unclear or absent. Pore openings are round to oval.

Megafusoolithus qiaoxiaensis (Wang et al. 2010), from the Chichengshan Formation of Zhejiang, China, are defined as 40 cm long by 13 cm wide, with an elongation index of 3.07. Ornamentation is lineartuberculate along most of the egg,

however poles are smooth. Eggshell is 1.45 – 1.6 mm thick (excluding ornamentation), the CL:ML ratio is 3:1, and the boundary between the CL and ML is unclear.

Macroelongatoolithus goseongensis (Kim et al. 2011) is defined on the basis of a partial clutch, containing six eggs, discovered in the Goseong Formation, Gyeongsang, South Korea. Eggs are 39 cm long and 11.5 cm wide with an elongation index of 3.39. Eggshell is 2.3 – 3.1 mm thick with a CL:ML ratio of 2.5:1 – 4.8:1. Ornamentation is lineartuberculate and the CL-ML boundary is abrupt and undulating.

Distribution includes: Lower Cretaceous Cedar Mountain and Dakota Formations, Emery County, Utah, USA; Albian – Maastrichtian Gaogou, Zoumagang, Liangtoutang, and Chichengshan Formations, Henan and Zhejiang Provinces, China; and the Campanian Goseong Formation of Gyeongsang, South Korea.

Ellipsoolithus Mohabey 1998

An oddity among the elongatoolithid egg type, *Ellipsoolithus* have an elliptical rather than elongate shape, and are relatively small at 9.8 - 11 cm long by 6.5 – 8 cm wide. The single oospecies *Ellipsoolithus khedaensis* is described from the Maastrichtian Lameta Formation of Gujarat, India. Clutches occur as a single layer of horizontally distributed eggs. Eggshell thickness varies from 1.2 – 1.64 mm, ornamentation has weak relief and grades from dispersituberculate at the poles to lineartuberculate toward the midpoint of the eggs, the CL:ML ratio is typically 4:1, and the CL-ML boundary is abrupt.

Trachoolithus Mikhailov 1994a

Trachoolithus was described by Mikhailov (1994) from a collection of eggshell fragments from the Lower Cretaceous Dushi Ula Formation (Neocomian – Aptian) of Ubur – Khangay, Mongolia. Eggshell fragments from the single oospecies *Trachoolithus faticanus* have fine lineartuberculate ornamentation and are significantly thinner than most other elongatoolithid eggs, at 0.3 – 0.5 mm thick. Ornamentation has high relief, making up 2/3 of eggshell thickness. Ornamentation is dispersituberculate to ramotuberculate and CL:ML ratio varies from 3-4:1.

Heishanoolithus Zhao and Zhao 1999

Known from material from the Lower Cretaceous Shahai Formation, Liaoning Province, China, *Heishanoolithus changi* is defined on the basis of eggshell fragments. Eggshell is 1.2 – 1.3 mm thick with dense nodular and lineartuberculate ornamentation. CL:ML ratio is 7:1. This oogenus is distinguished from other elongatoolithid eggs by its small mammillary layer height in comparison to the total eggshell thickness and dominant ramotuberculate ornamentation.

Ornitholithus Donaire
and Lopez-Martinez 2009

Described from the Paleocene of France and Spain, these 20 to 40 cm long eggs likely belong to a giant bird. The authors declined to assign an oospecies, but erected a new oogenus for this material. Of Elongatoolithidae, *Ornitholithus* is the only oogenus described as exhibiting a branching pore system, and is also likely the only avian egg included in the oofamily.

Paraelongatoolithus Wang,
Wang, Zhao, and Jiang 2010

Described from the Chichengshan Formation, Zhejiang Province, China, *Paraelongatoolithus reticulatus* is defined by a single elongate egg with an estimated length of 17 cm by 7.2 cm wide. Ornamentation is 'reticulate'. Eggshell thickness varies from 0.50 to 0.60 mm (0.70 – 0.85 mm with ornamentation), CL:ML ratio is 2:1, and the CL-ML boundary is abrupt.

Undulatoolithus Wang,
Zhao, Wang, Li, and Zou 2013

Described from the Upper Cretaceous Zhoutian Formation of Jiangxi Province, China, *Undulatoolithus pengi* is defined by eggs 19.36 cm long and 8.35 cm wide. Eggs are asymmetrical, paired, and occur in a ring shaped clutch. CL:ML ratio varies from 4:1-8:1 and the CL-ML boundary is gradational. Authors differentiate this new taxon from *Macroolithus* specimens by ornamentation height, which makes up nearly half of total eggshell thickness of 1.3 mm.

Elongatoolithid and *Oviraptor* Associations

In the early 1920s a theropod dinosaur in close association with a clutch of elongated eggs was collected from the Upper Cretaceous Djadokhta Formation of Mongolia (Osbourn 1924; Clark et al. 1999; Dong and Currie 1996; Norell et al. 1995). The abundant elongate eggs were initially interpreted as belonging to *Protoceratops*, as this ceratopsian was also prevalent in the formation. The bizarre new theropod, whose odd beak was in close proximity to these eggs, thus gained the name *Oviraptor* or "egg

stealer", and was assumed to have been preying on the eggs of the small ceratopsian. At the time of publication, however, Osborn cautioned that such an interpretation may turn out to falsely vilify the *Oviraptor*, and that a strict assessment of the theropod's behavior was not to be clung to. Since that discovery multiple lines of evidence, from skeleton-egg associations (Norell et al. 1995; Clark et al. 1999, 2001; Dong and Currie 1996; Fanti et al. 2012) to embryos in ovo (Norell et al. 1994; Cheng et al. 2008), have come to light indicating a strong link between eggs of the oofamily Elongatoolithidae and oviraptorosaurs.

Elongatoolithus and *Macroolithus*

Oviraptorosaur embryonic material adhering to the internal surface of an elongatoolithid egg was first identified by Norell et al. (1994), in the description of a elongatoolithid nest containing a single in ovo individual as well as the remains of perinatal troodontids. Subsequent oviraptorosaur embryos within elongatoolithid eggs were reported from the Djadokha and Nemegt Formations of Mongolia (Norell 2001, Weishampel et al. 2008), and the Nanxiong Formation of China (Cheng et al. 2008; Sato et al. 2005). Weishampel et al. (2008) state that eggshell associated with embryonic material is most similar to *E. andrewsi* and *E. elongatus*, however Cheng et al. (2008) assign associated eggshell to *Macroolithus*.

Descriptions of *Citipati osmolskae* and *Nemegtomaia barsboldi* specimens in brooding postures over *Elongatoolithus* and *Macroolithus* clutches (Norell et al. 1995; Clark et al. 1999, 2001; Dong and Currie 1996; Fanti et al. 2012), in addition to an *Oviraptor philoceratops* specimen in close proximity to an elongatoolithid clutch

(Osborn 1924) suggest a relationship between oviraptorid theropods and the elongatoolithid eggs. More recently, eggs preserved within the body cavities of two individuals have been discovered (Sato et al. 2005; He et al. 2012). Sato et al. (2005) refer associated eggs to *Macroolithus yaotunensis*. In both Sato et al. (2005) and He et al. (2012) two eggs are described in association with a single oviraptorid individual. The former describes a specimen with two eggs within the body cavity, while the individual in the latter paper, specimen M8829, has a single egg within the body cavity and one in close association with the hips and tail. The presence of embryos within eggs and eggs within the body cavities of oviraptorids substantiates the claim of a parent-egg relationship between oviraptorosaurs and elongatoolithid eggs. It is this evidence that then allows for the interpretation of nesting and reproductive behaviors in oviraptorosaurs based on clutch morphology, gas conductance, and microstructure of elongatoolithid eggs, discussed below.

Macroelongatoolithus

A perinatal oviraptorid specimen preserved in contact with four *Macroelongatoolithus* eggs has been documented (Grellet-Tinner 2005; Grellet-Tinner et al. 2006) but not thoroughly discussed in published literature. Eggshell from this specimen, known as “Baby Louie” (LACM7477/149736a) was definitely assigned to *M. xixiaensis* by Grellet-Tinner (2005) and an edentulous premaxillary, a trait associated with oviraptorosaurs, was tentatively identified in the associated perinatal individual (Grellet-Tinner 2005; Grellet-Tinner and Makovicky 2006).

Reproductive Behaviors of Elongatoolithid Egg Laying Animals

Clutches of elongatoolithid eggs consist of paired eggs arranged in a ring with a large central space and up to three superimposed layers of eggs in some cases (Carpenter 1999; Clark et al. 1999; Liang et al. 2009). Egg pairing in these specimens has been cited as evidence that the parent animals had two functioning oviducts and were capable of holding two shelled eggs within the body at a time (Varricchio et al. 1997; Clark et al. 2001; Grellet-Tinner 2005; Grellet-Tinner et al. 2006). A description of a gravid oviraptorosaur by Sato et al. (2005) lends additional support to this hypothesis as the animal was preserved with two eggs within the body cavity. Additionally, large clutch size compared to adult body size has been used to suggest paternal care and possibly multiple females contributing to a single clutch (Varricchio et al. 2008). Slight asymmetry in elongatoolithid eggs has been documented and interpreted as evidence of an air cell at one end of the egg. In extant birds egg cell formation occurs via evaporation of fluids in subaerially exposed nests (Ar and Rahn 1980), while egg shape is thought to result from influence of peristaltic muscular contractions on a single egg within an oviduct (Iverson and Ewert 1991). As egg shape and air cell formation have not been shown to correlate in modern birds the presence of an air cell in fossil eggs based on egg asymmetry is tenuous. Linear ridges and nodes common to the ornamentation of elongatoolithid eggs have been hypothesized as structures used to direct air circulation (Grellet-Tinner et al. 2006; Sabath 1991).

Early research regarding the nesting environment of these eggs suggested the clutches might have been subaerially exposed in a desert environment due to the narrow

nature of pores in the angustacanuliculate system (VanStraelen 1925). However, later reported gas conductance values are higher than modern birds and indicate the eggs may have been partially buried in a substrate or covered with vegetation while in the nest (Mou 1992, Seymour 1979). Contact between the gastralia of 'brooding' specimens suggests that partial burial is most likely, as the close association of skeletal elements indicates direct contact between the parent animal and eggs (Clark et al. 1998; Varricchio et al. 1999; Grellet-Tinner 2005; Jackson et al. 2008).

Oviraptor embryos found in elongatoolithid eggs are typically near the end of the developmental period, with well-ossified bones (Weishampel et al. 2008). This suggests that such oviraptorids were precocial, hatching with functional limbs and in need of little parental care compared to altricial hatchlings (Weishampel et al. 2008). Association of adult oviraptorids on top of egg clutches may suggest oviraptorids were caring for their egg clutches in some way, either for the purpose of temperature regulation or in order to protect the clutch from predators. It has also been suggested that the presence of the parent's carcass over an egg clutch may be attributed to extended brooding, similar to that seen in the paleognath *Dromaius novahollandiae* (emu), in which the parent goes without food or water for an extended period of time (Grellet-Tinner et al. 2005). The weakened state caused by such behavior may have allowed the animals to be overcome by dune collapse (Grellet-Tinner 2005).

Review of Gas Conductance Studies

Previous studies have suggested a link between water vapor conductance across an amniote eggshell (with relation to mass of the egg), and nesting environment (Ar et al.

1974; Seymour 1979). Several authors suggest dinosaur eggs typically had greater gas conductance rates than those seen in open nesting bird eggs of equivalent mass, and were thus buried in a substrate (Sabath 1991; Mikhailov et al. 1994; Deeming 2006). However, many of these studies rely on calculations of water vapor conductance based on data collected from eggshell fragments alone.

It was not until recently that the impact of variation in microstructure and porosity across an egg was considered in relation to this variations impact on estimated gas conductance rates in non-avian dinosaur eggs (Varricchio et al. 2013). This more recent work suggest that while single eggshell fragment calculations of water vapor conductance may be a useful starting point for estimating nesting mode in extinct taxa, a more detail regional analysis is necessary to obtain a more accurate gas conductance range. The difference between values estimated from isolate fragments and the range of gas conductance calculated from a thorough zonal study may easily mean the difference between reconstructing a buried nesting mode and an open-air nesting one. *Macroelongatoolithus* gas conductance has previously been estimated as 600 mg H_2O mg $torr^{-1}day^{-1}$, suggesting a moderately humid nesting environment (Deeming 2006).

CHAPTER 3

MATERIALS AND METHODS

Materials

Wayan Formation

Eggshell fragments were discovered by USDA Forest Service Paleontologist Steve Robison (Fig 3.1A) in the Caribou-Targhee National Forest and on state lands, Bonneville County, Idaho. Dave Varricchio and Frankie Jackson undertook later excavations at two localities, Jackknife Creek and Brockman Creek (Fig. 3.1B-C, Fig. 3.2) with the assistance of Bob Jackson, Joey Stielger, Paul Ullmann, Darrin Strosnider, Jason More, and Jamie Kern.

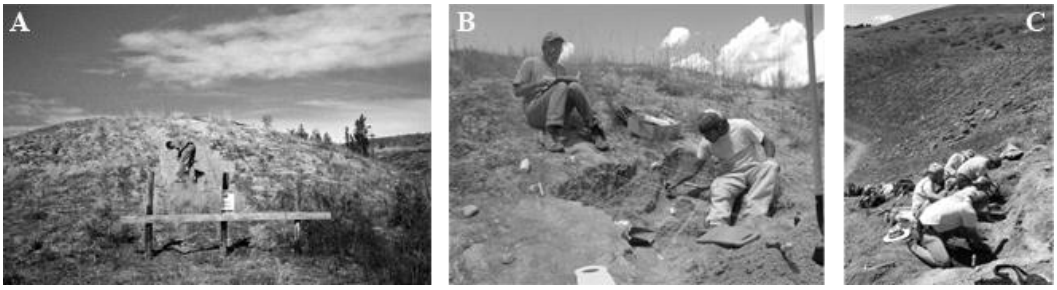

Figure 3.1 Excavation of Wayan Formation Localities in 2007. A. Jackknife Creek locality IMNH 2428. Steve Robison collecting first eggshell fragments discovered in area. B. Jackknife Creek locality IMNH 2428. Bob Jackson and Joey Stiegler creating quarry map of initial excavation area. C. Brockman Creek locality IMNH 2427. Front to back: Bob Jackson, Frankie Jackson, Joey Stiegler, Paul Ullmann, Darrin Strosnider, and Dave Varricchio, working on initial excavation.

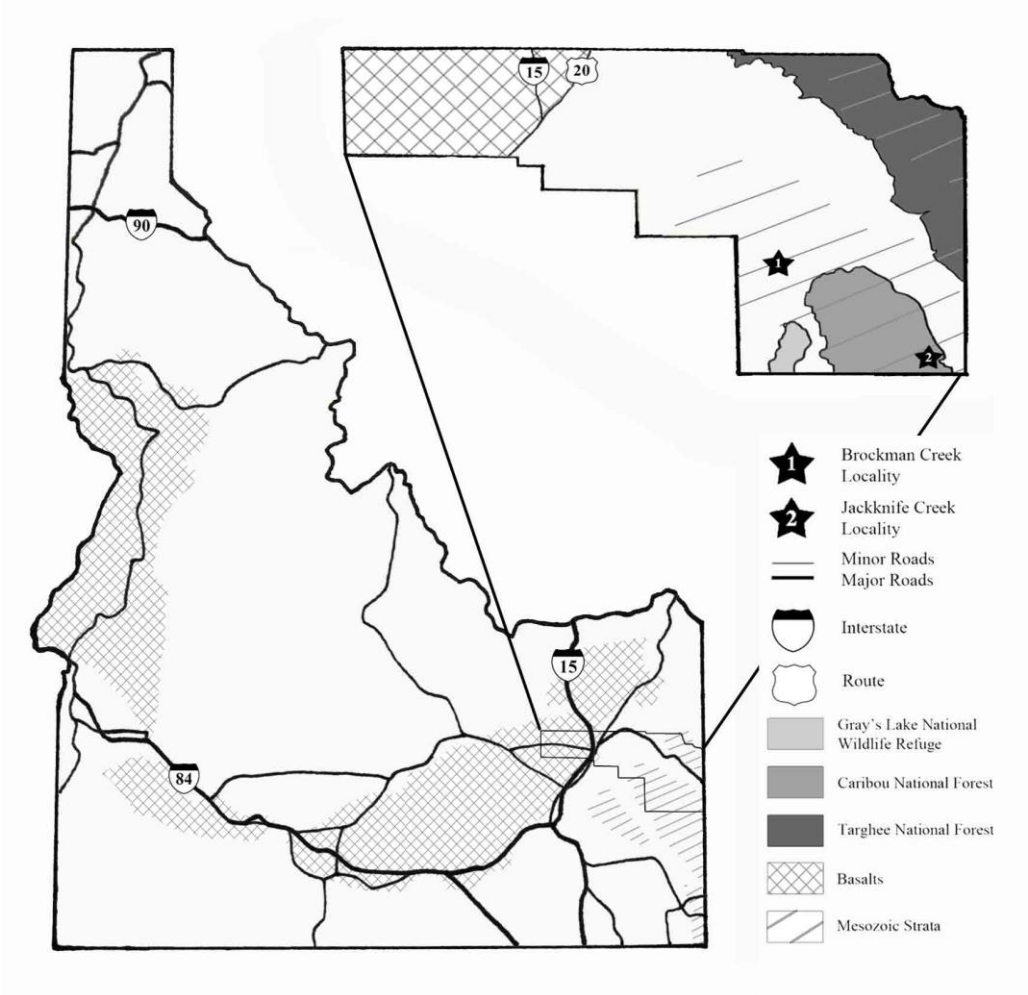

Figure 3.2 Idaho Locality Map. Inset shows detail view of Bonneville County.

Brockman Creek Material Eggshell fragment concentrations (IMNH 2427\49604, 49606; Fig 3.3 A-B) and eggshell concentration with fragmentary egg portions (IMNH 2427\49605; Fig 3.3 C). These specimens are housed in the Idaho Museum of Natural History, Pocatello, ID. Loose fragments collected from Brockman Creek are temporarily housed in the Varricchio Family Paleontology Lab, Gaines Hall, MSU, Bozeman, MT.

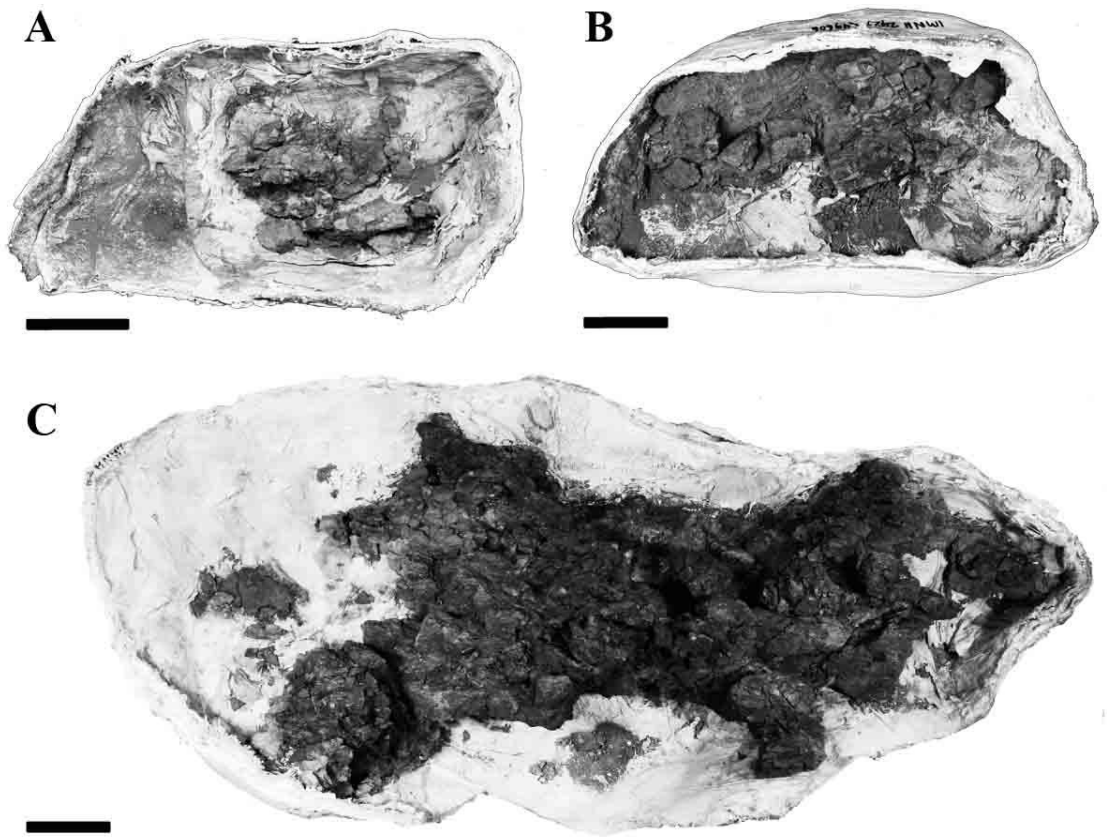

Figure 3.3 IMNH 2427 Brockman Creek Specimens. A. IMNH 2427\49604. B. IMNH 2427\49606. C. IMNH 2427\49605. Scale bars equal 10 cm.

Jackknife Creek Material Eggshell fragment accumulations (IMNH 2428\49607, IMNH 2428\69609-49612 ; Fig 3.4 A-E), in situ collected eggshell fragments (IMNH 2428\49613), and partially preserved egg pair (IMNH 2428\49608; Fig 3.4F – 3.5). These specimens are housed in the Idaho Museum of Natural History, Pocatello, ID. Thin sections ES390-ES395, ES461-ES470 are housed in the Earth Sciences Department, MSU, Bozeman, MT.

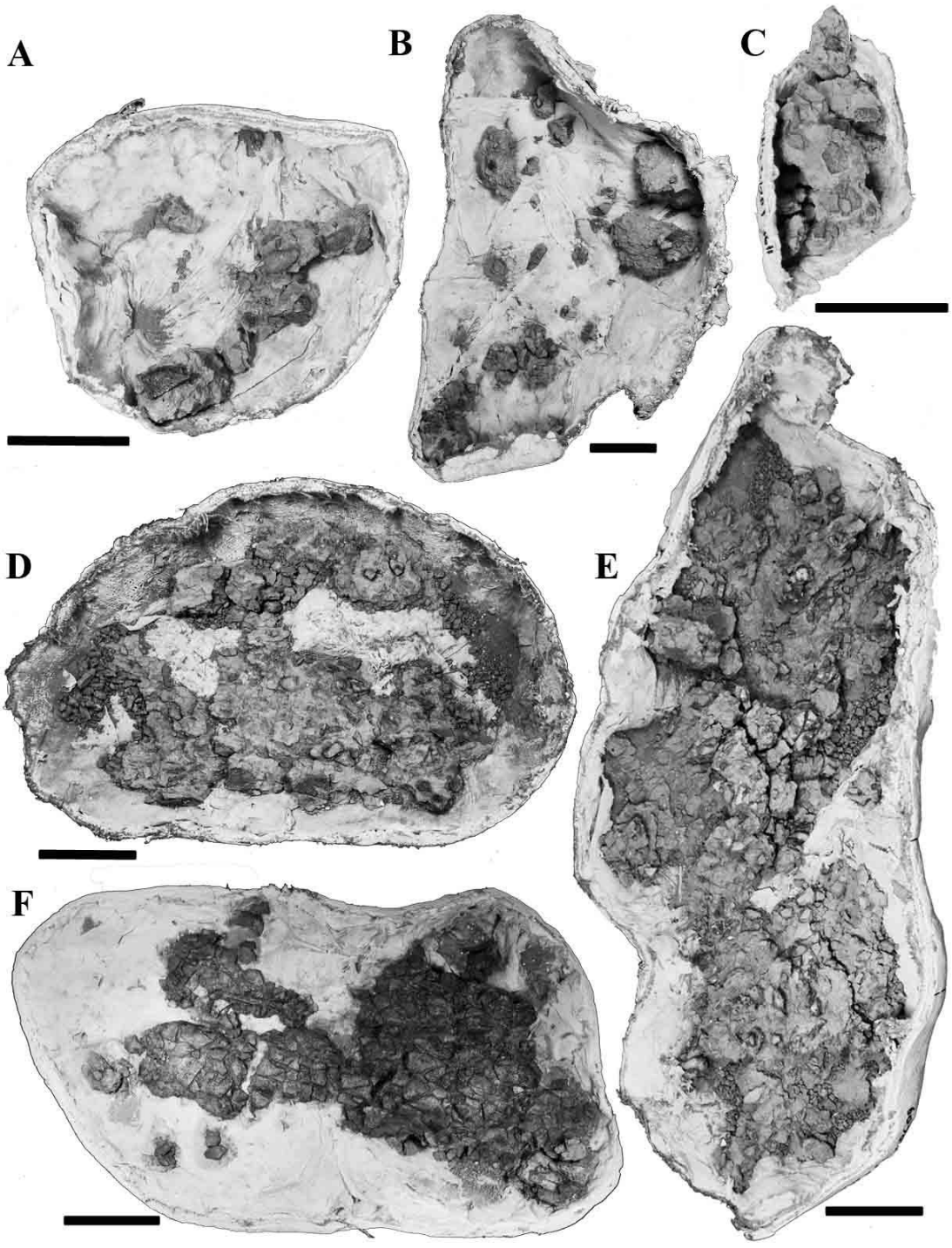

Figure 3.4 IMNH 2428 Jackknife Creek Specimens. A. IMNH 2428\49610. B. IMNH 2428\49612. C. 2428\49611. D. IMNH 2428\49607. E. IMNH 2428\49609. F. IMNH 2428\49608. Scale bars equal 10 cm.

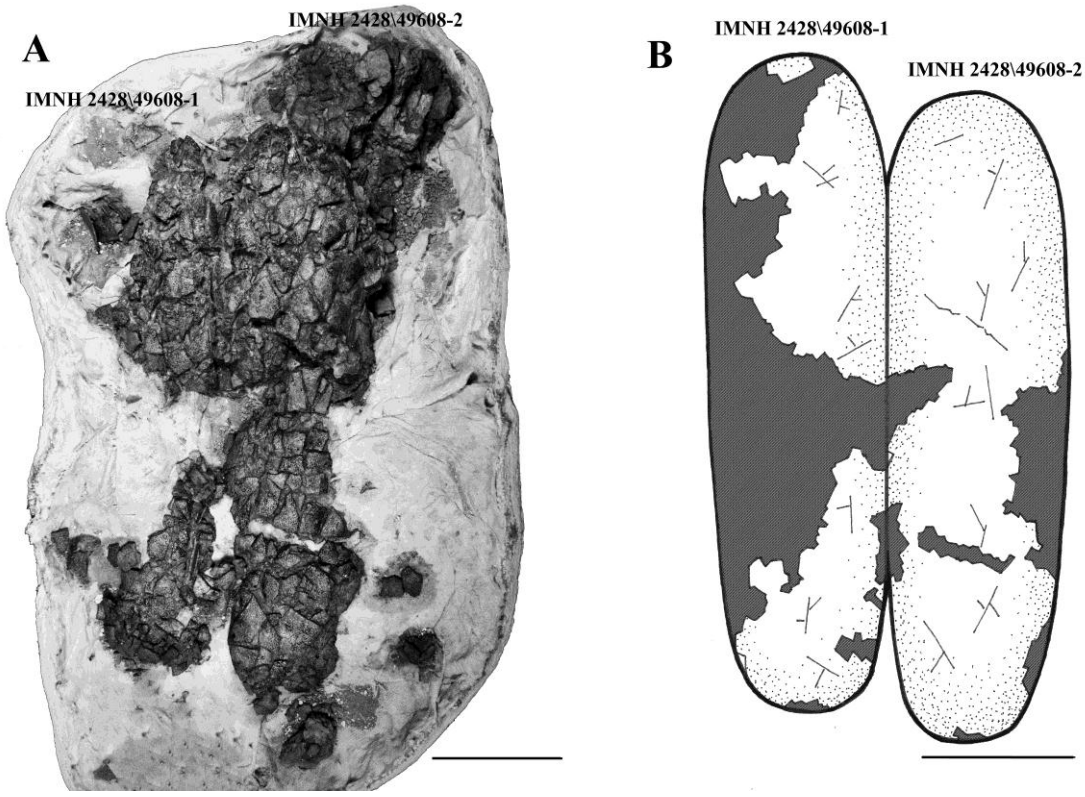

Figure 3.5 IMNH 2428\49608. A. Detail view of specimen. B. Line drawing of specimen, reconstructing probable outline of both eggs. Shading indicates missing egg portions. Scale bar equals 10 cm.

Geology and Faunal Composition The Lower Cretaceous Wayan Formation, located in the thrust belt of southeastern Idaho, is approximately 1344 m thick (Krumenacker et al. 2010) and composed of interbedded pebble conglomerates, sandstones, and grey/red mudstones (Schmitt and Moran 1982; Krumenacker 2005). Palynomorph evidence suggests an Albian age, however more recent work utilizing dating of detrital zircon crystals expands this age range to the Albian-Cenomanian (Krumenacker et al. 2010).

Highly mottled grey/red siltstones and claystones are the dominant rock type of the formation, interspersed with lenses and laterally continuous packages of siltstones and

fine-grained sandstones. This lithology indicates an upland meandering stream complex associated with a well-drained floodplain (Schmitt and Moran 1982; Dorr 1985). The mottled nature of the mudstones in addition to the presence of calcareous nodular development is interpreted as evidence for a semi-arid floodplain with soil horizon development (Schmitt and Moran 1982; Dorr 1985; Krumenacker et al. 2010).

Known fauna from the Wayan Formation include ornithopods (*Oryctodromeus*, *Tenontosaurus* and iguanodontids), dromaeosaurids, tyrannosaurids, ankylosaurs, and neoceratopsians (Dorr 1985; Weishampel et al. 2002; Chapman et al. 2004; Krumenacker 2005; Varricchio et al. 2007; Krumenacker et al. 2011). Dinosaur eggshell fragments were reported from the Wayan Formation as early as 1985 (Dorr 1985), but remained un-described/classified until this study.

Blackleaf Formation

Material Examined MOR 1638 Surface collected eggshell fragment from locality BL-390, Vaughn Member, Blackleaf Formation, Beaverhead County, MT. ES 301 Thin section made from collected material housed in the Earth Sciences Department, MSU, Bozeman, MT. Eggshell fragments were collected from the Blackleaf Formation of South-western Montana by David Varricchio and Frankie Jackson. These fragments were found in association with bone fragments at locality BL-390.

Geology and Faunal Composition Equivalent in age to the Wayan Formation of Idaho, the Blackleaf Formation of Montana is composed of between 425 and 600 meters of varying lithologies that represent near shore fluvial-deltaic deposition with variable

volcaniclastic input towards the top of the section (Dyman and Nichols 1988; Krumenacker et al. 2010; Ullmann et al. 2012) limestones, and sandstone beds, while the uppermost members show a shift toward non-marine fluvial-deltaic sandstones, mudstones, and bentonitic beds (Dyman and Nichols 1988; Krumenacker et al. 2010). U-Pb zircon dates for this formation are approximately 93 – 99 MA (Albian – Cenomanian) (Zartman et al. 1995).

Previously, the reported dinosaur fauna of the Blackleaf was limited to the small ornithopod *Oryctodromeus* (Varricchio et al. 2007). Recent analysis of microsites producing teeth identified as those of dromaeosaurids, tyrannosauroids, hadrosaurids, hypsilophodonts, and ankylosaurs has greatly expanded the diversity of this faunal assemblage (Ullmann et al. 2012).

Thomas Fork Formation

Material Examined Surface collected eggshell fragments, Thomas Fork Formation, Lincoln County, WY. ES 304-306, ES 385 thin sections made from collected material (Housed in the Earth Sciences Department, MSU, Bozeman, MT).

Geology and Faunal Composition Considered to be a tongue of the Wayan Formation, the Thomas Fork Formation of Wyoming is characterized by color-variegated mudstones with calcareous nodule development (Dorr 1985; Krumenacker 2010). Dorr reported dinosaur eggshell fragments from the Thomas Fork Formation as early as 1985, but eggshell fragments from the formation remained un-described/classified until this study.

Liangtoutang Formation

Material Examined ZMNH M8705. Partially preserved egg pair. Specimen consists of the concave or ventral portion of two eggs, one intact along the length of the egg (ZMNH M8705-1) and one preserved along roughly 2/3^{rds} of estimated length (ZMNH M8705-2)(Fig. 3.6). Eggshell thin sections ES456 – ES460 housed in the Earth Sciences Department, MSU, Bozeman, MT.

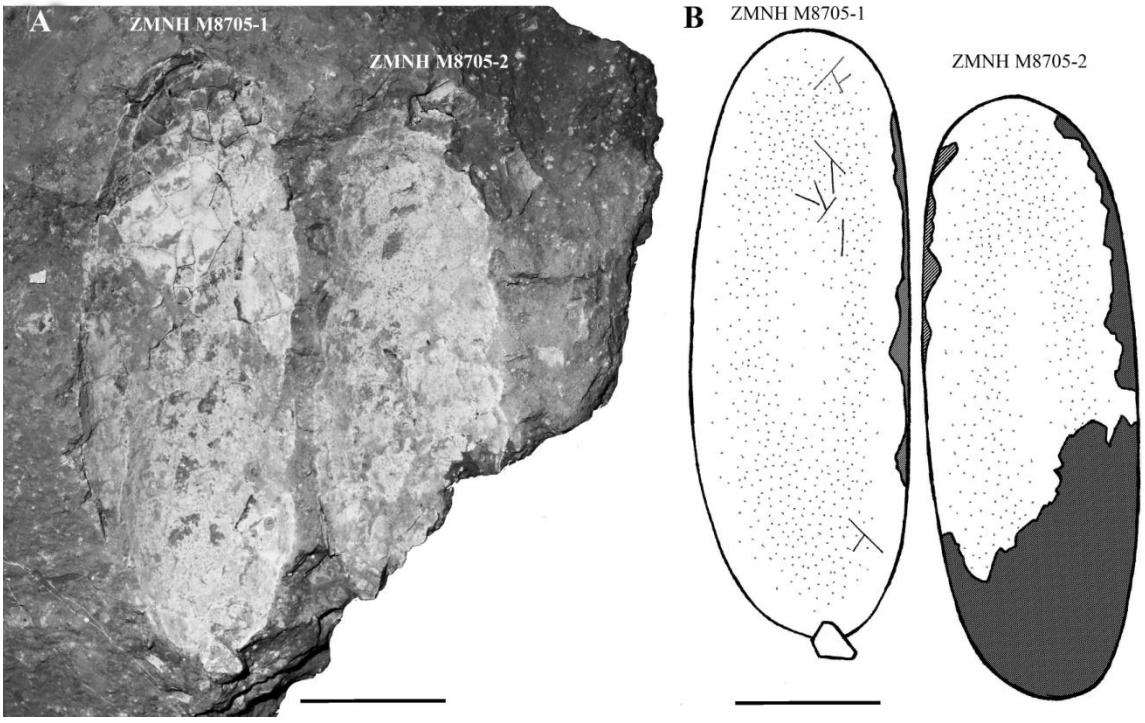

Figure 3.6 ZMNH M8705. A. Detail view of specimen. B. Line drawing of specimen, reconstructing probable outline of both eggs. Shading indicates missing egg portions. Scale bar equals 10 cm.

Geology and Faunal Composition The Tangshang, Liangtoutang, and Chichengshan Formation are the mid-Cretaceous components of the Qujiang group, exposed throughout the Tiantai basin of Zhejiang Province, China. The Liangtoutang

Formation is primarily composed of red siltstones and fine-grained sandstones, with some pebbly sandstone reported (Jin et al. 2007; Zheng et al. 2012). This lithology is interpreted as indicative of a shallow laucustrine setting with intermittent subaerial exposure of the sediments (Wang et al. 2000; Jin et al. 2007; Zheng et al. 2012; Barta et al. 2014). Radiometric dating places the formation at 105.9 – 103.2 MA (Albian) (Wang et al. 2000). In Zheng et al. 2012 this radiometric data is combined with biostratigraphic correlation to date the Liangtoutang as Albian – Cenomanian, identical to the most recent age estimate for the Wayan Formation of Idaho, US. More recent U-Pb zircon analysis of Tiantai strata has constrained these formations to 91 – 99 MA (Cenomanian – Turonian) (He et al. 2013).

Methods

Wayan Formation Field Work

During the 2006 and 2007 excavations Frankie Jackson and Dave Varricchio mapped and recorded orientation (i.e., concave up (CCU) or down (CCD))of in situ eggshell fragments at both localities. During a subsequent locality visit in 2012 stratigraphic sections were measured perpendicular to bed strike for the entire length of accessible outcrop at both localities. During stratigraphic sectioning samples were collected at boundaries of lithologic changes at the subunit level. Significant changes in color, grain size, or rock type were considered the beginning of a new unit and streaks, calcite veins, and subunits containing nodules or of varying color and lithology were noted.

Laboratory Preparation of
Wayan Formation Specimens

All jackets were prepared from the stratigraphic bottom up, as is common with egg specimens in order to preserve any potentially intact egg morphology. Rock was removed in one-centimeter thick horizons and any eggshell found within each horizon was mapped and CCU/CCD data was recorded. This data was then combined with field collected CCU/CCD data for in situ material that was removed during excavation at each site. Orientation ratios were compared to orientation data recorded in previous literature to determine if the Wayan Formation eggshell accumulations represent in situ or transported assemblages. Eggshell fragments were mapped and removed until either cohesive sections of egg were uncovered or the jacket was prepared down to the last 1-2 cm.

Specimens were prepared in the Varricchio Family Paleontology Lab in Gaines Hall at Montana State University. During preparation any lithologic changes were noted and rock samples were collected from each jacket. When preparation was complete eggshell removed from jackets was bagged and labeled with the appropriate IMNH ID number. Any eggshell remaining in the jackets was consolidated using Vinac and specimens were photographed using a Nikon D60 digital SLR camera. All jackets were assigned numbers in accordance with the Idaho Museum of Natural History specimen numbering system.

Prior to thin sectioning casts were made of each sample in order to decrease any affect sampling had on the overall appearance of IMNH 2428\49608-2. Molds of each eggshell were made using SilPutty RTV silicone. Casts were poured with Smooth-On

EpoxAcast 650 resin and cured with Smooth-On 101 Fast Hardener epoxy curative. Smooth-On So Strong black pigment was added to casting resin in order to dye casts. Varricchio Paleontology Lab manager Michael Holland painted casts to match the color of the original specimen using craft grade acrylic paint from Plaid, Inc. Eggshell fragment casts were then placed into the area from which samples were initially removed.

X-ray Diffraction

Rock samples from two jackets from Brockman Creek and Jackknife Creek (IMNH 2427\49605, IMNH2427\49606, and IMNH 2428\49607, IMNH 2428\49608, respectively) were collected and analyzed using X-ray Powder Diffraction (XRD) in order to determine bulk mineralogy, with specific emphasis on clay mineral identification. A concretion from IMNH 2428\49607 was also collected and analyzed. All samples were ground with a mortar and pestle, then sieved through a USA Standard Testing Sieve # 230 (equivalent to a Tyler 250 Mesh, 63 μm openings) and stored in 2-dram glass vials.

In order to determine mineralogy of Brockman Creek and Jackknife Creek mudstones each sample was divided into four components for analysis: one sample was packed into a disc mount for a bulk compositional analysis, while the remaining powder samples were used to create three oriented slides per sample for clay mineral identification. A single un-oriented powder mount was analyzed to identify the mineralogical composition of the concretion ES 386. To create oriented slides mudstone samples were put in suspension with water and a small amount of 5% solution sodium metaphosphate de-flocculating agent. This solution was then pumped through a glass

filter and dual beaker set-up with a paper filter in place. Once all water was pumped out of the sample the paper filter coated in the settled pulverized rock was placed on the side of a bottomless glass cylindrical flask using tweezers (to avoid contamination), then rolled onto a smooth glass slide to create an oriented sample. Three oriented slides were made for each of the mudstone samples using this method, for a total of 12 oriented slides. For each sample the three slides were subjected to three different drying treatments- glycolating, baking at 500 C, and air-drying.

X-ray Diffraction of samples was analyzed using an X-Ray Powder Diffraction Spectrometer and SCINTAG X1 Diffraction System. Peak charts for these three treatments were analyzed using Jade 9 software. All equipment used for XRD analysis is located at the Image and Chemical Analysis Laboratory (ICAL), Montana State University (MSU). Electron Dispersive X-ray (EDX) backscatter analysis was used to identify elements present within the mudstone samples. This allows for more accurate determination of peak analyses, as minerals with similar peaks can be resolved based on the presence or absence of elements noted by EDX. Comparison of peaks and peak destruction between the three treatments applied to each sample were also compared to a flowchart available from USGS to corroborate clay mineral composition (U. S. Geological Survey Open-File Report 01-041). Electron Dispersive X-ray Backscatter data was obtained using a JEOL 6100 SEM with Backscattered Electron Imaging (BEI) and a Noran Voyager Dispersive X-ray (EDX) system, also located at ICAL, MSU.

Microscopic Examination

Eggshell samples were cleaned and each sample was broken into three fragments. Two fragments of each sample were prepared as standard 30 μm thick petrographic thinsections, one radial and one tangential for each sample. These thin sections were studied with polarized light microscopy (PLM), in both plane polarized light (PPL) and cross-polarized light (XPL) using a Nikon Eclipse LV100 POL microscope with attached Nikon Digital Sight DS-5Mc camera. Epoxy pucks containing eggshell leftover from the thin sectioning process were cut to 1.5 mm thickness with a Hillquist Trim Saw and polished using a Buehler Ecomet 3 variable speed grinder-polisher with an eight inch wheel and 1 micron grit Buehler Micropolish. Epoxy pucks were then cleaned using distilled water and a Cole-Parmer 8891 ultrasonic bath, dried on a Thermolyne nuova II stir plate, and viewed using a Nikon Eclipse 50i petrographic microscope with attached Nikon Digital Sight DS-2Mv camera and Relion Industries Cathodolumenesence Detector and Alctel vacuum pump in order to assess diagenetic alteration of specimens.

Remaining fragments of each sample were sputter coated with 10 nm of gold, mounted on aluminum stubs, and imaged using a J.R. Lee Instrument Personal Scanning Electron Microscope (SEM) located at the Museum of the Rockies. Scale bars were added to photomicrographs of specimens using Adobe Photoshop CS 5 software. Microstructural features were then measured using public domain ImageJ software developed by the National Institutes of Health (NIH) available without charge through the NIH website: imagej.net.

Zonal Microstructural Analysis

In order to assess and quantify any microstructural variation along the length of an egg the most intact egg from each specimen, IMNH 2428\49608-2 and ZMNH M8705-1, were divided into five zones. This method was modeled after methods established in Varricchio et al. (2013) to quantify variation in gas conductance along *Troodon* eggs. Zones were evenly divided by length of the egg, with poles (Zone 1 and Zone 5) representing 12.5% of total egg length, and Zones 2 through 4 representing 25% of total egg length (Figs. 3.7 – 3.8). Three samples were taken from each zone of IMNH 2428\49608-2 and one sample was taken from each zone of ZMNH M8705-1. Sample size was limited in order to minimize specimen destruction. These fragments were prepared as outlined in Microscopic Examination methods listed above.

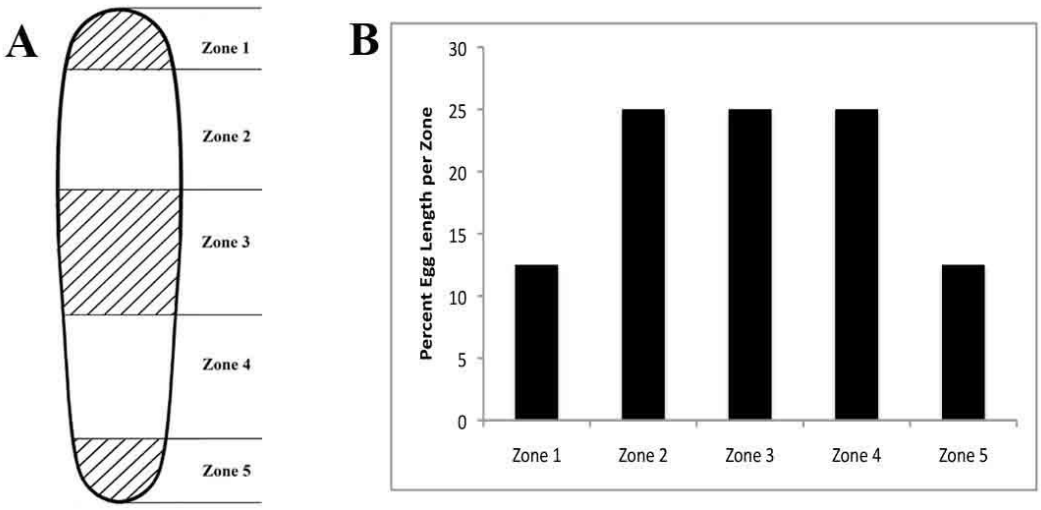

Figure 3.7 Defined Zones for IMNH 2428\49608-2. A. Idealized egg shape with Zones 1, 3, and 5 shown by diagonal lines, Zones 2 and 4 with no fill. B. Zones as defined by percent of total egg length.

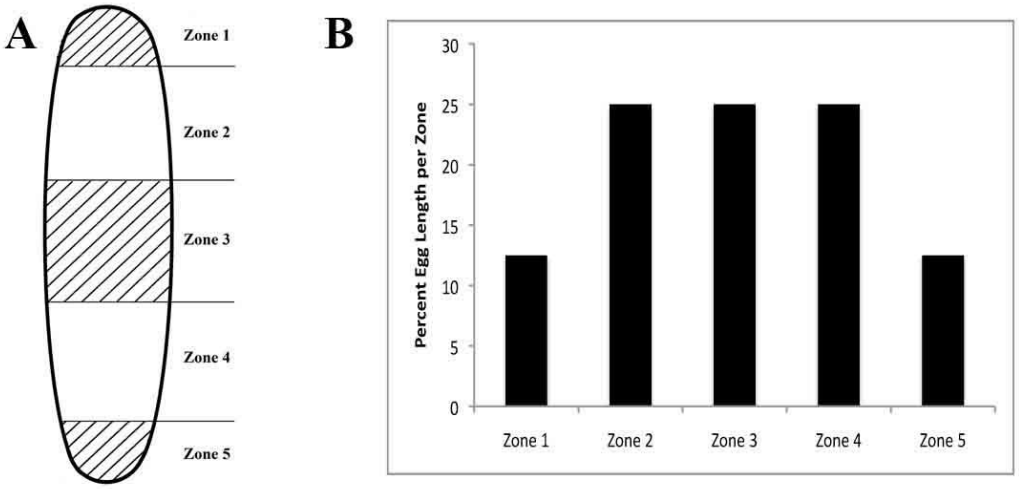

Figure 3.8 Defined Zones for ZMNH M8705-1. A. Idealized egg shape with Zones 1, 3, and 5 shown by diagonal lines, Zones 2 and 4 with no fill. B. Zones as defined by percent of total egg length.

Zonal Gas Conductance

Tangential thin sections were made from portions of the three samples taken from each zone of IMNH 2428\49608-2 and the single sample taken from each zone of ZMNH M8705-1. Samples were prepared and examined as outlined in Microscopic Analysis methods listed above and were used to identify pores and the area and diameter of each was measured using Image J software. Individual pore areas were summed for each zone and divided by the total examined shell area for each zone in order to calculate a fractional pore area ($_fA$). This fractional pore area was then multiplied by zonal surface area to calculate the total pore area for each zone (A_p). Effective porosity was then calculated by dividing zonal pore area by the average pore length per zone (L_s) (Table 3.2). Average pore length here was assumed to be equal to average shell thickness.

The most complete egg of each pair, IMNH 2428/49608-2 and ZMNH M8705-1, was divided into five zones based on egg length (as defined above under Zonal

Microstructural Analysis methods). Those zones were then split into geometric shapes that best fit the dimensions of that zone in order to create the most accurate geometric model of the egg possible. Hemispheres, spherical caps, conical frustrums, and cylinders were used to accomplish this. Surface area and volume were calculated for each shape and summed where appropriate to determine zonal values. These calculations were compared to surface area and volume calculations made from equations used in previous gas conductance studies to estimate surface area and volume of eggs with an 'avian shape' (Table 3.3).

Table 3.1 Geometric Equations

Hemisphere	Volume = $\frac{4}{3}\pi r^3$ Surface Area = $2\pi r^2$	Cylinder	Volume = $\pi r^2 h$ Surface Area = $2\pi rh$ Where h = height of section and r = radius of cylinder
Spherical Cap	Volume = $\frac{1}{3}\pi h^2(3r-h)$ Surface Area = $2\pi rh$ Where h = height of section and r = radius of projected complete sphere	Ellipsoid	Volume = $\frac{4}{3}\pi abc$ Surface Area = $4\pi\left(\frac{a^p b^p + a^p c^p + b^p c^p}{3}\right)^{\frac{1}{p}}$ Where a = z axis radius, b = x axis radius, c = y axis radius, and $p = 1.6$
Conical Frustrum	Volume = $\frac{1}{3}\pi h(r_1^2 + r_1 r_2 + r^2)$ Surface Area = $\pi(r_1 + r_2)\sqrt{((r_1 - r_2)^2 + h^2)}$ Where h = height of section, r_1 = radius at base of conical frustrum, r_2 = radius at top of conical frustrum		

A simplified equation, derived by Varricchio et al. (2013), was used calculate gas conductance for each zone of both specimens (Table 3.2). Total gas conductance values for each egg were calculated by summing zonal values. Similarly, total egg surface area and volume were also calculated by summing zonal values. Water vapor conductance values were then compared to those established for avian taxa by Ar and Rahn (1984). Those authors compiled a data set of mostly open air nesting avian taxa (with the

inclusion of only a few aquatic or burrow nesting birds). A regression equation based on the curve of this data is used to calculate predicted gas conductance for open-air nesting avian eggs of similar size to the examined dinosaur eggs (Table 3.3).

Table 3.2 Gas Conductance Equations and Associated Variables.

Gas Conductance	$G_{H_2O} = (c/RT) \times D_{H_2O} \times (A_p/L_s)$
Conversion Factor	$c = 1.5552 \times 109$ *sec mg* H_2O *day*$^{-1}$ *mol*$^{-1}$
Universal Gas Constant	$R = 6.236 \times 10^4$ *cm*^{3} *Torr mol*$^{-1}$ °K^{-1}
Temperature	*Assumed to be 25°C, 298.15°K*
Binary Diffusion Coefficient of Water Vapor in Air	D_{H_2O} *at 25°C* $= 0.252$ *cm*^{2} *s*$^{-1}$ (Varricchio et al. 2013)
Simplified Gas Conductance	$G_{H_2O} = 2.109$ *mg* H_2O *day*$^{-1}$ *mol*$^{-1}$ $\times$ (A_p/L_s) (Varricchio et al. 2013)
Fractional Pore Area	${}_fA$ = *observed pore area / observed shell area*
Zonal Area	A_z = *Surface Area for each zone, calculated using geometric shape modeling of egg*
Total Pore Area per Zone	$A_p = {}_fA \times A_z$
Pore Length	L_s = *assumed = to average shell thickness per zone*

Table 3.3 Regression Equations

Egg Volume	$V_{egg} = 0.51\ LB^2$ (Hoyt 1979)
	Where L = length of egg and B = maximum egg breadth
Egg Surface Area	$S_{egg} = 4.951\ V^{0.666}$ (Paganelli et al. 1974)
Predicted Conductance	${}_pG_{H_2O} = 0.3786M^{0.818}$ (Jackson et al. 2008)
	Where $Mass = \rho \times V$, and ρ is assumed to = 1.08 based on avian data (Jackson et al. 2008)

Institutional Abbreviations

ES, Department of Earth Sciences, Montana State University, Bozeman, Montana, U.S.A.; **IMNH**, Idaho Museum of Natural History, Pocatello, Idaho; **MOR**, Museum of the Rockies, Bozeman, Montana, U.S.A.; **ZMNH**, Zhejiang Museum of Natural History, Hangzhou, China.

CHAPTER 4

SEDIMENTOLOGY OF THE WAYAN FORMATION *MACROELONGATOOLITHUS* EGG AND EGGSHELL LOCALITIES

Eggshell material was excavated from Brockman Creek and Jackknife Creek localities from the Wayan Formation of Idaho. Rock samples and stratigraphic sections were used to reconstruct the paleo environment of the egg-bearing strata. Rock samples from within jacketed material were analyzed using XRD and a return visit to the field sites was undertaken in order to measure detailed stratigraphic sections near both excavation sites.

Stratigraphy

Brockman Creek

A detailed stratigraphic section of Brockman Creek reveals a lithology composed overwhelmingly of mottled grey/red/brown mudstones and siltstones (Fig 4.1). Sporadic, narrow intervals of (1-2 cm diameter) calcareous nodules are present and interspersed with rare fine-grained sandstone lenses. This matches the overall lithologic pattern of the Wayan Formation. Eggshell concentrations from this locality are restricted to mottled red-brown mudstones.

Unit 1 consists of 208.65 cm of red-brown blocky siltstone and grey and red-brown mudstone interspersed with thin (less than 1 cm thick) calcite veins. Thin intervals of small (1-2 cm diameter) nodule development occur through out the unit.

Unit 2 is composed of 201.85 cm of mottled grey-green and red-brown mudstone with thin nodule intervals. These nodule occurrences are typically concentrated, however small nodules occur between the nodule dense intervals. No bedding plane or structure is visible within this unit. Dark red spots are visible throughout unit.

Unit 3 consists of 114.11 cm of blocky grey-green mudstone interbedded with thin calcite rich red streaks and calcite veins along the base of the unit.

Unit 4 consists of 145 cm of fine sandstone with calcareous cement, interbedded with calcareous siltstone. Sandstone beds average 22 cm in height and range from well indurated at the base to friable toward the top of the unit.

Unit 5 marks an abrupt transition to 189.05 cm of siltstone with sparse oxidized red patches throughout and is separated from Unit 4 by a calcite vein. Siltstone varies from grey to red-brown, with distinct mottling in one subunit. Small (1-2 cm diameter) nodules form a thin lens within the mottled subunit. Soft, grey, muddy siltstones dominate the base of Unit 5 while blocky red-brown siltstones are present toward the top of the unit. Thin, grey calcite rich streaks are interspersed through the red-brown subunit and effervesce strongly with exposure to dilute hydrochloric acid (HCL). Eggshell concentrations are restricted to mottled grey/red and red-brown siltstones within this unit.

X-ray Diffraction analysis of rock samples from IMNH 2427\49606 (Unit 5) shows a quartz-rich composition with calcite and siderite present in small quantities (Fig. 4.2), whereas XRD analysis of rock samples from IMNH 2427\49605 (Unit 5) indicate mineralogy dominated by quartz and calcite (Fig. 4.3). Peak collapse comparisons from

IMNH 2427\49606 and IMNH 2427\49605 analyzed using the USGS flowchart highlighted three major peak identifications at 7Å, 10Å, and 14Å. These were identified as clay minerals kaolinite, interstratified illite-montmorillanite, and chlorite, respectively.

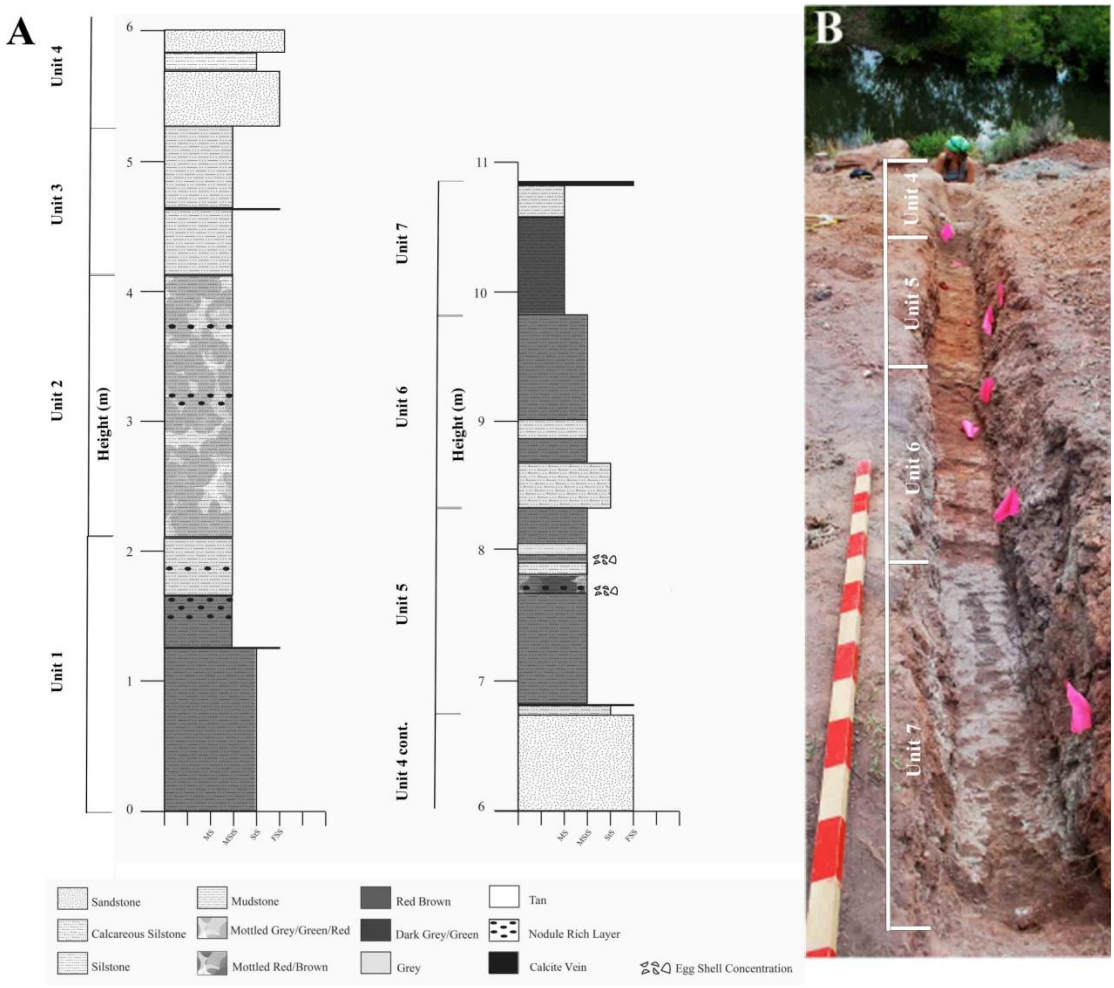

Figure 4.1 Brockman Creek Stratigraphy. A. MS = Mudstone, MStS = Muddy Siltstone, StS = Siltstone, FSS = Fine Sand Stone. B. Trench showing lithology, with 1.5 m Jacob's staff for scale. Photo taken from top of section, Jamie Fearon is shown collecting samples from lower units. Note that angle of photo prevents labeling of units below Unit 4 and distorts size of each unit.

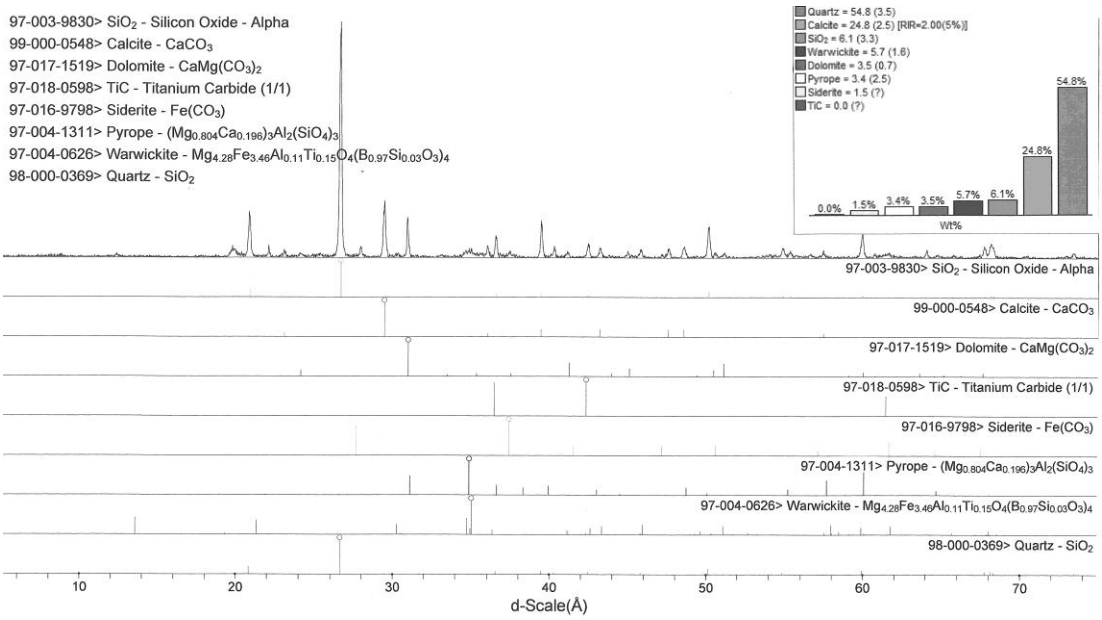

Figure 4.2 XRD Analysis of IMNH 2427\49606. Inset shows mineralogy by weight percent of specimen

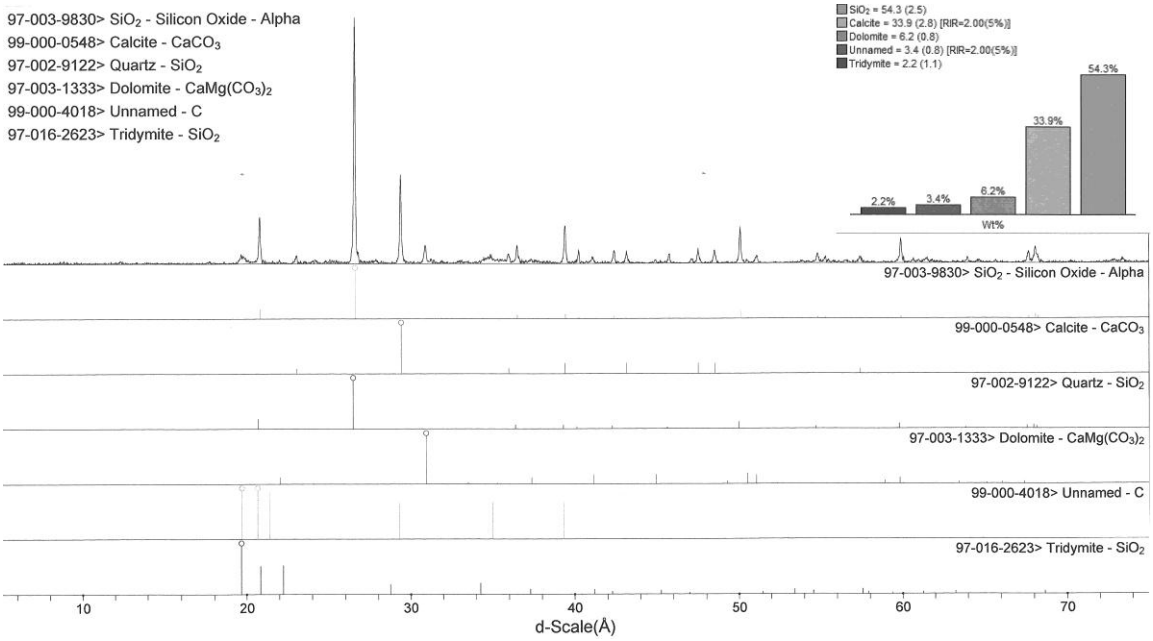

Figure 4.3 XRD Analysis of IMNH 2427\49605. Inset shows mineralogy by weight percent of specimen.

Unit 6 is composed of 147.2 cm of grey and brown siltstones. Grey calcareous blocky siltstone at the base of the unit transitions to grey and brown muddy siltstones.

Unit 7 consists of 99.94 cm of dark grey/green to light grey mudstone, capped by a 3 cm thick calcite vein.

Jackknife Creek

A detailed stratigraphic section of Jackknife Creek reveals a lithology dominated by mudstones ranging in color from light-dark grey, bright red, and brick red (Fig 4.4). This matches mudstone units observed within the Wayan Formation. Egg and eggshell finds at this locality are restricted to light grey mudstones.

Unit 1 is composed of 45 cm of light grey calcareous blocky mudstone, which effervesced strongly with dilute HCL. No bedding planes or structure are visible within unit.

Unit 2 consists of 60 cm of brick red calcareous mudstone with no visible bedding or structure. Samples effervesced strongly with contact to dilute HCL and are slightly more well-indurated than other units in section.

Unit 3 is composed of 65 cm of grey calcareous blocky mudstone with a mottled red and grey subunit 35 cm in height. Samples effervesced strongly with dilute HCL. Small (~1cm diameter) calcareous nodules are present in IMNH 2428\49607, excavated from Unit 3 (Fig. 4.5 – 4.6).

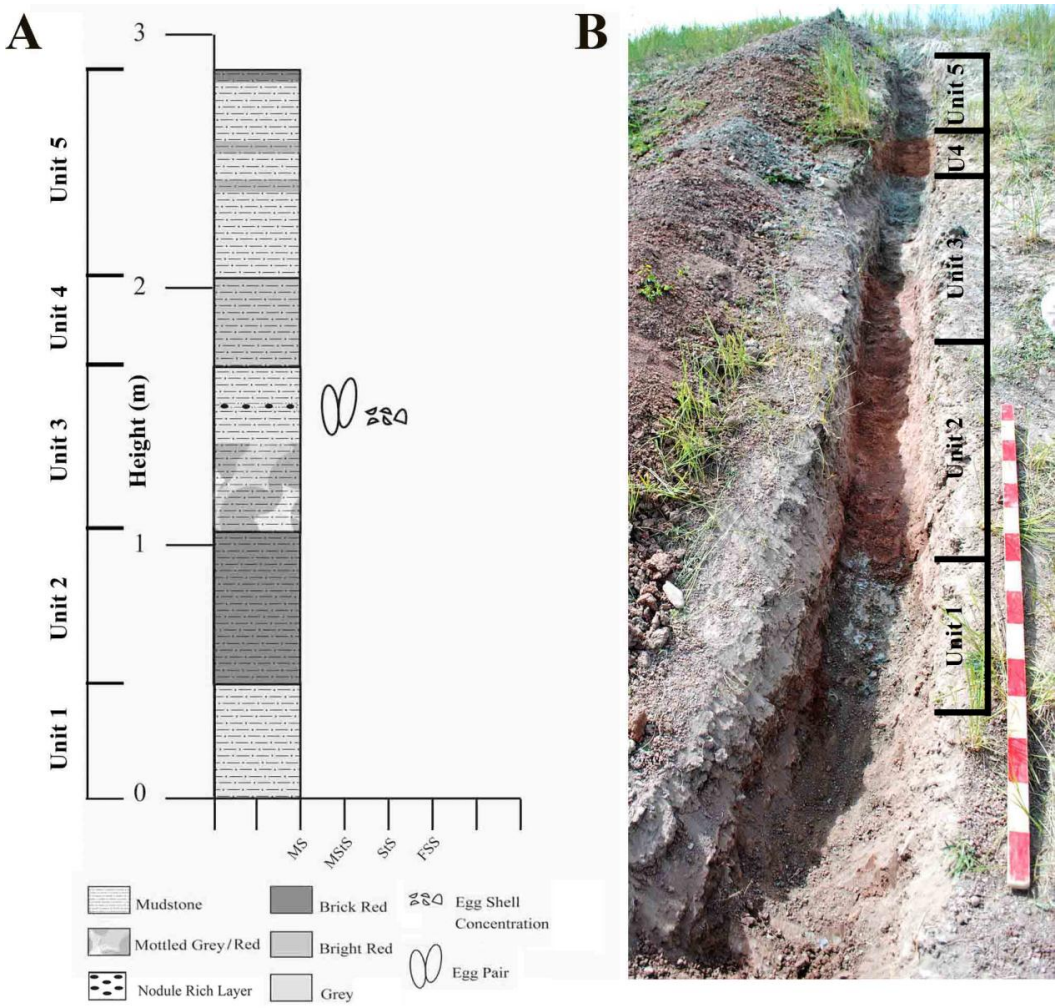

Figure 4.4 Jackknife Creek Stratigraphy. A. Stratigraphic Section. MS = Mudstone, MStS = Muddy Siltstone, StS = Siltstone, FSS = Fine Sandstone. B. Trench showing lithology, with 1.5 m Jacob's staff for scale. Photo taken from bottom of section. Note angle of photo distorts size of units.

Figure 4.5 Concretions from Mudstone in IMNH 2428\49607. Scale bar equals 1 cm. Specimen on the far right was ground for XRD analysis. Scale bar equals 1 cm.

X-ray Diffraction analysis of mudstone samples from the same specimen indicates the presence of the clay minerals metahalloysite and kaolinite (Fig. 4.7), while XRD analysis of rock samples from IMNH 2428\49608 (egg pair) indicates the presence of illite and muscovite (Fig. 4.8). Peak collapse comparisons from IMNH 2428\49607 analyzed using the USGS flowchart highlighted three major peak identifications at 7Å, 10Å, and 29Å. These were identified as clay minerals kaolinite, glauconite, and interstratified chlorite-montmorillanite, respectively. Peak collapse comparisons of rocks within IMNH 2428\49608 using the same method highlighted peaks at 7Å and 14Å – identified as chlorite, and 10Å – identified as interstratified illite-montmorillanite.

Unit 4 is composed of 35 cm of bright red calcareous mudstone, which effervesced strongly with dilute HCL. No bedding structures visible in unit.

Unit 5 consists of 82 cm of grey calcareous blocky mudstone with prominent bright red and brick red streaking throughout unit. Most notable red subunits occur at 5, 28, and 43 cm down from top of unit. Rock samples effervesced strongly with contact to dilute HCL.

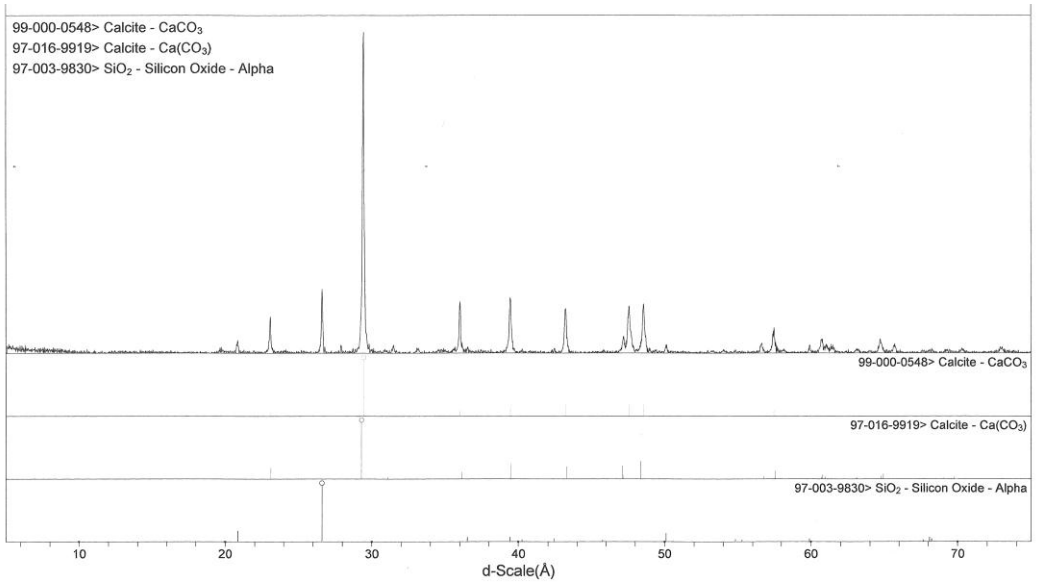

Figure 4.6 XRD Analysis of IMNH 2428\49607 Concretion.

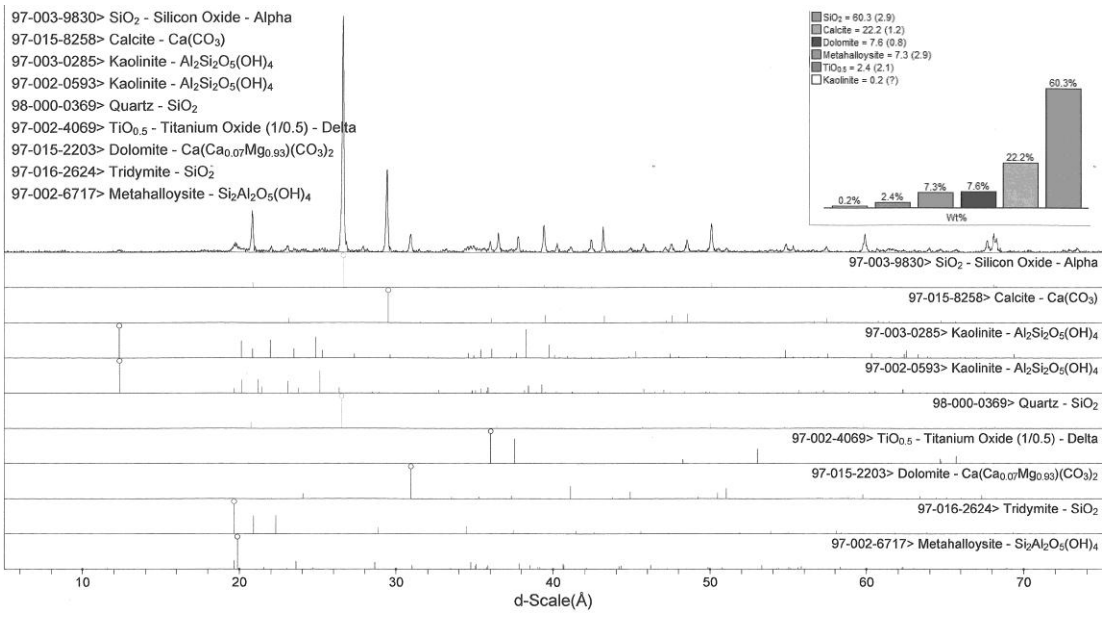

Figure 4.7 XRD Analysis of Mudstones Sample from IMNH 2428\49607. Inset shows mineralogy by weight percent of specimen.

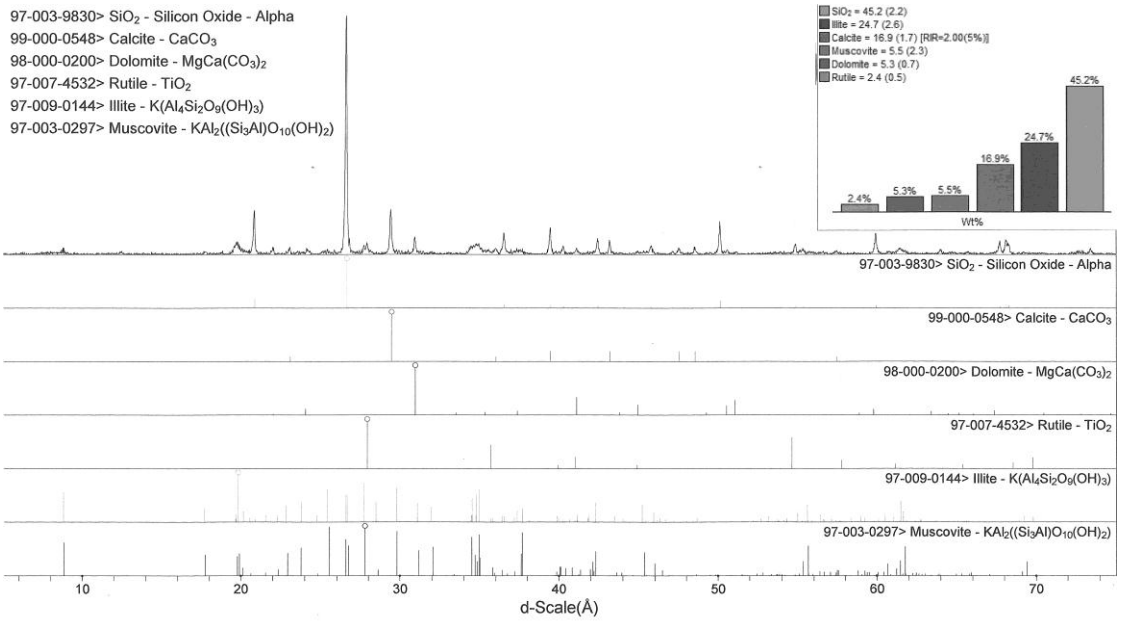

Figure 4.8 XRD Analysis of Mudstones Sample from IMNH 2426\49608. Inset shows mineralogy by weight percent of specimen.

Taphonomy and Paleoenvironment of the Wayan Formation Nesting Site

Previous studies have established a correlation between the ratios of CCU to CCD fragments at a site with the manner in which those fragments were accumulated (Owen and Hayward 1997; Hayward et al. 1997, 2000, 2011; Imai 2012). Fragments from Brockman Creek and Jackknife Creek eggshell accumulations have a total distribution of 59.8% CCU, 40.3% CCD and 56.15% CCU, 43.85% CCD, respectively. Mudstones analysis via stratigraphic sectioning and XRD allows a finer scale understanding of the make up of eggshell bearing localities. The presence or absence of clay minerals, especially those in the smectite group, provides detail used to reconstruct the paleoenvironment these eggs were laid in, while eggshell fragment orientation can be used to reconstruct the taphonomic history of the specimens.

Orientation Data

Brockman Creek

IMNH 2427 Orientation data was recorded for a total of 291 fragments, 86 of these were from fragments removed during the initial excavation of the Brockman Creek site. Of these 174 (59.8%) were recorded as CCU and 117 (40.2%) were recorded as CCD (Table 4.1). The remaining eggshell fragments were oriented at a vertical or near vertical position relative to the surround rock.

Table 4.1 Brockman Creek Eggshell Orientation Data. *Fragments removed and mapped during initial excavation of site.

Specimen Number	CCU	CCD	Total	% CCU	%CCD	Total
IMNH 2427\49604	36	13	49	73.5	26.5	100
IMNH 2427\49605	72	54	126	57.1	42.9	100
IMNH 2427\49606	22	8	30	73.3	26.7	100
Fragments*	44	42	86	51.2	48.8	100
TOTALS	**174**	**117**	**291**	**59.8**	**40.2**	**100**

All Brockman Creek specimens show a higher percent of CCU fragments than CCD, ranging from 51.2 – 73.5% CCU. The percent of CCU fragments in IMNH 2427\49604 – IMNH 2427\49606 is most similar to distributions documented for in situ nesting cites in both extant avian theropods and dinosaurs (Fig 4.9, 4.10) (Hayward et al. 1997, 2000, 2011).

Jackknife Creek

IMNH 2428 Orientation data was recorded for a total of 260 fragments, 56 of these were from fragments removed during the initial excavation of the Jackknife Creek site.

Of the total recorded fragments 146 (56.15%) were recorded as CCU and 114 (43.85%) were recorded as CCD (Table 4.2).

Table 4.2 Jackknife Creek Eggshell Orientation Data. *Fragments removed and mapped during initial excavation of site.

Specimen Number	CCU	CCD	Total	% CCU	% CCD	Total
IMNH 2428\49607	20	3	23	86.96	13.04	100
IMNH 2428\49608	2	4	6	33.33	66.67	100
IMNH 2428\49609	-	-	-	-	-	-
IMNH 2428\49610	48	7	55	12.73	12.73	100
IMNH 2428\49611	8	15	23	65.22	65.22	100
IMNH 2428\49612	46	51	97	52.58	52.58	100
Fragments*	22	34	56	60.71	60.71	100
TOTALS	**146**	**114**	**260**	**56.15**	**43.85**	**100**

Data collected from Jackknife Creek specimens are considerably more variable, with IMNH 2428\49607 and IMNH 2428\49610 showing a clear CCU orientation preference (87% and 87.3% CCU, respectively) while IMNH2428\49611-12 have moderately higher percentages of CCD oriented fragments. Eggshell fragments collected during initial excavation also show a CCD orientation preference.

Sedimentology

Clay mineral content of mudstones from both localities, combined with observations of sedimentary structures within jacketed material and the orientation data outlined above, allow for a detailed analysis of the nesting horizon. Within IMNH 2428\49608-2 slight displacement of the stratigraphic-up oriented half of the blunt pole of the egg relative to the stratigraphic-down portion indicates minor shearing of the specimen in a lateral plane. Small-scale (1 to 2 cm) slickensides are present within the matrix of several jackets, and powdered XRD analysis allowed for the identification of

clay minerals illite, kaolinite, chlorite, glauconite, and montmorillanite within mudstones samples from both localities. Interstratified illite – montmorillanite and chlorite – montmorillanite were also identified.

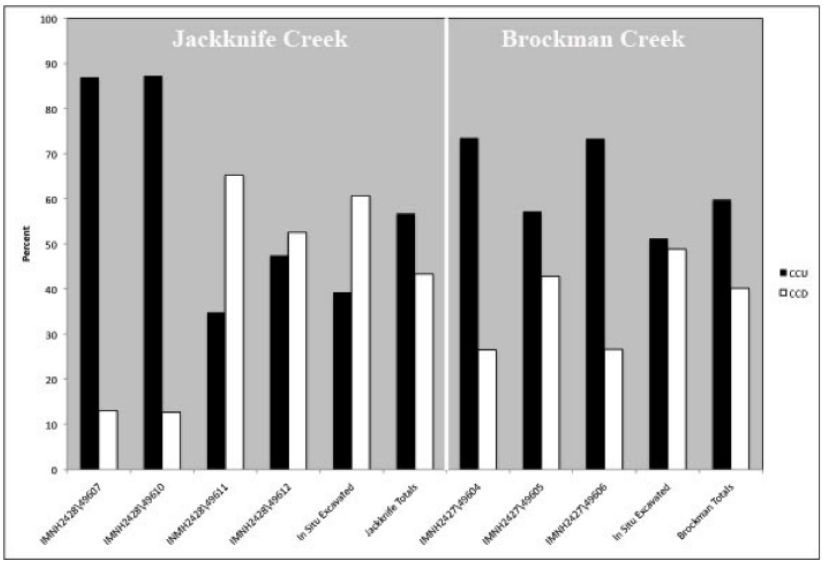

Figure 4.9 Eggshell Orientation Data for Wayan Formation Localities. "In situ excavated" material mapped by Frankie Jackson and David Varricchio during initial excavation.

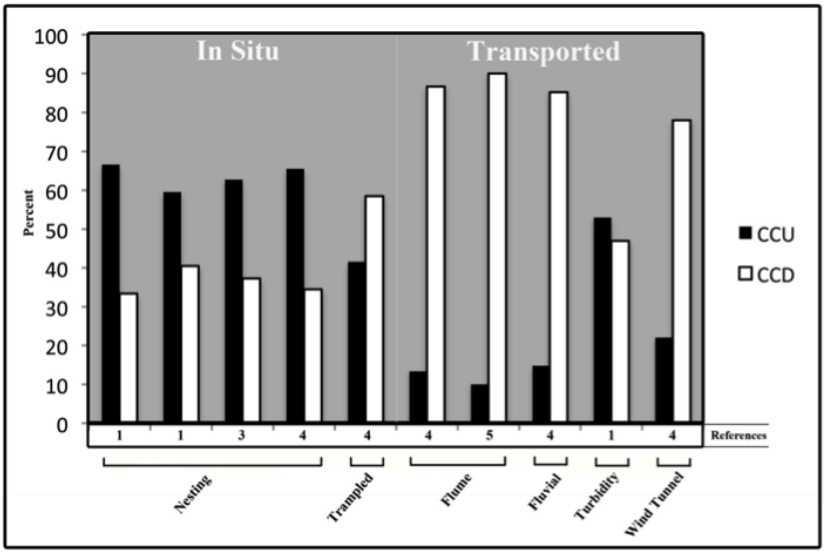

Figure 4.10 Eggshell Orientation for In Situ and Transported Assemblages. 1) Hayward et al. 1997, 2) Owen and Hayward 1997, 3) Hayward et al. 2000, 4) Hayward et al. 2011, 5) Imai 2012.

Intermittent concentrations of small nodule development indicate that the calcite rich sediments represent well drain floodplain soil horizons exposed to periodic wet and dry conditions. Calcareous nodule horizons typically from the precipitation of concentrated calcite within soils due to evaporation of groundwater and suggest a dry climate punctuated by brief wet periods (Miall 1996; Prothero and Schwab 2004).

Conclusions

Shrink-swell clay disruption of the sediments likely played a role in the displacement of the Wayan Formation eggshell material, indicated by the presence of slickensides and smectite-group clay minerals. A prevalence of CCU oriented eggshell fragments suggests that specimens excavated from both Brockman Creek and Jackknife Creek represent autochthonous assemblages, in which specimens were not transported from the original nesting cite (Figs. 4.9 – 4.10). Overall, CCU/CCD values are most similar to in situ nesting sites and trampled in situ assemblages and differ significantly from ratios representative of transported assemblages. The prevalence of fine-grained mudstones representative of a well drained floodplain also support an in situ interpretation of the egg and eggshell material, as the low velocity fluvial system would be insufficient to transport intact eggs and eggshell. Additionally, the paring of the ventral intact egg and egg portion within IMNH 49608 supports an in-situ interpretation of the Jackknife Creek egg site, as transported eggs are unlikely to retain a biologically imposed paired orientation.

As these specimens are in situ, the surrounding mudstones represent the environment in which the parent-animal chose to nest. The nesting environment can be

reconstructed as a well drained soils of a meandering stream flood plain with prolonged subaerial exposure of soil horizons, resulting in the formation of nodule concentrations. Powder sample XRD identification of the clay minerals illite and kaolinite, combined with field identification of intermittent calcareous nodule development corroborate previous assessment (Schmitt and Moran 1982; Krumenacker 2010) of the Wayan Formation mudstones as indicative of a semi-arid floodplain with well-developed soil horizons.

CHAPTER 5

GROSS MORPHOLOGY AND MICROSTRUCTURE OF EXAMINED EGGS AND EGGSHELL

Ootaxonomic assignment of eggshell material is a necessary step before comparisons of variation within taxa can be assessed. Gross morphological and microstructural aspects of whole eggs from the Wayan Formation of Idaho and the Liangtoutang Formation of Zhejiang Province China were used to assign the eggs to an oospecies. Fragmentary material from the Blackleaf Formation of Montana and the Thomas Fork Formation of Wyoming was also examined and assigned. Eggshell microstructure of all specimens was then compared to one another and to known *Macroelongatoolithus* oospecies.

Results

Wayan Formation

Seven accumulations of eggshell material were jacketed and excavated from the Jackknife Quarry. These accumulations were found within a 2 meter by 1 meter area. Three closely spaced eggshell accumulations were excavated from an area roughly 1.5 by 2 meters within the Brockman Creek quarry. After lab prep of the ten total collected jackets, seven contained eggshell fragment concentrations. Of the remaining three jackets, one was found to contain a partial egg pair (IMNH 2428\49608-1 and IMNH 2428\49608-2) (Fig. 5.1); the second revealed fragmentary portions of one or more eggs (IMNH 2427/49605) (Fig. 3.3C); and the third contained only mudstone.

Preparation of IMNH 2428\49608 revealed a partially preserved egg pair, consisting of nearly the entire ventral portion of one egg (IMNH 2428\49608-2) with a second, abutting, fragmentary ventral egg portion (IMNH 2428\49608-1). The dorsal portions of both eggs appear to be extensively weathered and were recognized in the field as a fragmentary eggshell mass. IMNH 2427\49605 contained portions of at least one egg, however these egg portions were incomplete and distributed throughout the jacket in a manner that suggested extreme disruption by either shearing or shrink-swell clay induced sediment disruption. As noted in Chapter 4, eggshell orientation data is consistent with eggshell distribution via disruption of the sediments and specimens prior to lithification. This was likely exaggerated further by later deformation of the Wayan Formation, and finally overprinted slightly by extant mammal-sediment interactions. Field notes from initial excavation mention extensive pocket gopher habitation in both localities and make specific note that this has visibly disrupted the egg and eggshell distribution both vertically and laterally.

Brockman Creek

IMNH 2427\49604-49606 Eggshell fragment accumulations. Rock within these jackets is homogenous reddish brown silty mudstone and within IMNH 2427\49605 contain yellow streaking and patches.

Jackknife Creek

IMNH 2428\49607, IMNH 2428\49609-49612 Eggshell fragment accumulations. Rock within these jackets is homogenous light grey silty mudstone. Sparse oblong and

roughly spherical nodules less than 1 cm in diameter were found in IMNH 2428\49607 (Fig. 4.5). These are composed of calcite, as shown by XRD of crushed samples (Fig. 4.6).

IMNH 2428\49608 Ventral portions of a partially preserved egg pair and associated fragments (Fig. 5.1). Eggs are lithostatically crushed, making the determination of a three dimensional egg shape is difficult. However, lack of significant telescoping at edges of specimen, and a lack of overall distortion to egg shape, allowed for construction of a conservative geometric model of the egg in three dimensions as described in Chapter 3. The most intact egg, IMNH 2428\49608-2, appears to be 39.8 cm long, 10.8 cm wide at the midpoint, and is slightly asymmetrical – pole size varies by 0.50 cm.

Zonal Description of IMNH 2428\49608-2

Ornamentation is highly variable along the long axis of IMNH 2428\49608-2 and among surface collected fragments (IMNH 2428\49813). All values reported in this study include ornamentation as part of eggshell thickness. Varieties include fine and coarse dispersituberculate, ramotuberculate, and lineartuberculate. Poles have smooth portions, but overall show dispersituberculate ornamentation. This grades from both poles into ramotuberculate and lineartuberculate ornamentation toward the midpoint of the egg. White calcite overgrowth is visible over most of the specimen and obscures the ornamentation to a minor degree.

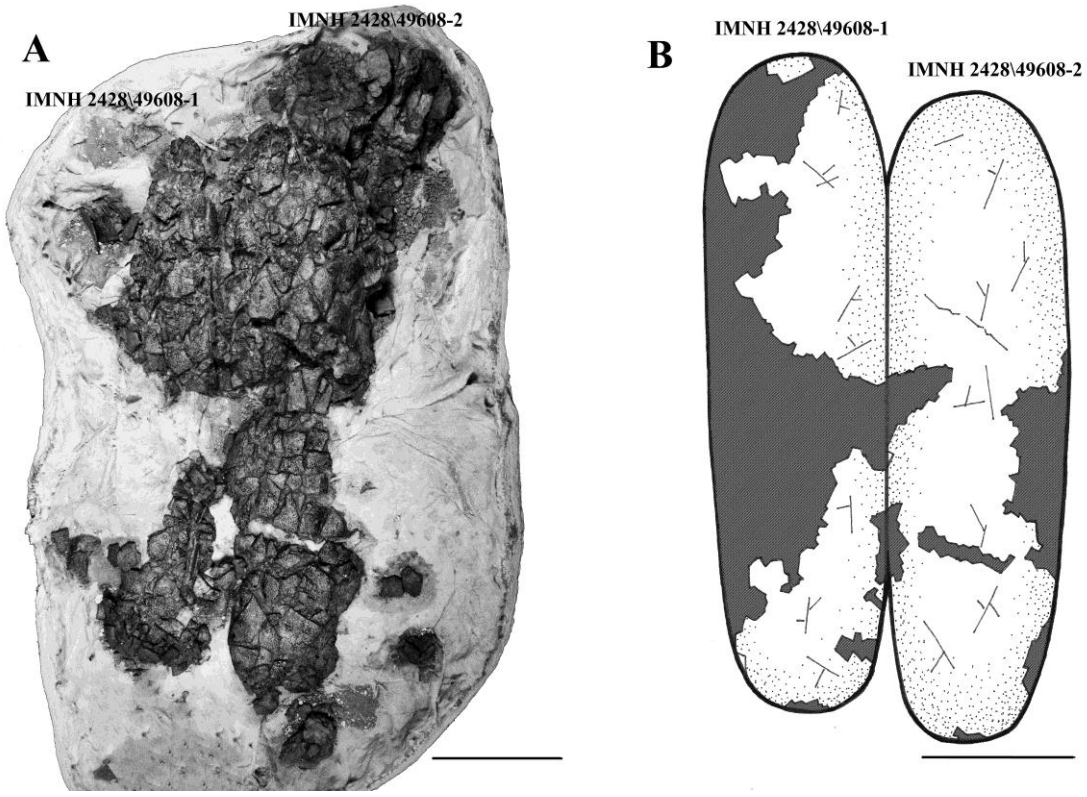

Figure 5.1 IMNH 2428\49608. A. Detail view of specimen. B. Line drawing of specimen, reconstructing probable outline of both eggs. Shading indicates missing egg portions. Scale bar equals 10 cm.

Eggshell consists of two structural layers of calcite separated by a distinct and strongly undulating boundary (Fig 5.2A). The mammillary layer is composed of radiating crystals, which, at random intervals, splay into the overlaying cryptoprismatic layer (Fig 5.2B). Close examination of the cryptoprismatic layer reveals the presence prisms with tabular crystal growth (Fig 5.2C), similar to that previously documented in *Macroelongatoolithus* but generally not mentioned in elongatoolithid egg descriptions. Squamatic structure is prevalent in nearly all thin sections.

Accretion lines are visible throughout the cryptoprismatic layer and bend along ornamentation contours to varying degrees –occasionally nearly flat through ornamentation, but in other instances bending to match contours. While the degree to which accretion lines follow ornamentation contours varies, in no instance observed here do the accretion lines truncate perpendicularly against naturally occurring divots in surface structure (valleys between ornamentation peaks), but rather bend along with the outer eggshell surface. At pores accretion lines typically bend downward abruptly before truncating against the pore wall.

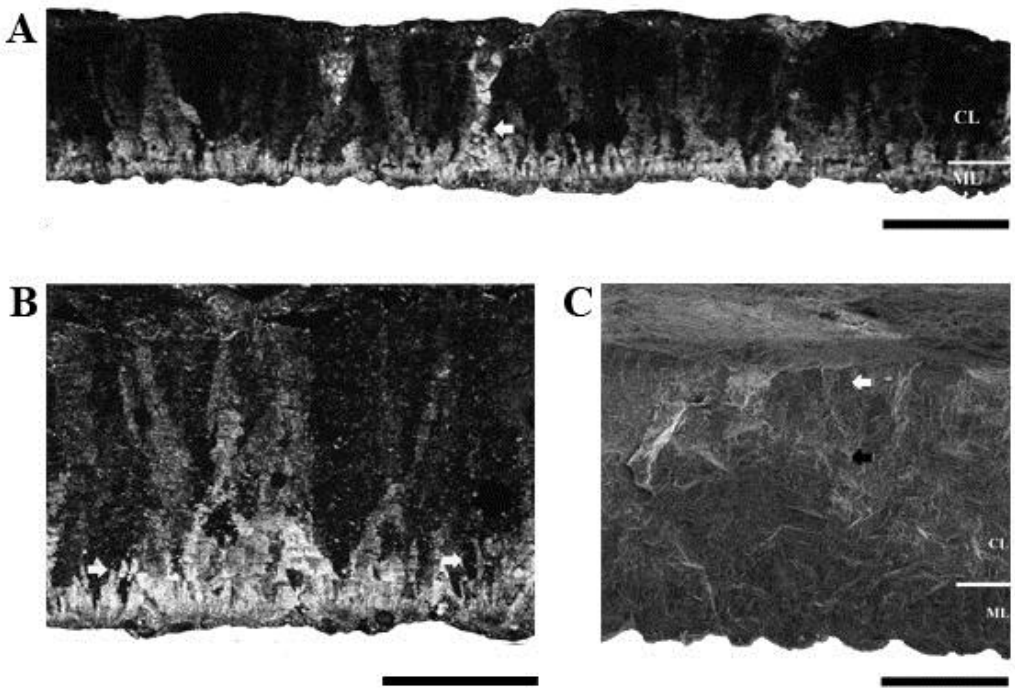

Figure 5.2 Microstructure of IMNH 2428\49608. A. ES462-1, Zone 1. Overview of eggshell microstructure at 20x magnification, XPL. White arrow indicates pore. White bar notes rough boundary between ML and CL, note undulating nature of this boundary across the specimen. Scale bar equals 1 mm. B. ES462-1, Zone 1. 100x magnification, XPL. White arrows indicate crystal splaying across the ML-CL boundary. Scale bar equals 0.5 mm. C. ES390-2, Zone 1. SEM. White arrow indicates visible boundary of prisms. Black arrow indicates tabular structure of prisms within the CL. White bar indicates ML-CL boundary. Scale bar equals 0.5 mm.

Pores are typically located at low points in ornamentation, between nodes. Eggshell thickness varies widely along the egg, average eggshell thickness across the entire egg is 1.44 mm (SD = 0.16 mm), with an absolute range of 1.01 – 1.82 mm (including ornamentation), and is generally thickest at the midpoint, in Zones 3 and 4 (Table 5.1 – 5.2, Fig. 5.3).

In Zone 1 the CL-ML boundary, while visible, is difficult to measure due to eggshell alteration and erosion of mammillary cone bases. In some samples this prevented an accurate measurement of ML thickness, thus precluding an assessment of CL:ML ratio. In such samples this data was not recorded in order to avoid underestimating the ML thickness. The undulating nature of the ML-CL contact creates highly variable ML and CL thickness measurements, which can result in a wide range for CL:ML ratios across an eggshell sample. Average CL:ML ratio is 5.16:1 (SD = 1.67), and the ranges from 2.92:1 – 7.68:1 across the specimen (Tables 5.1 – 5.2).

Table 5.1 Total Range of Microstructural Variation in IMNH 2428\49608-2. *Including ornamentation.

IMNH 2428\49608-2	Shell Thickness mm*	CL:ML	Mammillary Cone Width mm	Nucleation Spacing mm
Zone 1	1.01-1.411	-	0.109-0.206	0.074-0.165
Zone 2	1.317-1.565	2.920-6.347	0.097-0.264	0.091-0.239
Zone 3	1.386-1.823	3.239-7.681	0.103-0.177	0.08-0.185
Zone 4	1.388-1.658	3.297-7.681	0.099-0.247	0.084-0.252
Zone 5	1.332-1.766	3.774-7.657	-	-
Whole Egg	**1.01-1.82**	**2.920-7.681**	**0.099-0.247**	**0.074-0.252**

Table 5.2 Microstructural Variation in IMNH 2428\49608-2, Zonal Averages. Average zonal measurements and standard deviation are shown. *Including ornamentation.

IMNH 2428\49608-2	Shell Thickness mm*	CL:ML	Mammillary Cone Width mm	Nucleation Spacing mm
Zone 1	1.178 +- 0.078	-	0.16	0.122
Zone 2	1.452 +- 0.050	4.62	0.175	0.164
Zone 3	1.594 +- 0.088	4.439	0.14	0.133
Zone 4	1.488 +- 0.064	4.781	0.161	0.133
Zone 5	1.515 +- 0.141	5.602	-	-
Whole Egg	**1.442 +- 0.163**	**5.158 +- 1.666**	**0.161 +- 0.044**	**0.135 +- 0.018**

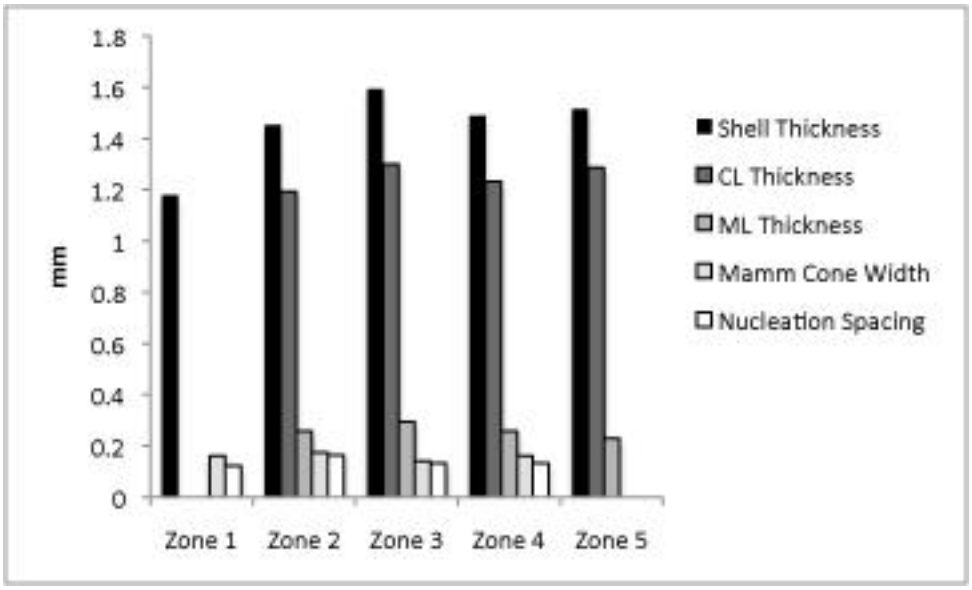

Figure 5.3 Microstructural Variation Across Zones of IMNH 2428\49608-2. ML and CL thickness values were not recorded for Zone 1 due to alteration of the eggshell samples from this zone.

Blackleaf Formation

MOR 1638/ES385 has lineartuberculate ornamentation. As only one eggshell fragment was examined, variable ornamentation was not observed. Eggshell consists of two structural layers of calcite separated by a distinct, undulating boundary (Fig 5.4A). The mammillary layer is composed of radiating crystals and crystal splaying across the ML/CL boundary is present (Fig 5.4B). Squamatic structure is prevalent. Accretion lines are visible throughout the cryptoprismatic layer and conform to topology of ornamentation toward the outer surface of the eggshell.

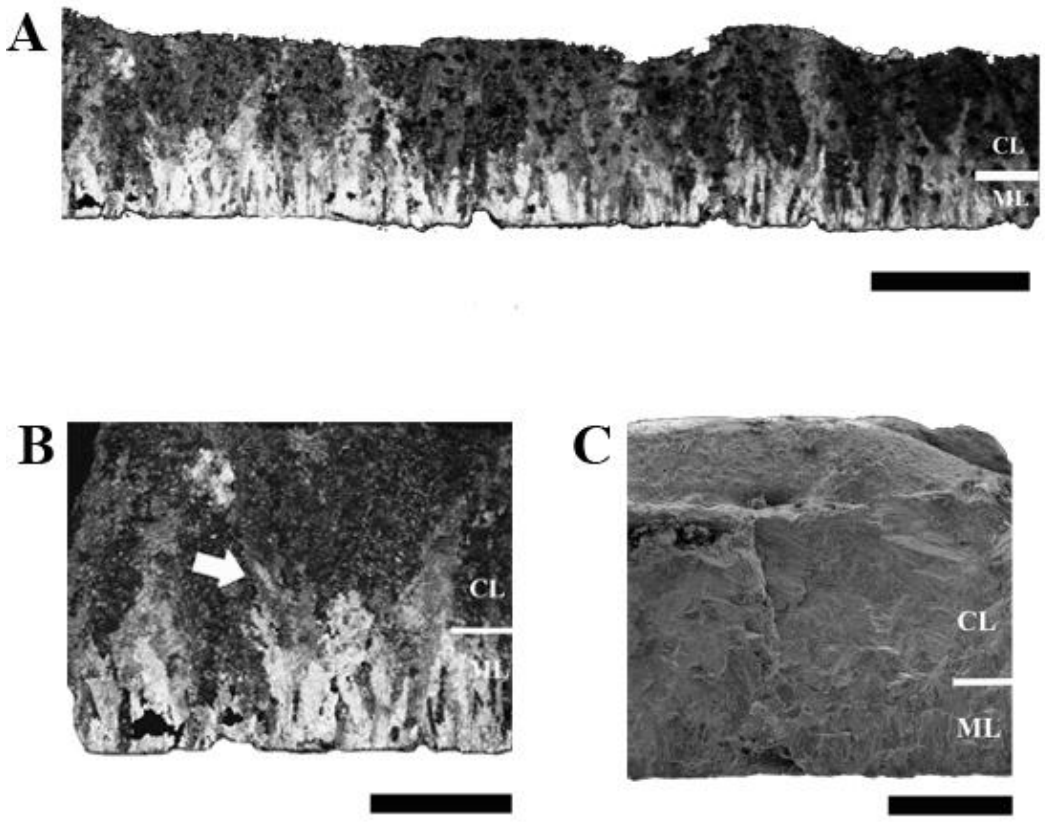

Figure 5.4 Microstructure MOR1638/ES385, Blackleaf Eggshell. A. ES385-1. Overview of eggshell microstructure at 20x magnification, XPL. White bar notes rough boundary between ML and CL, note undulating nature of this boundary across the specimen. Scale bar to lower right equals 1 mm. B. ES385-1. 100x magnification, XPL. White arrow indicates crystal splaying across the ML-CL boundary. Scale bar to lower right equals 0.5 mm. C. ES385-2. SEM. White bar indicates ML-CL boundary. Scale bar equals 0.5 mm.

Eggshell thickness varies from 1.08 – 1.28 mm (average = 1.17 mm, SD = 0.06 mm) (Table 5.3, 5.4). Where clear, the CL-ML boundary is undulating and the CL:ML ratio ranges from 2.64:1 – 4.23:1 (average = 3.29:1, SD = 0.799). Most mammillary cones were altered or eroded, preventing accurate measurements. Where unaltered cones are visible mammillary cone width is 0.098 mm. Nucleation spacing ranges from 0.063 – 0.072 mm (average = 0.068 mm, SD = 0.0064 mm).

Thomas Fork Formation

Ornamentation of the Thomas Fork sample, ES 301, ES304-306, could not be assessed, as only thin sections were examined. Eggshell consists of two structural layers of calcite separated by a distinct, undulating boundary (Fig 5.5A). The mammillary layer is composed of radiating crystals and crystal splaying across the ML/CL boundary is present (Fig 5.5B). Squamatic structure is prevalent. Accretion lines are visible throughout the cryptoprismatic layer and conform to topology of ornamentation toward the outer surface of the eggshell. Eggshell thickness varies from 1.28 – 2.02 mm (average = 1.52 mm, SD = 0.174 mm) (Tables 5.1 – 5.2). Where clear, the CL-ML boundary is undulating. CL:ML ratio range is 2.05:1 – 7.21:1 (average = 3.52:1, SD = 2.66), mammillary cone width varies from 0.063 – 0.17 mm, and nucleation spacing ranges from 0.056 – 0.179 mm (average = 0.0.107 mm, SD = 0.036 mm).

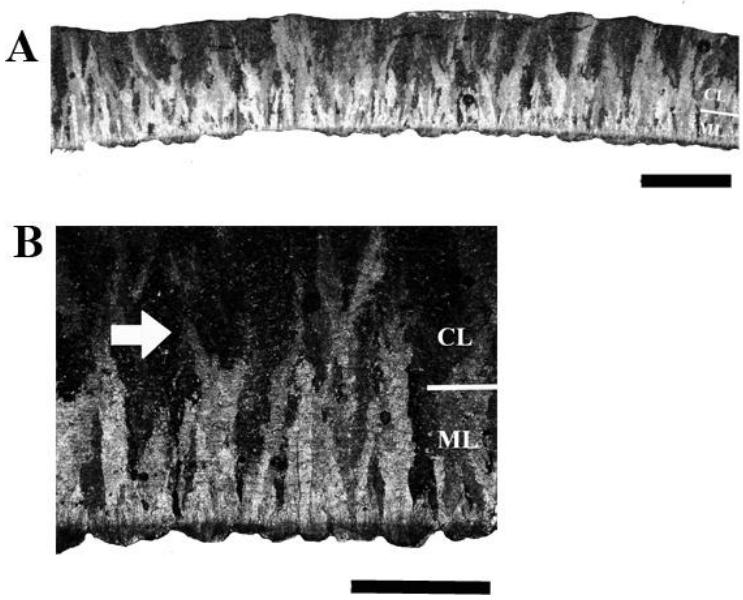

Figure 5.5 Microstructure ES305, Thomas Fork Eggshell. A. ES305. Overview of eggshell microstructure at 20x magnification, XPL. White bar notes rough boundary between ML and CL, note undulating nature of this boundary across the specimen. Scale bar equals 1 mm. B. ES305. 100x magnification, XPL. White arrow indicates crystal splaying across the ML-CL boundary. Scale bar equals 0.5 mm.

Table 5.3 Total Range of Microstructural Variation, Blackleaf and Thomas Fork Specimens. Including Ornamentation.

Specimen	Formation	Shell Thickness mm	CL:ML	Mammillary Cone Width mm	Nucleation Spacing mm
ES385-1	Blackleaf	1.075-1.282	2.64:1-4.23:1	0.098	0.063-0.072
ES301, ES304-306	Thomas Fork	1.28-2.02	2.05:1-7.21:1	0.063-0.170	0.056-0.179

Table 5.4 Average Microstructural Variation, Blackleaf and Thomas Fork Specimens. Values shown are averages +- standard deviation. Including Ornamentation.

Specimen	Formation	Shell Thickness mm	CL:ML	Mammillary Cone Width mm	Nucleation Spacing mm
ES385-1	Blackleaf	1.174 +- 0.063	3.29:1 +- 0.799	0.098	0.068 +- 0.0064
ES301, ES304-306	Thomas Fork	1.522 +- 0.174	3.516 +- 2.659	0.116 +- 0.029	0.107 +- 0.036

Liangtoutang Formation

Gross Morphology Ornamentation is variable along the long axis of ZMNH M8705-1. Varieties include dispersituberculate and ramotuberculate. A more extensive variety of eggshell may be present along ZMNH M8705-1, however limited sampling and calcite overgrowth of specimens precludes further examination. Poles have smooth portions, but overall show dispersituberculate ornamentation.

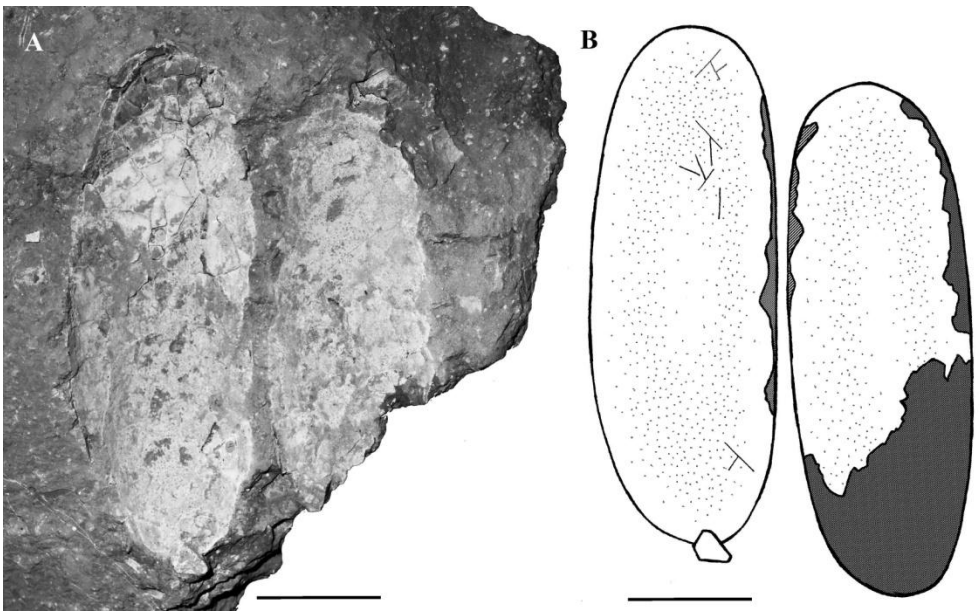

Figure 5.6 ZMNH M8705. A. Detail view of specimen. B. Line drawing of specimen, reconstructing probable outline of both eggs. Shading indicates missing egg portions. Scale bar equals 10 cm.

Zonal Microstructure Eggshell consists of two structural layers of calcite separated by a distinct and undulating boundary (Fig 5.8A). This boundary is obscured in several specimens due to eggshell alteration, making some measurements (such as mammillary cone width and nucleation site spacing) difficult or impossible to assess. The mammillary layer is composed of radiating crystals, which, at random intervals, splay into the overlaying cryptoprismatic layer (Fig 5.8 B). Squamatic structure is prevalent in nearly all thin sections. Accretion lines are visible throughout the cryptoprismatic layer and bend along ornamentation contours to varying degrees – occasionally nearly flat through ornamentation, but in other instances bending to match contours.

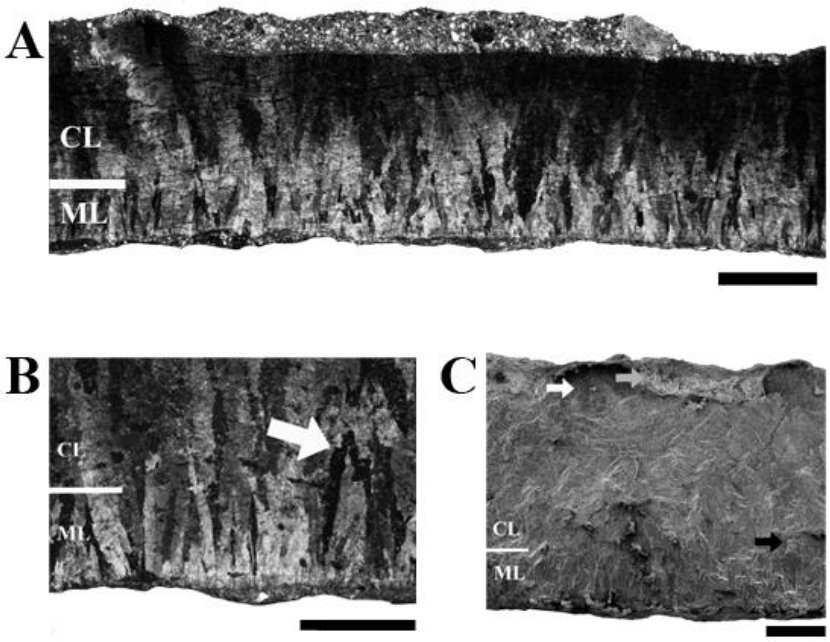

Figure 5.7 Microstructure of ZMNH M8705-1. A. ES457-1, Zone 2. Overview of eggshell microstructure at 20x magnification, XPL. White bar notes rough boundary between ML and CL, note undulating nature of this boundary across the specimen. Scale bar to lower right equals 1 mm. B. ES459-1, Zone 4. 100x magnification, XPL. White arrow indicates crystal splaying across the ML-CL boundary. Scale bar to lower right equals 0.5 mm. C. ES456-3, Zone 1. SEM. White arrow indicates visible boundary of prisms. Black arrow indicates crystal splaying across the CL-ML boundary. Grey arrow indicates calcite overgrowth along upper eggshell surface. White bar indicates ML-CL boundary. Scale bar equals 0.5 mm.

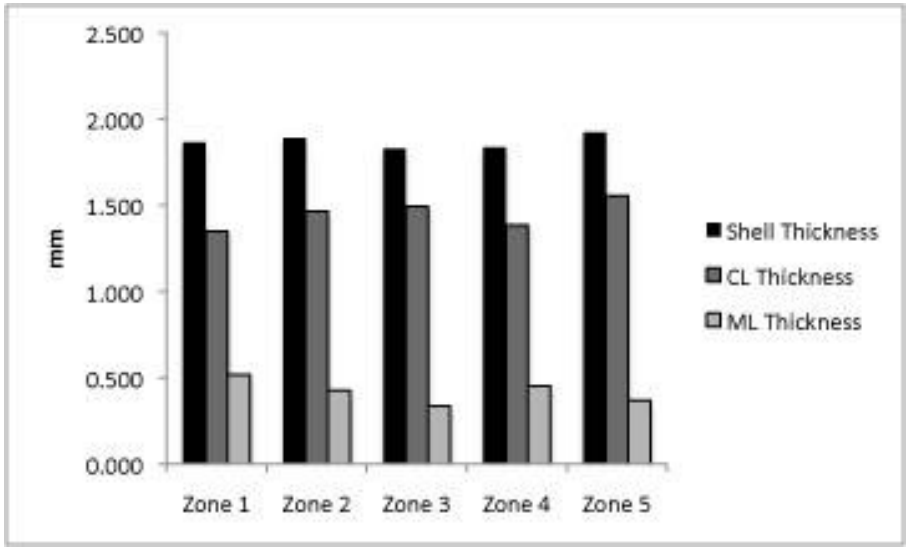

Figure 5.8 Microstructural Variation Across Zones of ZMNH M8705-1.

ZMNH M8705-1 pair is 41.65 cm long, 14.28 cm wide at the midpoint, and slightly asymmetrical – pole width varies by 0.3 cm. Eggshell thickness varies along the egg, with an absolute range of 1.60 – 2.17 mm, and is thickest at poles (Zones 1 and 5) (Tables 5.5 – 5.6, Fig. 5.8). This is potentially a taphonomic feature, as Zones 2-5 show altered eggshell structure and heavily eroded mammillary cone bases. Average eggshell thickness across the entire egg is 1.87 mm (SD = 0.11 mm). The undulating nature of the ML-CL contact creates highly variable ML and CL thickness measurements, which can result in a wide range for CL:ML ratios across an eggshell sample. This effect is seen in other reports of *Macroelongatoolithus* material- the oogenus has a markedly variable CL:ML range when compared to other oogenera. The CL:ML ratio across ZMNH M8705-1 ranges from 2.12:1 – 6.15:1, and is 3.76:1 on average (SD = 1.20).

Table 5.5 Total Range of Microstructural Variation in ZMNH M8705-1. *Including ornamentation.

M8705	Shell Thickness mm*	CL:ML	Mammillary Cone Width mm	Nucleation Spacing mm
Zone 1	1.765-2.141	2.118:1-3.737:1	-	-
Zone 2	1.763-2.166	2.470:1-5.242:1	-	-
Zone 3	1.601-2.000	3.126:1-5.536:1	-	-
Zone 4	1.753-1.893	2.637:1-3.584:1	-	-
Zone 5	1.884-1.967	3.034:1-6.153:1	-	-
Whole Egg	**1.601-2.166**	**2.118:1-6.153:1**	-	-

Table 5.6 Microstructural Variation in ZMNH M8705-1, Zonal Averages. Average zonal measurements and standard deviation are shown. *Including ornamentation.

M8705	Shell Thickness mm*	CL:ML	Mammillary Cone Width mm	Nucleation Spacing mm
Zone 1	1.866 +- 0.091	2.604:1	-	-
Zone 2	1.892 +- 0.134	3.443:1	-	-
Zone 3	1.828 +- 0.141	34.447:1	-	-
Zone 4	1.837 +- 0.053	3.059:1	-	-
Zone 5	1.923 +- 0.024	4.220:1	-	-
Whole Egg	**1.869 +- 0.111**	**3.764:1 +- 1.201**	**-**	**-**

Table 5.7 Comparison of Examined Eggs and Eggshell.

Specimen Number	Egg LxW cm	Elong. Index	Ornament	Shell Thickness mm	Crystal Splaying	CL:ML Ratio	CL/ML Boundary	Nuc. Spacing mm	Mamm Cone Width mm	Pore Opening Shape	Pore Diameter mm
IMNH 2428\49608-2 Wayan Fm	39.8 x 10.2	3.9:1	Disp-Linear	1.01-1.82	Present	2.92:1-7.68:1	Unclear-abrupt	0.074-0.252	0.097-0.264	Round-oval	0.026-0.267
ES305 Blackleaf Fm	-	-	Linear	1.075-1.28	Present	2.64:1-4.23:1	Mod. Clear, wavy	0.063-0.072	0.098	Round-oval	-
ES301, ES304-306 Thomas Fork Fm	-	-	-	1.28-2.02	Present	2.05:1-7.21:1	Mod Clear, wavy	0.56-0.179	0.063-0.170	Round-oval	-
ZMNH M8705-1 Liangtoutang Fm	41.65 x 14.28	2.92:1	Disp-Linear	1.601-2.17	Present	2.12:1-6.15:1	Unclear-abrupt	-	-	Round-oval	0.041-0.744

Ootaxonomic Assignment of Examined Material

All examined eggshell consists of two structural layers of calcite separated by a distinct and strongly undulating boundary. The mammillary layer is composed of radiating crystals that splay into the overlaying cryptoprismatic layer at random intervals. Squamatic structure is prevalent in nearly all thin sections. Accretion lines are visible throughout the cryptoprismatic layer and bend along ornamentation contours to varying degrees –occasionally nearly flat through the CL, but typically conforming to surface topology toward the outer eggshell surface. Pore system varies from angusticanaliculate to obliquicanaliculate. These features allow the diagnosis of all material described here to the oofamily Elongatoolithidae.

Extremely large egg size, 38.9-41 cm long by 10.8 – 14 cm wide, eggshell thickness of 1.01 – 2.17 mm, CL:ML ratio range of 2.06:1 – 7.68 allow the further assignment of this material to the oogenus *Macroelongatoolithus* and oospecies *Macroelongatoolithus carlylei*. *M. xixiaensis* was established as a junior synonym of *M. carlylei* by Zelenitsky et al. 2000, while Wang, Zhao et al. 2010 refer *M. zhangi* as a

junior synonym of *M. xixiaensis*, and Huh et al. 2014 synonymize *M. goseongensis* with *M. xixiaensis*. As *M. carlylei* has priority (Zelenitsky et al. 2000), *M. zhangi*, *M. xixiaensis*, and *M. goseongensis* are here formally recognized as junior synonyms of *M. carlylei*. *Megafusoolithus qiaoxiaensis* is also established as a junior synonym of *M. carlylei*, as Wang, Zhao et al. 2010 fail to establish unique features separating this oospecies from *M. xixiaensis* (See Tables 5.8a, 5.8b, 5.9 and discussion below).

Table 5.8a Gross Morphology and Microstructure of all *Macroelongatoolithus* Specimen. [+]Re-assessed values for *M. zhangi* from Wang, Zhao et al. 2010.

Oospecies	Province/State, Country	Formation, Age	Egg L x W cm	Elong. Index	Asymmetrical	Ornament.
Macroelongatoolithus carlylei	Idaho, US	Wayan Fm Albian-Cenomanian	39.8 x 10.2	3.9:1	Slight	Disp-Linear
	Montana, US	Blackleaf Fm Early Late Cretaceous	-	-	-	-
	Wyoming, US	Thomas Fork Fm Early Late Cretaceous	-	-	-	Disp-Linear
	Zhejiang, China	Liangtoutang Fm Albian-Cenomanian	41.65 x 14.28	2.92:1	Slight	Disp-Linear
	Utah, US	Cedar Mt and Dakota Fm Lower Cretaceous	-	-	-	Disp-Linear
Longiteresoolithus xixiaensis	Henan, China	Gaogou Fm Cenomanian-Turonian	34.5-61 x 14-27	2.6:1	-	-
	Henan, China	Zoumagang or Gaogou Fm Cenomanian-Maastrichtian	34-61 x 14-27	2.5:1-2.9:1	-	Nodes-weak linear
Macroelongatoolithus xixiaensis	Henan, China	Zoumagang Fm Maastrichtian	34-61 x 14-27	2.3:1-3.63:1	Yes	Disp-Linear
	Henan, China	Zoumagang Fm Maastrichtian	38-60 x 16.5	2.86:1-2.93:1	-	Disp-Linear, Smooth Poles
	Henan, China	-	40-41 x 14	2:1-3.2:1	-	-
	Zhejiang, China	Liangtoutang Fm Albian-Cenomanian	39.9-51.6 x 13-17.9	3:1	Yes	Disp-Linear, Smooth Pole
	Zhejiang China	Chichengshan Cenomanian	43-14.5	2.56:1-2.81:1	-	Disp-Ramo
	Gyeongsang, South Korea	Goseong Fm Campanian	41-45 x 15-17	2.7:1	Slight	Ramo-Linear
Macroelongatoolithus zhangi	Zhejiang, China	Liangtoutang Fm Albian-Cenomanian	45[+] x 15	3:1	-	Linear
Macroelongatoolithus goseongensis	Gyeongsang, South Korea	Goseong Fm Upper Cretaceous	39 x 11.5	3.39:1	-	Linear
Megafusoolithus qiaoxiaensis	Zhejiang, China	Chichengshan Fm Cenomanian	~40 x 13	~3.07:1	-	Linear, Smooth Poles

Table 5.8b Gross Morphology and Microstructure of all *Macroelongatoolithus* Specimens Continued. 1) Zelenitsky et al. 2000, 2) Wang and Zhou 1995, 3) Liang et al. 2009, 4) Fang et al. 1998, 5) Grellet-Tinner 2005, 6) Li et al. 1995, 7) Jin et al. 2007, 8) Wang, Zhao et al. 2010, 9) Huh et al. 2014, 10) Fang et al. 2000, 11) Kim et al. 2011. * Excluding ornamentation.

Shell Thickness mm	Crystal Splaying	CL:ML Ratio	CL/ML Boundary	Nuc.Site Spacing mm	Mamm Cone Width mm	Pore Opening Shape	Pore Diameter mm	Reference
1.01-1.82	Present	2.92:1-7.68:1	Unclear-abrupt, wavy	0.074-0.252	0.097-0.264	Round-oval	0.026-0.267	This study
1.075-1.28	-	2.64:1-4.23:1	Mod. Clear, wavy	0.063-0.072	0.098	Round-oval	-	This study
1.28-2.02	-	2.05:1-7.21:1	Mod. Clear, wavy	0.056-0.179	0.063-0.170	Round-oval	-	This study
1.601-2.17	Present	2.12:1-6.15:1	Unclear-abrupt, wavy	-	-	Round-oval	0.041-0.744	This study
1.5-3	-	2:1-4:1	Unclear-abrupt	-	-	-	-	1
1.2-3	-	-	-	-	-	-	-	2
1.2-3.1	-	-	-	-	-	-	-	3
1.5-1.6	-	3:1	Abrupt, wavy	-	-	-	-	4
1.2-1.58*	-	2.72:1	Mod. Clear	-	-	-	-	5
2-3.2	-	7:1-8:1	-	-	-	-	-	6
1.65-2.45	Present	1.62:1-2.3:1	Abrupt, wavy	-	-	Round-subround	-	7
1.38-2.05	-	2:1-5:1	Abrupt, wavy	-	0.1-0.3	Round-oval	0.08-0.4	8
2.99-4.75	Present	2.07:1-3.98:1	Abrupt, wavy	-	-	-	-	9
2	-	1.5:1	Abrupt	-	-	-	-	10
2.3-3.1	-	2.5:1-4.8:1	Abrupt	-	-	-	-	11
1.45-1.60*	-	3:1	Unclear	-	0.6	Round-oval	0.1-0.3	8

Table 5.9 Summary of Gross Morphology and Microstructure of Examined Eggs and Eggshell with Established Oospecies. [+]Length as determined by Wang, Zhao et al. 2010 via re-evaluation of *M. zhangi* specimen photos.
[1]

Oospecies	Spec. Number / Formation	Egg LxW cm	Elong Index	Ornament	Shell Thickness mm	CL:ML Ratio	CL/ML Boundary	Crystal Splaying	Refs
Macroelongatoolithus carlylei	IMNH 2428\49608-2 Wayan Fm, Idaho	39.8 x 10.8	3.7:1	Dispers-Linear	1.01-1.82	2.9:1-7.7:1	Unclear-abrupt	Present	This Study
	ES305 Blackleaf Fm, Montana	-	-	Linear	1.08-1.28	2.6:1-4.2:1	Mod. Clear	Present	This Study
	ES301, ES304-306 Thomas Fork Fm, Wyoming	-	-	-	1.28-2.02	2.1:1-7.2:1	Mod. Clear	Present	This Study
	ZMNH M8705-1 Liangtoutang Fm, Zhejiang China	41.65 x 14.28	2.92:1	Disper-Linear	1.60-2.17	2.1:1-6.2:1	Unclear, abrupt	Present	This Study
	Cedar Mt/Dakota Fm, Utah	-	-	Disper-Linear	1.5-3	2:1-4:1	Unclear, abrupt	-	1, 6, 13
Macroelongatoolithus xixiaensis	Various	34-61 x 13-14.28	2:1-3.63:1	Dispers – Ramo-Linear	1.2-4.75	1.6:1-8:1	Unclear-abrupt	-	2, 4-5, 7, 9-12
Macroelongatoolithus zhangi	Liangtoutang Fm, Zhejiang China	45 x 11.5[+]	-	Linear	2	3:1	Abrupt	-	3, 12
Megafusoolithus qiaoxiaensis	Chichengshan Fm, Zhejiang China	40 x 13	3.07:1	Linear, Smooth Poles	1.45-1.6	3:1	Unclear	-	12
Macroelongatoolithus goseongensis	Gyeongsang, South Korea	39 x 11.5	3.39:1	Linear	2.3-3.1	2.5:1-4.8:1	Abrupt	-	8

Systematic Paleontology

Oofamily ELONGATOOLITHIDAE Zhao, 1975

Macroelongatoolithidae Wang and Zhou 1995 (see also Wang, Zhao et al. 2010)

Included oogenera

Elongatoolithus (=*Oolithes elongatus*, Young 1954), Zhao and Jiang 1974; *Macroolithus* (=*Oolithes rugustus*, Young 1965) Zhao, 1975; *Nanhsiungoolithus* (=*Oolithes nanhsiungensis* Young, 1965) Zhao, 1975; *Ellipsoolithus* Mohabey, 1998; *Trachoolithus* Mikhailov, 1994a; *Macroelongatoolithus* Li et al. 1995 (see Wang and Zhou 1995 for oofamily Macroelongatoolithidae and Wang, Zhao et al. 2010 for assignment of oogenus *Macroelongatoolithus* to oofamily Macroelongatoolithidae, and

introduction of the oogenus *Megafusoolithus*); *Heishanoolithus* Zhao and Zhao, 1999; *Paraelongatoolithus* Wang, Wang et al. 2010; *Undulatoolithus* Wang et al. 2013.

Revised Diagnosis

Eggs 9 cm to 61 cm long with an elongation index from 2 – 3.9. Eggshell 0.8 – 4.74 mm thick depending on oogenus and oospecies, CL:ML ratio 2:1 to 8:1. Eggshell with two distinct structural layers, a mammillary layer consisting of radiating calcite crystals and a second structural layer lacking well-defined shell units separated by a clear boundary. Angusticanaliculate, oblicucanuliculate, or rimocanuliculate pore system. Dispersituberculate, ramotuberculate, and lineartuberculate ornamentation common.

Oogenus *MACROELONGATOOLITHUS* Li, Yin, and Liu 1995

Macroolithus Zhao, 1975, p. 108, figure caption.

Boletuoolithus Bray, 1998, p. 221-222, fig. 1-3, 4A, 4B.

Longiteresoolithus Wang and Zhou, 1995, p. 262; Zhou et al. 1999, p. 298-299, fig. 1B, 1D; Zhou et al. 2001, p. 98; Liang et al. 2009, fig. 2 H.

Megafusoolithus Wang, Zhao et al. 2010, figs 5A-E.

Type Oospecies- *Macroelongatoolithus carlylei* (Jensen 1970)

Included Oospecies- *Macroelongatoolithus carlylei* Jensen 1970

Distribution

Upper Cretaceous Zoumagang, Majiacun, Gaoguou, Zhaoying, and Sigou Formations, Henan Province, Xixia Basin, China; Albian – Cenomanian Liangtoutang

Formation and Upper Cretaceous Chichengshan Formation, Zhejiang Province, Tiantai Basin, China; Upper Cretaceous Goseong Formation, South Gyeongsang Province, South Korea; Lower Cretaceous Cedar Mountain, Kelvin, and Dakota Formations, UT; Albian – Cenomanian Wayan Formation, Bonneville County, Idaho, U.S.A.; Albian – Cenomanian Blackleaf Formation, Beaverhead County, MT; early Late Cretaceous Thomas Fork Formation, Lincoln County, WY; Cenomanian – Turonian Liangtoutang Formation, Zhejiang Province, Tiantai Basin, China.

Revised Diagnosis

Large, elongate eggs over 34 long and 10 to 16.5 cm wide, elongation index 2.6 to 3.9. Eggshell thickness, including ornamentation, is 1.38 to 4.75 mm. CL:ML ratio 2:1 to 8:1. Abrupt, wavy boundary separates the CL and ML. Ornamentation is variable both in type and relief, and may grade from dispersituberculate at the poles to lineartuberculate along the middle portion of the length of the egg. Clutches consist of paired eggs in a ring-shaped configuration with an external clutch diameter of 2 or more meters.

Oospecies MACROELONGATOOLITHUS CARLYLEI

Macroelongatoolithus xixiaensis Li et al. 1995, pl. 1; Fang et al. 1998, p1. 17, fig. 10; Grellet-Tinner et al. 2006, figs. 6D-6F, figs. 7A-7F; Wang, Zhao et al. 2010, figs. 3A-3D and 4A-4D; Huh et al. 2014, figs. 3, 5A, 6A-D, and 7-8.

Longiteresoolithus xixiaensis Wang and Zhou, 1995, pl. 1; Zhou et al. 1999, fig 1B, 1D.

Macroelongatoolithus xixia Carpenter 1999, fig. AII.22.

Macroelongatoolithus sp. Carpenter 1999, fig. 10.12.

Macroelongatoolithus goseongensis Kim et al. 2011, figs. 2A, 5A-H

Megafusoolithus qiaoxianensis Wang, Zhao et al. 2010, figs. 5A-5E

Type Specimen – BYU-200, eggshell fragment and thin section.

Revised Diagnosis – Same as for oogenus.

Distribution – Same as for oogenus.

Referred Specimens

Eggshell fragments IMNH 49613, eggshell accumulations IMNH 49604-49607 and IMNH 49609-49612, and a partially preserved egg pair IMNH 49608, Albian – Cenomanian Wayan Formation, Bonneville County, ID; Surface collected eggshell fragment MOR 1638, Blackleaf Formation, Beaverhead County, MT; Surface collected eggshell fragments, early Late Cretaceous Thomas Fork Formation, Lincoln County, WY; Egg pair ZMNH M8705, Albian – Cenomanian Liangtoutang Formation, Zhejiang Province, Tiantai Basin, China.

Description

White calcite overgrowth is visible over eggshell within both IMNH 2428\49608 and ZMNH M8706, and obscures the ornamentation to a minor degree. Ornamentation is highly variable along the long axis of IMNH 2428\49608-2, along ZMNH M9705-1, and among surface collected fragments IMNH 2428\49813. Varieties include fine and coarse dispersituberculate, ramotuberculate, and lineartuberculate. Poles have smooth portions,

but overall show dispersituberculate ornamentation. This grades from both poles into ramotuberculate and lineartuberculate ornamentation toward the midpoint of the egg. The most complete egg from the Wayan Formation (IMNH 2428\49608-2) and Liangtoutang Formation (ZMNH M8705-1) specimens measure 39.8 cm long by 10.8 cm wide and 41.65 cm long by 14.28 cm wide, respectively. IMNH 2428\49608-2 eggshell thickness ranges from 1.01 to 1.82 mm and ZMNH M8705-1 varies from 1.60 to 2.17 mm including ornamentation. Eggshell thickness of Blackleaf Formation material (ES 305) and Thomas Fork Formation material (ES 301,ES304-306) also fall within similar ranges, the former measuring 1.08 to 1.28 mm and the latter 1.28 to 2.02 mm (Table 5.7). The total eggshell thickness range for all material examined is 1.01 to 2.17 mm (average range 1.174 to 1.869 mm). These values compare favorably with described eggshell thickness ranges of *M. xixiaensis*, *M. zhangi*, *M. carlylei*, *M. goseongensis*, and *Megafusoolithus qiaoxianensis* (Table 5.7a-b, Table 5.8).

CL:ML ratios of all specimens are comparable and fall within 2.05:1 – 7.68:1, values that fall within the broad range described for *M. xixiaensis*. Close examination of the cryptoprismatic layer reveals the presence prisms with tabular crystal growth in IMNH 2428\49608-2 and ZMNH M8705-1, a feature previously documented in *M. xixiaensis* (Jin et al. 2007) but generally not noted in *Macroelongatoolithus* egg descriptions. Nucleation spacing and mammillary cone width measurements are generally narrower in ES305 (Blackleaf Formation) and ES301/ES304-306 (Thomas Fork Formation) compared with IMNH 2428\49608-2 and ZMNH M8705-1, however there is some overlap in the range of these features. Unfortunately, measurements of

these last features are not well documented for other specimens within *Macroelongatoolithus*, and so cannot be used for diagnostic purposes at this time.

Ootaxonomic Considerations and Synonymy within *Macroelongatoolithus*

Macroelongatoolithidae

Wang et al. (2010) report a specimen of *M. xixiaensis* that exhibits nodose ornamentation along the entirety of the egg, in contrast to the typical ramotuberculate to lineartuberculate gradational pattern of other known *Macroelongatoolithus* specimens. On this basis Wang et al. (2010) reinstated the use of a previously disregarded oofamily Macroelongatoolithidae Wang and Zhou 2005, claiming the large size of *Macroelongatoolithus* and predominately nodular ornamentation of a subset of this group as cause for their removal from Elongatoolithidae. The former oogenus was subsequently placed into Macroelongatoolithidae and split into two oogenera, *Macroelongatoolithus xixiaensis* and *Megafusoolithus qiaoxiaensis* (the former oogenus and species extrapolated from a partially preserved egg alone), on the basis of variability in ornamentation and minor variation of the ML:CL ratio (Wang, Zhao et al. 2010).

However, weathering of the specimen reported by Wang, Zhou et al. (2010) and partial preservation of the eggs renders this taxonomic revision suspect. When weathered or eroded, linear ridges– typically made up of closely spaced nodes arranged in a straight or faintly undulating line (Grellet-Tinner 2005) – may appear similar to isolated nodes. Additionally, clutch features used to justify a separate oofamily for *Macroelongatoolithus* specimens include size of the eggs, clutch diameter, and the lack of multiple tiers of eggs.

These differences may simply reflect the large size of the egg-laying animal rather than taxonomic variance of sufficient significance to warrant splitting the oofamily Elongatoolithidae. Due to the ambiguous nature of the ornamentation presented by Wang et al. (2010), combined with the strong microstructural similarity of M*acroelongatoolithus* to other oogenera within Elongatoolithidae, I recommend against continued use of the oofamily Macroelongatoolithidae.

Macroelongatoolithus zhangi
as a Junior Synonym of *M. xixiaensis*

Wang, Zhao et al. (2010) assert that the scale bar pictured in Wang and Zhou's (1995) description of *M. zhangi* was misread in the original paper and the true length of the specimen is 45 cm, contradicting the 25 cm length noted in Wang and Zhou (1995). With this correction the egg size for *M. zhangi*, previously distinguishing it from other *Macroelongatoolithus* species, is no longer unique. On this basis Wang, Zhao et al. (2010) establish *M. zhangi* as a synonym of *M. xixiaensis*.

Megafusoolithus qiaoxiaensis
as a Junior Synonym of *M. xixiaensis*

Megafusoolithus qiaoxiaensis was defined on the basis of a single, partially preserved egg half. Wang, Zhao et al. (2010) differentiates this oospecies on the basis of variability in ornamentation and minor variation of the ML:CL ratio. These features are not significantly different enough from established microstructural and ornamentation ranges of *Macroelongatoolithus xixiaensis* to warrant a separate oogenus and oospecies as ML:CL ratio is an extremely variable feature within *Macroelongatoolithus* and highly variable ornamentation, from nodose to lineartuberculate, is noted in most specimens.

Additionally, weathering of linear ornamentation could result in the superficial appearance of a node-dominated ornament (Grellet-Tinner et al. 2005). Here *Megafusoolithus qiaoxiaensis* is considered a synonym of *M. xixiaensis* until such a time as a complete specimen is described with microstructure or gross morphology that differ significantly from previously established oospecies.

M. goseongensis as a Junior Synonym of *M. xixiaensis*

Extremely large clutch size (3 m diameter) was proposed by Kim et al. 2011 as the basis to establish the new oospecies *Macroelongatoolithus goseongensis*. However, Wang, Zhao et al. 2010 cite a 3.3 meter diameter *Macroelongatoolithus xixiaensis* clutch first described by Wang and Zhou 1995, which contradicts the former authors' assertion that *M. goseongensis* eggs are arranged in a uniquely large clutch. As Kim et al. (2011) plainly state the similarity in egg size and microstructure between specimens described in their paper to previous established *M. xixiaensis* specimens, *M. goseongensis* can be considered a junior synonym of *M. xixiaensis* and therefore, a junior synonym of *M. carlylei*. The overlap in diagnostic features such as egg size, eggshell thickness, and CL:ML ratio is seen in Table 5.8.

Macroelongatoolithus xixiaensis as a Junior Synonym of *Macroelongatoolithus carlylei*

Intermittent splaying of radial ML crystals across the ML-CL boundary was first noted in *Macroelongatoolithus xixiaensis* in 2007 (Jin et al. 2007), seven years after Zelenitsky proposed that *M. xixiaensis* represented a junior synonym of *M. carlylei*. In

all other respects the two oospecies are identical, and it is thus logical to assign the Wayan Formation egg pair to the previously established North American *Macroelongatoolithus* oospecies. While crystal splaying was not noted in Zelenitsky et al.'s 2000 diagnosis of *M. carlylei*, the character is not listed as diagnostic for *M. xixiaensis* and is therefore considered here to be a feature noted within some *Macroelongatoolithus* specimens, rather than an apomorphy of *M. xixiaensis*.

Additionally, Figure 3B of Bray (1998) shows flaring crystal contacts between the ML and CL similar to those contacts seen when the radial crystals of the ML splay out into the CL as documented in Jin et al. (2007) and specimens described in this study. This may suggest the presence of crystal splaying the *M. carlylei*, however image quality is too poor for a definitive assessment of this character. At present, the presence/absence of crystal splaying is the only definite distinguishing microstructural feature between *Macroelongatoolithus* oospecies (Table 5.8). As this is a recently described feature, specimens described prior to the description of crystal splaying should be re-examined in order to properly ascertain the presence or absence of this character within Elongatoolithidae.

Conclusions

It is most parsimonious to assign all material described here to *M. carlylei* and treat *M. zhangi, M. xixiaensis, M. goseongensis* and *Megafusoolithus qiaoxianensis* as junior synonyms of *Macroelongatoolithus carlylei*, as partly suggested by Zelenitsky et al. 2000. In the systematic paleontology portion of their 2000 paper, Zelenitsky et al. officially synonimized *M. xixiaensis* with *M. carlylei*. In the discussion the authors

suggest that re-naming all established Asian *M. xixiaensis* material should wait until whole eggs were found from North America to strengthen the diagnosis of *M. carlylei*. As intact North American specimens identifiable as *M. carlylei* are described in the present study, all material previously defined as *M. xixiaensis* can be synonimized with *M. carlylei*. Additionally, as no literature prior to Zelenitsky et al. 2000 (or since) established a type species for the oogenus, the designated type within Zelenitsky et al. 2000 as *M. carlylei* stands.

CHAPTER 6

ZONAL GAS CONDUCTANCE STUDY OF NORTH AMERICAN MACROELONGATOOLITHUS (OOFAMILY ELONGATOOLITHIDAE) AND A COMPARISON TO ASIAN SPECIMENS

Among modern birds and reptiles, high gas conductance values are linked to buried or humid nest environments, while low values are indicative of subaerially exposed eggs in an open nest (Ar et al. 1974; Ar and Rahn 1985; Seymour 1979). This trend has been extrapolated to gas conductance values calculated for dinosaur eggs to varying degrees of effectiveness (Sabath 1991; Deeming 2006; Jackson et al. 2008; Varricchio et al. 2013). Samples taken along the length of two complete *Macroelongatoolithus* eggs are used to evaluate variation in gas conductance along egg length, in order to compare total egg gas conductance calculated from longitudinal zonal sampling with those values established from single eggshell fragments, and to reconstruct the nesting mode of *Macroelongatoolithus* egg laying animals.

Results

IMNH 2428\49607

IMNH 2428\49608-2 is 39.8 cm long, 10.8 cm wide at the midpoint, and slightly asymmetrical; pole size varies by 0.50 cm. Three models were used to calculate total volume and surface area: geometric modeling as described in Chapter 3 (Fig. 6.1, Table 3.1), an assumed ellipsoid egg shape (Table 3.1), and regression equations assuming an

avian egg shape for volume (Hoyt et al. 1979) and surface area (Paganelli et al. 1974) (Table 3.5).

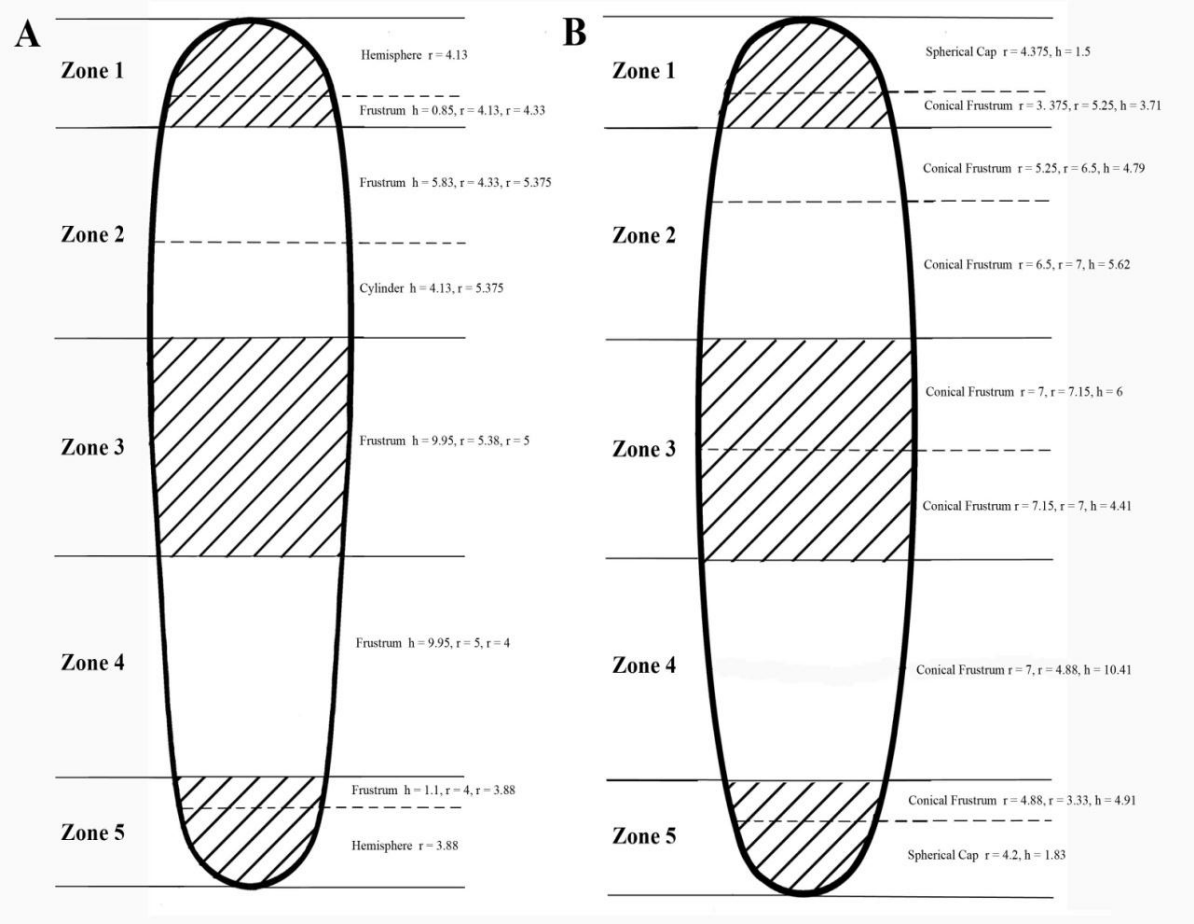

Figure 6.1 Geometric Modeling of Specimens. A. IMNH 2428\49608-2. B. ZMNH M8705-1.

Total egg volume and surface area calculated using the geometric modeling approach is 2,922 cm^3 and 1,178 cm^2, respectively (Table 6.2), higher than values calculated if the egg shape is assumed to be ellipsoid (V = 2,168.11 cm^3, SA = 1,024.53 cm^2). Using the regression equations established by Hoyt et al. 1979 and Paganelli et al. 1974 volume and surface area were calculated as 2,367.56 cm^3 and 874.94 cm^2. This last method resulted

in the lowest surface area calculation. Of the three methods, the geometric modeling approach allows for the most precise shape model and volume/surface area calculations.

Table 6.1 Surface Area and Volume of IMNH 2428\49608-2.

IMNH 2428\49608-2	Length cm	% Total Egg Length	Volume cm^3	% Volume	Surface Area cm^2	% Surface Area
Zone 1	4.98	12.50	341.69	11.58	130.23	11.05
Zone 2	9.95	25.00	806.53	27.33	319.68	27.12
Zone 3	9.95	25.00	841.55	28.52	324.54	27.53
Zone 4	9.95	25.00	635.60	21.54	282.75	23.98
Zone 5	4.98	12.50	297.31	10.07	121.74	10.33
TOTALS	**39.80**	**100**	**2922.67**	**100**	**1178.93**	**100**

Pore openings are circular and oval in cross section, range from 0.05 – 0.12 mm in average diameter, and are unevenly distributed across zones (Table 6.4). Gas conductance, calculated from the simplified gas conductance equation established in Varricchio et al. 2013 (Table 3.2), varies across zones from 2.18-598.46 mg H_2O mg $torr^{-1}$ day^{-1} and increases toward the midpoint of the egg from both poles. Total gas conductance for the specimen is 1,597.56 mg H_2O mg $torr^{-1}$ day^{-1} (Table 6.4). Microstructural features in Zone 5 are obscured by alteration of the specimen, possibly accounting for the extremely low porosity and gas conductance values calculated for that zone. Mass and predicted gas conductance was calculated using regression equations used in Jackson et al. 2008 (Table 3.3). Mass, based on the volume calculated from the geometric model approach, is 3,156.48g. Predicted gas conductance for an avian egg of equivalent mass to IMNH 2428\49608-2 is 275.758 mg H_2O $torr^{-1}$ day^{-1}.

Table 6.2 IMNH 2428\49608-2 Pore Attributes.

IMNH 2428\49608-2	# Pores Observed	% Pores Represented	Pore Density #/mm^2	% Pore Area	Avg Pore Diameter mm
Zone 1	72	16.253	0.707	29.298	0.0829 +- 0.032
Zone 2	141	31.828	0.570	23.610	0.1143 +- 0.046
Zone 3	155	34.989	0.707	29.302	0.1225 +- 0.045
Zone 4	69	15.576	0.389	16.104	0.1099 +- 0.035
Zone 5	6	1.354	0.041	1.685	0.0533 +- 0.017
TOTALS	**443**	**100**	**2.414**	**100**	

Table 6.3 IMNH 2428\49608-2 Gas Conductance.

IMNH 2428\49608-2	Obsv Pore Area mm^2	Obsv Shell Area mm^2	Fractional Pore Area	Total Zonal Area mm^2	Ap	Effective Porosity Ap/Ls	GH_2O mg H_2O torr^{-1}day^{-1}
Zone 1	0.730	101.788	0.007	13023.000	93.398	79.309	167.263
Zone 2	2.891	247.355	0.012	31967.800	373.629	257.312	542.672
Zone 3	3.054	219.099	0.014	32454.100	452.375	283.764	598.459
Zone 4	1.271	177.465	0.007	28274.700	202.503	136.076	286.983
Zone 5	0.019	147.484	0.000	12173.500	1.568	1.035	2.183
TOTALS	**7.965**	**893.191**		**117893.100**		**757.497**	**1597.560**

ZMNH M8705

ZMNH M8705-1 is 41.65 cm long, 14.28 cm wide at the midpoint, and is slightly asymmetrical – pole width varies by 0.3. Total egg volume and surface area calculated using the geometric modeling approach are 4,584.81 cm^3 and 1,581.79 cm^2, respectively (Table 6.5). Values calculated assuming an ellipsoid egg shape are slightly lower; volume = 4,447.45 cm^3, SA = 1,530.78 cm^2. Using the regression equations established by Hoyt et al. 1979 and Paganelli et al. 1974 volume and surface area were calculated as 4,332.56 cm^3 and 1,308.47 cm^2, respectively. Calculations based on an assumed avian egg shape resulted in the lowest estimate for both volume and surface area. As in IMNH 2428\49608-2, of the three methods geometric modeling allows for the most precise shape model and volume/surface area calculations.

Table 6.4 Surface Area and Volume of ZMNH M8705-1.

ZMNH M8705-1	Length cm	% Total Egg Length	Volume cm^3	% Volume	Surface Area cm^2	% Surface Area
Zone 1	5.21	12.50	247.35	5.39	153.78	9.72
Zone 2	10.41	25.00	1326.40	28.93	422.11	26.69
Zone 3	10.41	25.00	1574.18	34.33	454.95	28.76
Zone 4	10.41	25.00	1218.55	26.58	406.96	25.73
Zone 5	5.21	12.50	218.33	4.76	143.98	9.10
TOTALS	**41.65**	**100**	**4584.81**	**100**	**1581.79**	**100**

Pore openings are circular to oval in cross section, range from 0.079-0.131 mm in average diameter, and are unevenly distributed across zones (Table 6.6). Gas conductance varies across zones from 16.23-759.69 mg H_2O mg $torr^{-1}$ day^{-1} and the total calculated for the specimen is 1,119.52 mg H_2O mg $torr^{-1}$ day^{-1} (Table 6.7). As in IMNH 2428\49608-2, values are lowest at poles and highest at the midpoint of the egg. Gas conductance of Zone 2 is extremely low compared with values for all other zones, though this may be related to alteration of the eggshell in this zone indicated by poor preservation of mammillary cone bases and the obscured ML/CL boundary observed in samples from this zone. Calculated mass for ZMNH M8705-1, based on the volume calculated from the geometric model approach, is 4,951.59 g. Predicted gas conductance for an avian egg of equivalent mass to this specimen is 398.55 mg H_2O $torr^{-1}$ day^{-1}.

Table 6.5 ZMNH M8705-1 Pore Attributes.

ZMNH M8705-1	# Pores Observed	% Pores Represented	Pore Density $\#/mm^2$	% Pore Area	Avg Pore Diameter mm
Zone 1	2	4.082	0.042	3.135	0.131 +- 0.018
Zone 2	1	2.041	0.021	1.554	0.082 +- 0.000
Zone 3	20	40.816	0.420	31.030	0.107 +- 0.152
Zone 4	15	30.612	0.479	35.413	0.098 +- 0.025
Zone 5	11	22.449	0.391	28.873	0.079 +- 0.031
TOTALS	**49**	**100**	**1.354**	**100**	

Table 6.6 ZMNH M8705-1 Gas Conductance.

ZMNH M8705-1	Obsv Pore Area mm^2	Obsv Shell Area mm^2	Fractional Pore Area	Total Zonal Area mm^2	Ap	Effective Porosity Ap/Ls	GH_2O mg H_2O $torr^{-1}day^{-1}$
Zone 1	0.044	47.124	0.001	15377.900	14.358	7.695	16.229
Zone 2	0.006	47.515	0.000	42211.300	5.330	2.818	5.943
Zone 3	0.689	47.602	0.014	45495.400	658.509	360.211	759.686
Zone 4	0.187	31.283	0.006	40696.100	243.269	132.433	279.301
Zone 5	0.104	28.137	0.004	14398.300	53.219	27.672	58.360
TOTALS	**1.107**	**201.661**		**158179.000**		**530.829**	**1119.518**

Comparison

Zones for both specimens were established based on length, with Zones 2-4 equal to 25% egg length and Zones 1 and 3 equal to 12.5 % of total egg length. Calculations of volume and surface area vary slightly from proportions expected for a perfectly cylindrical egg (Fig. 6.2, Fig. 6.3), likely due to the minor asymmetry of the specimens.

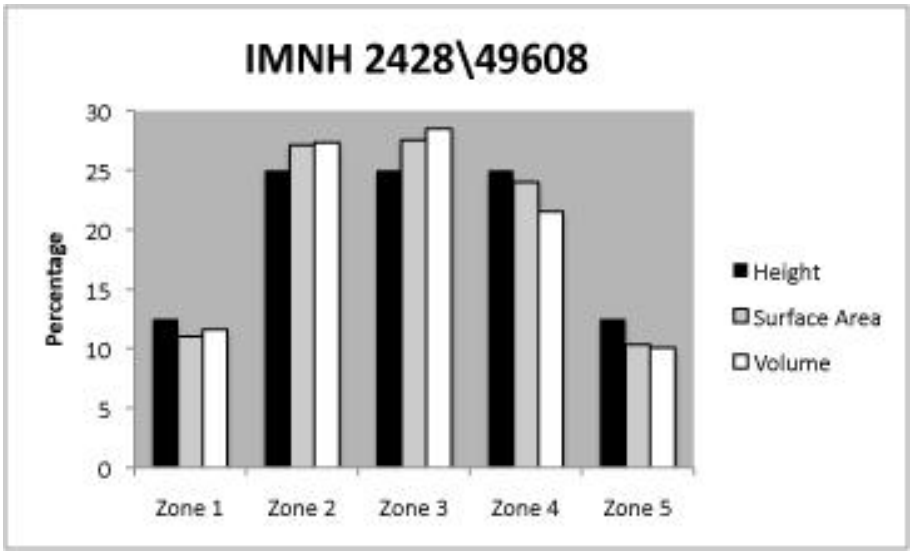

Figure 6.2 Percent Surface Area and Volume per Zone, IMNH 2428\49608-2.

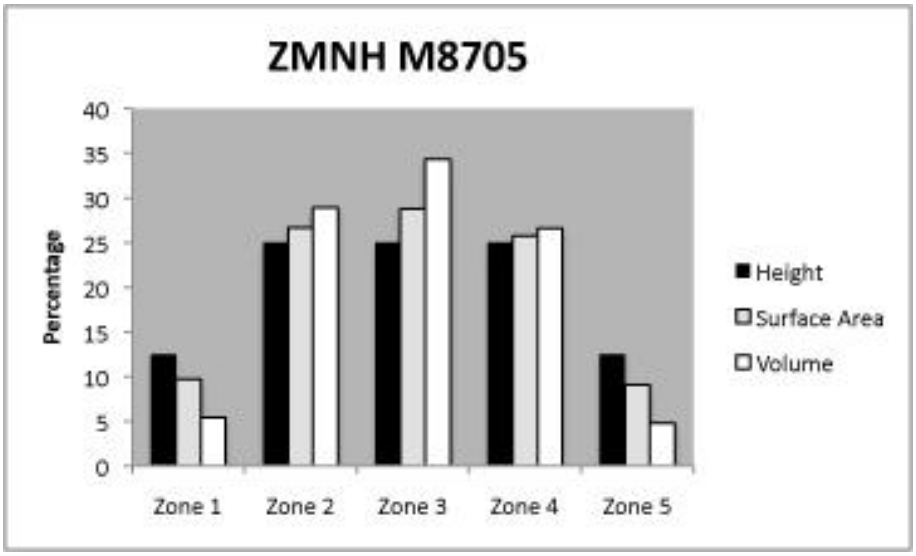

Figure 6.3 Percent Surface Area and Volume per Zone, ZMNH M8705-1.

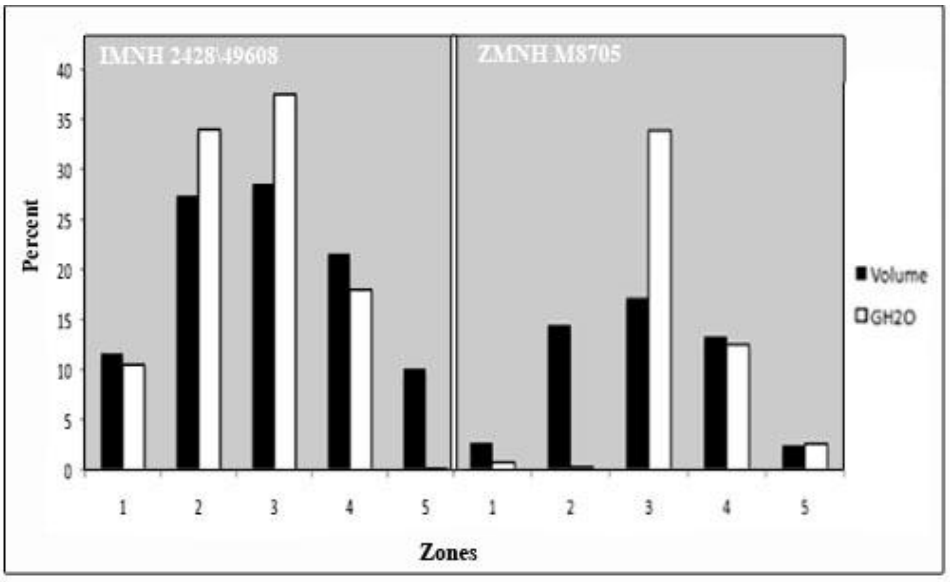

Figure 6.4 Percent Gas Conductance and Volume Per Zone.

Pore distribution and gas conductance are also distributed somewhat unevenly across both specimens. A comparison of the observed number of pores per zone with the expected number of pores per zone of an idealized egg with even pore distribution across zones was evaluated using a chi squared test. Disparity between observed values and

those expected for an even distribution of both pore distribution and gas conductance across the eggs is indicated in some zones (Table 6.8, Table 6.9). Pore area and gas conductance are concentrated in zones 3 and 4 of both specimens, while number of pores is highest in zones 2 and 3 of IMNH 2428\49608-2 and zones 3 and 4 of ZMNH M8705-1.

Table 6.7 Chi Squared Test of Pore Distribution Across IMNH 2428\49608-2 and ZMNH M8705-1. Degrees of freedom = v-1, where v = number of categories. Degrees of freedom = 4. For 4 degrees of freedom, an X^2 value higher than 9.5 indicates significant variation from expected values.

Zone	IMNH2428\49608 Obsv Pores	IMNH2428\49608 Expected Pores	IMNH2428\49608 X^2	ZMNHM8705 Obsv Pores	ZMNHM8705 Expected Pores	ZMNHM8705 X^2
1	72	103.520	9.597	2	5.584	2.300
2	141	104.379	12.848	1	13.570	11.643
3	155	104.570	24.320	20	12.020	5.298
4	69	68.721	0.001	15	9.736	2.847
5	6	61.810	50.393	11	8.091	1.046
Total	**443**	**443**	**97.160**	**49**	**49**	**23.135**

Table 6.8 Chi Squared Test of Gas Conductance Across IMNH 2428\49608-2 and ZMNH M8705-1. Degrees of freedom = v-1, where v = number of categories. Degrees of freedom = 4. For 4 degrees of freedom, an X^2 value higher than 9.5 indicates significant variation from expected values.

Zone	IMNH2428\49608 Obsv GH_2O	IMNH2428\49608 Expected GH_2O	IMNH2428\49608 X^2	ZMNHM8705 Obsv GH_2O	ZMNHM8705 Expected GH_2O	ZMNHM8705 X^2
1	167.26	176.47	0.48	216.23	108.84	78.80
2	542.67	433.19	27.67	5.94	298.75	286.99
3	598.46	439.78	57.25	759.69	322.00	594.95
4	286.98	383.15	24.14	279.30	288.03	0.26
5	2.18	164.96	160.63	58.36	101.90	18.61
Total	**1597.56**	**1597.56**	**270.16**	**1119.52**	**1119.52**	**979.61**

Effective porosity, a measure of zonal pore area divided by average pore length (assumed to be equal to average shell thickness), allows for a measure of porosity that does not rely on the assumed factors used in the gas conductance equation, such nesting temperature. However, as the established convention in previous studies is to report gas conductance rather than effective porosity the former is emphasized here. Both effective

porosity and gas conductance increase toward the midpoint of the eggs and are markedly low at one pole of each egg. These trends generally mirror the percent pore area of each zone, with the exception of ZMNH M8705-1 Zone 4, where percent pore area increases from Zone 3 to Zone 4, then decreases in Zone 5. In contrast, effective porosity and gas conductance decrease from Zone 3 through Zone 5 (Fig. 6.5-6.6).

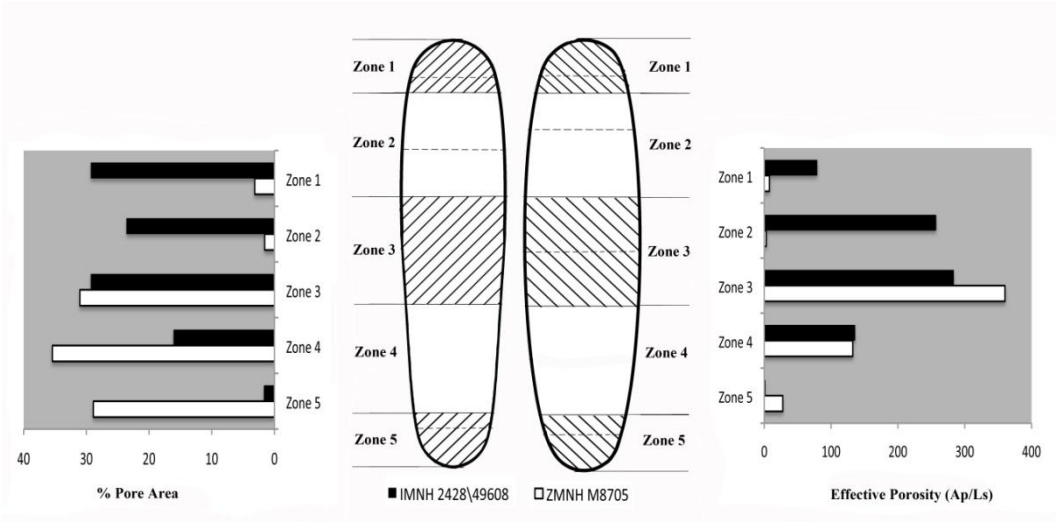

Figure 6.5 Percent Pore Area and Effective Porosity in IMNH 2428\49608-2 and ZMNH M8705-1.

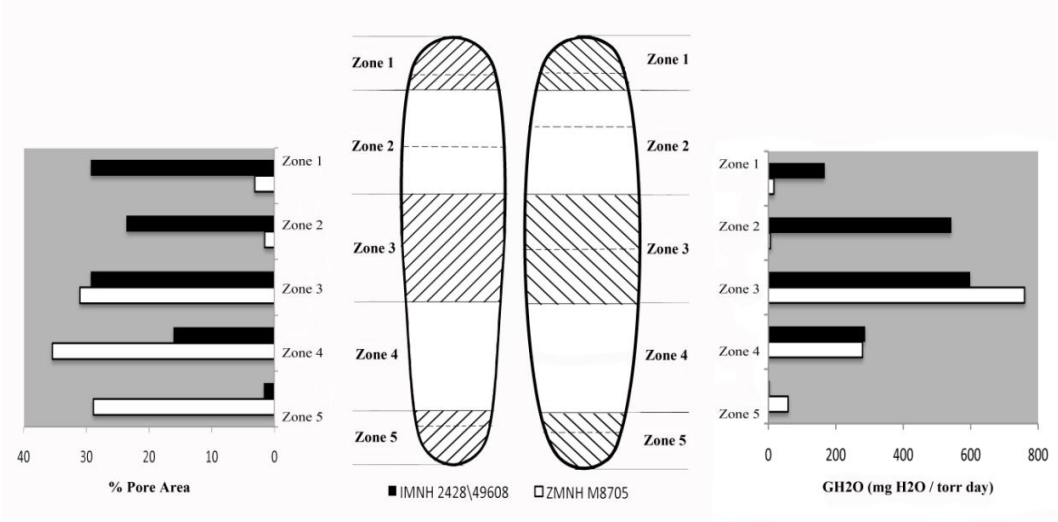

Figure 6.6 Percent Pore Density and Gas Conductance in IMNH 2428\49608-2 and ZMNH M8705-1.

Behavioral Implications

One pole of each examined specimen has significantly lower gas conductance values compared to the other zones (Zones 1-2 of IMNH 2428/49608, Zone 5 of ZMNH M8705-1) (Fig. 6.4), though gas conductance generally increases toward the equator of both specimens and is typically proportional to volume. Significantly higher values at the midpoint of both eggs compared to pole values reflect the high percent of egg volume represented by Zone 3 compared to other zones (Fig. 6.4). Low gas conductance compared to zonal volume, seen in Zones 1-2, ZMNH M8705-1, and Zone 5, IMNH 2428\49608-2, may be due to eggshell alteration in these zones. Poorly preserved mammillary cone bases and the obscured ML/CL boundary seen in IMNH 2428/49608 Zone 1 and ZMNH M8705-1 indicates alteration of the specimens, possibly accounting for the low porosity and gas conductance values calculated for Zones 5 and 1, respectively.

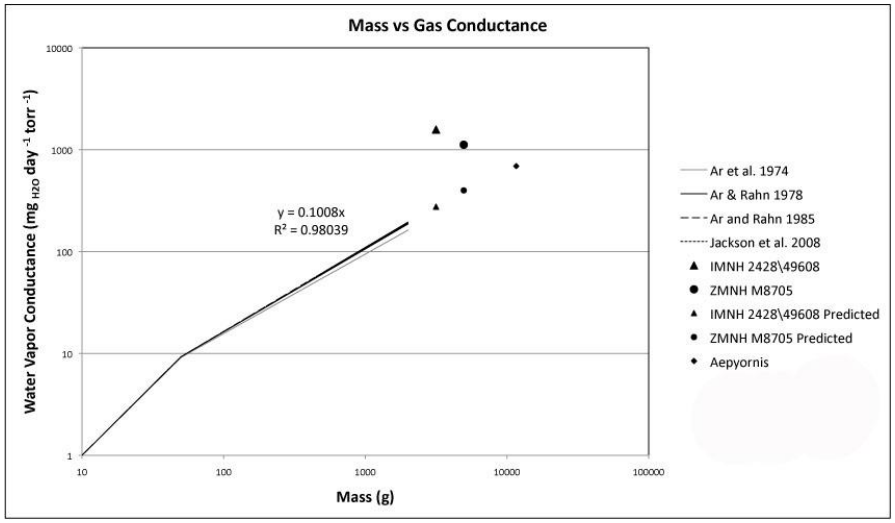

Figure 6.7 Gas Conductance Regression Equation with IMNH 2428\49608-2 and ZMNH M8705-1. "Predicted" values refer to calculations of gas conductance for an avian egg of equivalent mass to specimens. Logarithmic trend line shown for Jackson et al. 2008.

Table 6.9 Comparison of Calculated and Predicted Gas Conductance for Reptile, Avian, and *Macroelongatoolithus* Eggs. Modified from Jackson et al. 2008. 1) Packard et al. 1979, 2) Grigg and Beard 1985, 3) Dunson and Bramham 1981, 4) Lutz et al. 1980, 5) Dunson 1982, 6) Thompson 1985, 7) Harrision et al. 1978, 8) Ar et al. 1974, 9) Ar and Rahn 1985

Taxon	Species	Nesting Mode	Calculated GH_2O mg H_2O $torr^{-1}$ day^{-1}	Predicted GH_2O mg H_2O $torr^{-1}$ day^{-1}	Difference	Reference
Gecko	*Sphaerodactylus*	Open	1.1	5.5	0.20	3
	Lepidodactylus lugrubris	Open	1.7	3.4	0.50	5
	Hemidactylus garnoti	Open	2.6	4.4	0.60	5
Crocodilian	*C. porosus* (infertile)	Mound	622	810	0.77	2
	C. porosus (fertile)	Mound	2812	810	3.40	2
	C. actus	Buried	1185	825	1.40	4
	Alligator mississippiensis	Mound	2902	685	4.20	1
Turtle	*Emyduru macquarii*	Buried	1268	150	8.30	6, 7
	Trionyx spiniferus	Buried	810	150	5.46	1
Bird	*Gallus gallus*	Open	14	9.19	1.57	8
	Rhea Americana	Open	78	58.04	1.34	8
	Gavia immer (loon)	Open/Wet or Humid	98	23.3	4.20	9
	Podilymbus podiceps (grebe)	Open/Wet or Humid	13.02	4.51	2.90	9
	Alectura lathami (megapode)	Mound	48.15	28.75	1.70	9

Ootaxon	Specimen Number	Nesting Mode	Calculated GH_2O mg H_2O $torr^{-1}$ day^{-1}	Predicted GH_2O mg H_2O $torr^{-1}$ day^{-1}	Difference	Reference
M. carlylei	IMNH 2428\49608-2	-	1597.56	275.76	5.79	This
	ZMNH M8705-1		1119.52	398.55	2.81	Study

Total gas conductance values of both eggs are markedly high. IMNH 2428/49608-2, with a total gas conductance of 1,597.56 mg H_2O $torr^{-1}$ day^{-1}, has a conductance value 5.79 times higher than the gas conductance predicted for an avian egg of equivalent mass. Less drastic, but also significantly above predicted values, ZMNH M8705-1 has a total gas conductance of 1,119.52 mg H_2O $torr^{-1}$ day^{-1}, 2.8 times higher than predicted for a mass-equivalent avian egg (Fig. 6.6). The high total calculated gas conductance : predicted gas conductance ratios of these *Macroelongatoolithus carlylei* specimens are most similar to values seen in eggs of reptiles and bird eggs incubated in humid or covered nest environments (Table 6.10).

CHAPTER 7

DISCUSSION AND IMPLICATIONS

Parataxonomy and Microstructural Variation

Measured values of microstructural features typically used in ootaxonomic assignment vary within IMNH 2428\49608-2, and to a lesser degree within ZMNH M8705-1. Lesser-observed variation in the latter may be a result of lower sample size. High variability in shell thickness, cryptoprismatic layer to mammillary layer thickness ratio, and nucleation site spacing suggests that established methods for assigning ootaxa be re-assessed, or at least re-evaluated for the large and highly variable members of the oogenus *Macroelongatoolithus*. Variation documented here within a single specimen demonstrates the need to examine variation along egg specimens rather than establish these ranges from isolated fragments, and potentially to re-evaluate the ranges expected for microstructural features of an oospecies.

Future work documenting further comparisons of microstructural variation along the lengths of multiple eggs within a clutch, presumably laid by one or several member of the same species, may lend additional insight into the total range of variation possible within an ootaxon. Variation in *Macroelongatoolithus* gross morphology – length, width, and ornamentation type– indicates that these features are also subject to greater variation within a single oospecies than previously accounted for.

A careful and detailed re-evaluation of all documented *Macroelongatoolithus* material may lead to discernable groups and the re-establishment of ootaxa synonymized

here and in previous work, however until such a study is conducted the wide range of overlapping diagnostic features described in *Macroelongatoolithus* specimens are most parsimoniously interpreted as variation seen in a single oospecies, rather than the several separate oospecies named and variously synonymized since the oogenus was erected in 1995. The large size of eggs within this oogenus may superficially increase the apparent variation in microstructure and gross morphology. However, the highly undulating nature of the boundary seen in these eggs may also lead to the seemingly extreme variation documented these eggs.

Reproductive Biology and Nesting Behavior

Prior to this study, *Macroelongatoolithus* gas conductance was based on values from a single fragment, assumed to apply to an entire egg. At 600 mg H_2O mg $torr^{-1}$ day^{-1}, this calculation was assumed to be two times higher than the predicted gas conductance of a mass-equivalent egg, and therefore suggestive of high gas conductance and burial in a vegetation or sediment mound. However, as discussed in Jackson et al. (2008), a 2:1 calculated to predicted gas conductance ratio is, in reality, borderline and may be indicative of reptile or avian eggs in either open air nests or buried/humid nests (Table 6.10).

Evaluating gas conductance along a longitudinal profile expands the nesting mode of *Macroelongatoolithus* laying animals to include a more complex and definitive nesting mode than previously assumed. Low gas conductance values at poles combined with high values along the equator and extremely high overall gas conductance indicates burial in sediment or vegetation, creating a humid nest environment the eggs. Additionally, gas

conductance values for both specimens were quite similar, likely reflecting a shared nesting mode among oviraptorids in Asia and North America. Slightly lower values calculated for the Liangtoutang Formation specimen (ZMNH M8705-1) may reflect individual variation among egg-laying animals or perhaps minor differences in nesting environment between the semi-arid floodplain mudstones of the Wayan Formation in Idaho and the shallow laucustrine red siltstones and sandstones of the Liangtoutang Formation of Zhejiang, China.

Identity of the Egg-Laying Animal

While neither skeleton-clutch associations nor gravid adults are known for *Macroelongatoolithus* eggs, a single perinatal oviraptorid specimen preserved in contact with four *Macroelongatoolithus* eggs has been documented (Grellet-Tinner 2005; Grellet-Tinner et al. 2006). Unfortunately this specimen has not been thoroughly discussed in published literature. Contrary to this assignment, some researchers have claimed a link between *Macroelongatoolithus* eggs and tyrannosauroid theropods based on egg and clutch size alone (Qian et al. 2007; Qian et al. 2008). This relationship should be disregarded as it lacks concrete supporting evidence. The abundance of evidence indicating an oviraptorid-elongatoolithid relationship, in addition to the lack of any other dinosaurian taxa found intimately associated with elongatoolithid eggs, suggests that a large oviraptorid can be implicated as the *Macroelongatoolithus* egg-layer.

Temporal and Geographic Distribution of *M. carlylei*

Macroelongatoolithus carlylei distribution spans early to late Cretaceous strata of South Korea, eastern China, and the western United States. While *M. carlylei* was first

documented in the Lower Cretaceous Cedar Mountain, Kelvin and Dakota Formations of Utah, the diagnosis of *M. zhangi*, *M. xixiaensis*, *M. goseongensis* and *Megafusoolithus qiaoxianensis* as junior synonyms of *Macroelongatoolithus carlylei* broadens the oospecies' range to include formations and regions from which the synonymized ootaxa were described. These include the Upper Cretaceous Zoumagang, Majiacun, Gaoguou, Zhaoying, and Sigou Formations, Henan Province, Xixia Basin, China; Albian – Cenomanian Liangtoutang Formation and Upper Cretaceous Chichengshan Formation, Zhejiang Province, Tiantai Basin, China; and the Upper Cretaceous Goseong Formation, South Gyeongsang Province, South Korea. Material described in this study further expands this range to include the Albian-Cenomanian Wayan Formation, Bonneville County, ID, USA; Albian – Cenomanian Blackleaf Formation, Beaverhead County, MT, USA; and early Late Cretaceous Thomas Fork Formation, Lincoln County, WY, USA.

Paleobiogeography

Previously, an influx of Asian dinosaur taxa into North America was hypothesized to have occurred in the early Late Cretaceous based on the sudden presence of animals such as tyrannosaurids, ceratopsians, and hadrosaurids in western North America (Kirkland et al. 1998). Teeth identified from these taxa were found in the Albian-Cenomanian Blackleaf Formation of southwestern Montana, in addition to a tyrannosaurid tooth identified from the slightly older Cloverly Formation of Wyoming (Ullmann et al. 2011; Zanno and Makovicky 2011). The description of *Macroelongatoolithus* specimens from the early Late Cretaceous of Idaho adds further evidence of an Albian- Cenomanian date for an Asian – North American interchange.

Identification of the Wayan eggs to the primarily Asian oogenus *Macroelongatoolithus* establishes the co-occurrence of this oogenus in Asia and North America and strongly suggests the presence of an additional shared taxon, a giant oviraptorid similar to *Gigantoraptor* between the two continents.

CHAPTER 8

CONCLUSIONS

This study represents the first comprehensive comparison of gross morphology, microstructural variation, and gas conductance within a *Macroelongatoolithus* oospecies. The observed variation with and between IMNH 2428/49608 and ZMNH M86705 expands the range of expected allowable variation for an oospecies, and calls into question the over splitting of ootaxa on the basis of traits that may reflect individual variation or growth stage of the laying animal. The discovery and description of an intact *Macroelongatoolithus carlylei* specimen from North American confirms the synonymy of *M xixiaensis* into the previously named *M. carlylei* suggested by Zelenitsky et al. (2000), and expands the geographic and temporal distribution of the oogenus to include the early Late Cretaceous of North America.

Very recently the first published evidence of large bodied oviraptorosaur in North America was presented by Lamanna et al. (2014). While not as large as the estimated 8 meter long *Gigantoraptor* (Xu et al. 2007), the caegnathid *Anzu wyliei* is estimated to be 2.5 m long and 1.5 m tall at the hip and was discovered in the late Cretaceous Hell Creek Formation of Montana (Lamanna et al. 2014). The identification and analysis of *Macroelongatoolithus* eggs in early Late Cretaceous rocks of southeastern Idaho is an exciting indication that even larger oviraptorosaur roamed North America, nesting and perhaps caring for its eggs along the well-developed floodplain soils of meandering stream systems, despite the lack of skeletal remains to-date.

Future work comparing the gross morphology, microstructure, and gas conductance of *Elongatoolithus*, *Macroolithus*, and *Macroelongatoolithus* eggs and clutches will help broaden our understanding of how these eggs and the egg laying animals relate to each other and may shed some much needed light on any potential relationship between parent animal size and eggshell traits. Additionally, further microstructural and gross morphological examination of the available, and largely complete, Asian *Macroelongatoolithus* clutches could aid in refining how oospecies are defined within this group, and it may be possible to use microstructural variability within and between clutches to advance our understanding of nesting behaviors in large oviraptorosaurs.

REFERENCES CITED

Amo Sanjuan O, Canudo JI, Cuenca Bescos G. 2000. First record of Elongatoolithid eggshells from the lower Barremian (Lower Cretaceous) of Europe (Cuesta Corrales 2, Galve Basin, Teruel, Spain). First International Symposium on Dinosaur Eggs and Babies, Extended Abstracts.

Ar A, Paganelli CV, Reeves RB, Greene DG, Rahn H. 1974. The avian egg: water vapor conductance, shell thickness, and functional pore area. The Condor 76: 153-158.

Ar A, Rahn H. 1978. Interdependence of gas conductance, incubation length and weight of the avian egg. Respiratory function in birds, adult and embryonic: 153-158. Eds J Piiper. Springer, Heidelberg.

Ar A, Rahn H. 1985. Pores in avian eggshells: gas conductance, gas exchange, and embryonic growth rate. Respiration Physiology 61: 1-20.

Barta DE, Brundridge KM, Croghan JA, Jackson FD, Varricchio DJ, Jin X, Poust AW. 2014. Eggshell, eggs, and clutches of the Spheroolithidae from the Cretaceous Tiantai basin, Zhejiang Province, China. Historical Biology.

Bray ES. 1998. Dinosaur eggshell *Boletuoolithus carlylensis*, oogenus nov. from the Lower Cretaceous Cedar Mountain Formation of Utah. Lower and Middle Cretaceous Terrestrial Ecosystems. New Mexico Museum of Natural History and Science Bulletin No. 14.

Blatt H. 1992. Sedimentary Petrology. W.H. Freeman and Company, New York.

Canudo JI, Gasca JM, Aurell M, Badiola A, Blain HA, Cruzado-Caballero P, Gomez-Fernandez D, Moreno-Azanza M, Parrilla J, Rabal-Garces R, Ruiz-Omenaca JI. 2010. La Cantalera: an exceptional window onto the vertebrate biodiversity of the Hauterivian-Barremian transition in the Iberian Peninsula. Journal of Iberian Geology 36 (2): 205-224.

Carpenter K. 1999. Eggs, Nests, and Baby Dinosaurs: A Look at Dinosaur Reproduction. Indiana University Press.

Carpenter K. 2006. Assessing dinosaur faunal turnover in the Cedar Mountain Formation (Lower Cretaceous) of Eastern Utah, USA. Mesozoic Terrestrial Ecosystems, p. 21-25.

Carrano M, Mateus O, Mitchell J. 2013. First definitive association between embryonic *Allosaurus* bones and *Prismatoolithus* eggs in the Morrison Formation (Upper Jurassic, Wyoming, USA). Abstracts of the 73rd meeting of the Society of Vertebrate Paleontology.

Chao T, Chiang Y. 1974. Microscopic Studies on the Dinosaurian Egg-Shells from Laiyang, Shantung Province. Scientia Sinica 17 (1): 73- 90.

Cheng YN, Qiang JI, Wu XC, Shan HY. 2008. Oviraptorosaurian eggs (Dinosauria) with embryonic skeletons discovered for the first time in China. Acta Geologica Sinica 82(6): 1089-1094.

Chow, MM. 1954. Additional notes on the microstructure of the supposed dinosaurian egg shells from Laiyang, Shantung, Acta Scientaia Sinica, 2: 523-526.

Clark JM, Norell MA, Chiappe LM. 1999. An oviraptorid skeleton from the late Cretaceous of Ukhaa Tolgod, Mongolia, preserved in an avian like brooding position over an oviraptorid nest. American Museum Noviates 3265.

Currie PJ. 1996. The great dinosaur egg hunt. National Geographic: 101-108.

Dauphin YO. 1994. Comparison of microstructures and chemical composition between fossil egg shells from Southern France and Asia and those of recent birds. Neues Jahrbuch fur Geologie und Palaontologie Abhandlungen (New Yearbook for geology and paleontology, Treatises): 55-71.

Deeming DC. 2006. Ultrastructural and functional morphology of eggshells supports the idea that dinosaur eggs were incubated buried in a substrate. Palaeontology 49(1): 171-185.

Donaire M, Lopez-Martinez N. 2009. Porosity of Late Paleocene Ornitholithus Eggshells (Tremp Fm, South-Central Pyrenees, Spain): Palaeoclimatic Implications. Palaeogeography, Palaeoclimatology, Palaeoecology 279: 147-159.

Dong Z. 1979. Dinosaurs from the Cretaceous of South China. Mesozoic and Cenozoic Red Beds of South China. Selected Papers from the "Cretaceous-Tertiary Workshop", edited by Institute of Vertebrate Paleontology, Paleoanthropology and Nanjing Institute of Paleontology: 342-350.

Dong Z. 1980. Chinese Dinosaur Faunas and their Stratigraphic Position. Journal of Stratigraphy 4(4): 256-262.

Dong ZM, Currie PJ. 1996. On the discovery of an oviraptorid skeleton on a nest of eggs at Bayan Mandahu, Inner Mongolia, People's Republic of China. Canadian Journal of Earth Sciences 33: 631-636.

Dorr JA. 1985. Newfound Early Cretaceous dinosaurs and other fossils in Southeastern Idaho and Westernmost Wyoming. Contributions from the Museum of Paleontology, University of Michigan 27: 73-85.

Dunson WA. 1980. Low water vapor conductance of hard-shelled eggs of the gecko lizards *Hemidactylus* and *Lepidodactylus*. Journal of Experimental Zoology 219: 377-379.

Dunson WA, Bramham CR. 1981. Evaporative water loss and oxygen consumption of three small lizards from the Florida Keys: *Spanerodactylus cinereus*, *S. notatus*, and *Anolis sagrei*. Physiological Zoology 54: 253-259.

Dyman TS, Nichols DJ. 1988. Stratigraphy of Mid-Cretaceous Blackleaf and lower part of the Frontier Formations in parts of Beaverhead and Madison Counties, Montana. US Geological Survey Bulletin 1773.

Fang X, Lu L, Cheng Z, Zou Y, Pang W, Wang Y, Chen K, Yin Z, Wang X, Liu J, Xie H, Jin Y. 1998. On the Cretaceous fossil eggs of Xixia County, Henan Province. Geological Publishing House Beijing.

Fang X, Wang Y, Jiang Y. 2000. On the late Cretaceous fossil eggs of Tiantai, Zhejiang. Geological Review 46(1): 105-112.

Fang Z, Liwu L, Jiang Y, Yang L. 2003. Cretaceous fossil eggs from the Tiantai basin of Zhejiang, with a discussion on the extinction of dinosaurs. Geological Bulletin of China 22(7): 512-520.

Fang X, Li P, Zhang Z, Zhang X, Lin Y, Guo S, Cheng Y, Li Z, Zhang X, Cheng Z. 2009. Cretaceous Strata in Nanxiong Basin of Guangdong and the Evolution from the Dinosaur Egg to the Bird Egg. Acta Geoscientia Sinica 30(2): 167-186.

Fang X, Li P, Zhang Z, Zhang X, Lin Y, Gou S, Cheng Y, Li Z, Zhang X, Cheng Z. 2009. Cretaceous Strata in Nanxiong Basin of Guangdong and the Evolution from the Dinosaur Egg to the Bird Egg. Acta Geoscientia Sinica 30(2): 167-186.

Fanti F, Currie PJ, Badamgarav D. 2012. New specimens of *Nemegtomaia* from the Baruungoyot and Nemegt Formations (Late Cretaceous) of Mongolia. PLoSONE 7(2).

Grellet-Tinner G. 2005. A phylogenetic analysis of oological characters: A case study of saurischian dinosaur relationships and avian evolution [dissertation]. [Los Angeles (CA)]: University of Southern California.

Grellet-Tinner G, Chiappe L, Norell M, Bottjer D. 2006. Dinosaur eggs and nesting behaviors: A paleobiological investigation. Palaeogeography, Palaeoclimatology, Palaeoecology 232: 294-321.

Grellet-Tinner G, Makovicky P. 2006. A possible egg of the dromaeosaur *Deinonychus antirrhopus*: phylogenetic and biological implications. Canadian Journal of Earth Sciences 43: 705-719.

Grellet-Tinner G, Chiappe L, Norell M, Bottjer D. 2006. Dinosaur eggs and nesting behaviors: A paleobiological investigation. Palaegeography, Palaeoclimatology, Palaeoecology 232: 294-321.

Grigg GC, Beard L. 1985. Water loss and gain by eggs of *Crocodylus porosus*, related to incubation age and fertility. Biology of Australasian frogs and reptiles: 353-359. Eds G Grigg, R Shine, H Ehmann. Surry Beatty, Sydney.

Harrison KE, Bently TB, Lutz PL, Marszalek D. 1978. Water and gas diffusion in the American crocodile egg. American Zoologist 18: 637.

Hayward JL, Folsom SD, Elmendorf DL, Tambrini AA, Cowles DL. 1997. Experiments on the taphonomy of amniote eggs in marine environments. Palaios 12(5): 482-488.

Hayward JL, Zelenitsky DK, Smith DL. 2000. Eggshell taphonomy at modern gull colonies and a dinosaur clutch site. Palaios 15: 343-355.

Hayward JL, Dickson KM, Gamble SR, Owen AW, Owen KC. 2010. Eggshell taphonomy: environmental effects on fragment orientation. Historical Biology 23(1): 5-13.

He T, Varricchio DJ, Jackson FD, Jin X, Poust AW. 2012. An Oviraptorid Adult-Egg Association and the Origin of Avialan Reproductive Strategies. Programs and Abstracts of the 72nd Annual Meeting of the Society of Vertebrate Paleontology: 108.

He H, Wang X, Wang Q, Jiang S, Cheng J, Zhang Z, Zhou Z, Jiang Y, Yu F, Deng C, Yang J, Zhu R. 2013. SIMS zircon U-Pb dating of the Late Cretaceous dinosaur egg-bearing red deposits in the Tiantai Basin, southeastern China. Journal of Asian Earth Sciences 62:654-661.

Hoyt DF. 1979. Practical Methods of Estimating Volume and Fresh Weight of Bird Eggs. Auk 96: 73-77.

Huh M, Kim BS, Woo Y, Simon DJ, Paik IS, Kim HJ. 2014. First record of a complete giant theropod egg clutch from Upper Cretaceous deposits, South Korea. Historical Biology 26(2): 218-228.

Imai T. 2013. Sedimentological analysis of eggshell transport and deposition: implication and application to eggshell taphonomy [Master's thesis]. Bozeman, MT: Montana State University.

Iverson JB, Ewert MA. 1991. Physical characteristics of reptilian eggs and a comparison with avian eggs. In: Deeming DC, Ferguson MWJ, editors. Egg Incubation: Its Effect on Embryonic Development in Birds and Reptiles. New York, New York: Cambridge University Press: 87-100.

Jensen J. 1970. Fossil eggs in the lower cretaceous of Utah. Brigham Young University research studies. Geology Series. Geology Studies 17: 51-65.

Jin X, Azuma Y, Jackson FD, Varricchio DV. 2007. Giant Dinosaur Eggs from the Tiantai Basin, Zhejiang Province, China. Canadian Journal of Earth Sciences 44: 81-88.

Kim BS, Huh M, Moon KH, and Jang SJ. 2011. Excavation and preparation of a theropod nest from Aphae-do in Jeollanam-do province, South Korea. Journal of the Geological Society of Korea 47: 205-211.

Kim JY, Yang SY, Choi HI, Seo SJ, and Kim KS. 2011. Dinosaur eggs from the Cretaceous Goseong Formation of Tongyeong City, southern coast of Korea. Journal of the Paleontological Society of Korea 21(1): 13-26.

Kirkland JI, Lucas SG, Estep JE. 1998. Cretaceous dinosaurs of the Colorado Plateau. Lower and Middle Cretaceous Terrestrial Ecosystems. New Mexico Museum of Natural History and Science Bulletin No. 14, p. 79-89.

Krumenacker LJ. 2005. Preliminary report on new vertebrates from the Upper Gannett Group (Aptian) and Wayan Formation (Albian) of East Idaho. Paludicola 5(2): 55-64.

Krumenacker LJ. 2010. Chronostratigraphy and Paleontology of the mid-Cretaceous Wayan Formation of Eastern Idaho, with a Description of the First *Oryctodromeus* Specimens from Idaho [Master's thesis]. Bringham Young University.

Kundrat M, Cruickshank ARI, Manning TW, Nudds J. 2007. Embryos of therizinosaurid theropods from the Upper Cretaceous of China: diagnosis and analysis of ossification patterns. Acta Zoologica (Stockholm) 88.

Lamanna MC, Sues HD, Schachner ER, Lyson TR. 2014. A New Large-Bodied Oviraptorosaurian Theropod Dinosaur from the Latest Cretaceous of Western North America. PLOS ONE 9(3): 1-16.

Larson PL. 1998. The theropod reproductive system. GAIA N°15: 389-397.

Li Y, Yin Z, Liu Y. 1995. The discovery of a new genus of dinosaur egg from Xixia, Henan, China. Journal of Wuhan Institute of Chemical Technology 17(1): 38-41.

Liang X, Wen S, Yang D, Zhou S, Wu S. 2009. Dinosaur eggs and Dinosaur Egg-Bearing Deposits (Upper Cretaceous) of Henan Province, Chian: Occurrences, Palaeoenvirionments, Taphonomy, and Preservation. Progress in Natural Science 19: 1587-1601.

Loyal RS, Mohabey DM, Khosla A, Sahni A. 1998. Status and palaeobiology of the Late Cretaceous Indian theropods with description of a new theropod eggshell oogenus and oospecies, *Ellipsoolithus Kheaensis*, from the Lameta Formation, District Kheda, Gujarat, western India, Gaia, 15: 379-387.

Lutz PL, Bentley TB, Harrison KE, Marszalek DS. 1980. Oxygen and water vapor conductance in the shell and shell membrane of the American crocodile egg. Comparative Biochemistry and Physiology 66: 335-338.

Miall AD. 1996. The Geology of Fluvial Deposits. Springer-Verlag Berlin Heidelberg.

Mikhailov K. 1991. Classification of fossil eggshells of amniotic vertebrates. Acta Palaeontologica Polonica 36(2): 193-238.

Mikhailov K. 1994. Theropod and protoceratopsian dinosaur eggs from the Cretaceous of Mongolia and Kazakhstan. Paleontological Journal 28(2): 101-120.

Mikhailov K. 1995. Systematic, Faunistic, and Stratigraphic Diversity of Cretaceous Eggs in Mongolia, Comparison with China. Sixth Symposium on Mesozoic Terrestrial Ecosystems and Biota, Short Papers. China Ocean Press, Beijing: 165-168.

Mikhailov K. 1997. Fossil and recent eggshell in amniotic vertebrates: fine structure, comparative morphology, and classification. Special Papers in Palaeontology No 56. The Palaeontological Association of London.

Mikhailov K, Sabath K, Kurzanov S. 1994. Eggs and Nests from the Cretaceous of Mongolia. Dinosaur Eggs and Babies. Cambridge University Press.

Mohabey DM. 1998. Systematics of Indian Upper Cretaceous Dinosaur and Chelonian Eggshells. Journal of Vertebrate Paleontology 18(2): 348-362.

Mohabey DM. 2005. Late Cretaceous (Maastrichtian) Nests, Eggs, and Dung Mass (Coprolites) of Sauropods (Titanosaurs) from India. Thunder-Lizards, Tidwell and Carpenter (eds)., Indiana University Press.

Mou Y. 1992. Nest environments of the Late Cretaceous dinosaur eggs from Nanxiong basin, Guangdong Province, Unknown journal and date.

Nessov LA. 1995. Dinosaurs of northern Eurasia: new data about assemblages, ecology and paleobiogeography. Izdatelstvo Sankt-Peterburgskogo universiteta, St.-Petersburg 156.

Norell MA, Clark JE, Demberelyin D, Rhinchen B, Chiappe LM, Davidson AR, McKenna MC, Altangerel P, Novacek MJ. 1994. A theropod dinosaur embryo and affinities of the Flaming Cliffs dinosaur eggs. Science 266: 779-782.

Norell M, Clark JM, Chiappe LM, Dashzeveg D. 1995. A Nesting Dinosaur. Nature 378: 774-776.

Norell MA, Clark JM, Chiappe LM. 2001. An embryonic oviraptorid (Dinosauria: Theropoda) from the upper Cretaceous of Mongolia. American Museum Noviates 3315.

Osborn HF. 1924. Three new theropoda, protoceratops zone, central Mongolia. American Museum Novitates 144.

Osmolska H, Currie PJ, Barsbold R. 2004. Oviraptorosauria. The Dinosauria: 165-183.

Owen AW, Hayward JL. 1997. Orientation and dispersion of eggshell fragments in a fluvial environment. Journal of Vertebrate Paleontology Program Abstracts 17(3): 68A.

Packard GC, Taigen TL, Packard MJ, Shuman RD. 1979. Water-vapor conductance of testudinian and crocodilian eggs (Class Reptilia). Respiration Physiology 38:1-10.

Paganelli A, Olszowka A, Ar A. 1974. The Avian Egg: Surface Area, Volume, and Density. The Condor 76: 319-325.

Prothero DR, Schwab F. 2004. Sedimentary Geology. WH Freeman and Company. New York, NY.

Qian M, Xing G, Chen R, Jiang Y, Ding B, Yan Y, Zhang Q. 2007. Restoring the categories of Cretaceous dinosaurs from Tiantai fossil eggs in Zhejiang Province. Jiangsu Geology 31(2):81-89 (in Chinese).

Qian M, Jiang Y, Jiang Y, Zhang Y, Chen R, Li l, Xing G. 2008. New evidence on fossil eggs of Cretaceous Tyrannosaurs in eastern China. Jiangsu Geology 32:86-97.

Ruiz-Omeñaca JI, Canudo JI, Aurell M, Bádenas B, Barco JL, Cuenca-Bescós G, Ipas J. Estado de las investigaciones sobre los vertebrados del Jurásico Superior y Cretácico Inferior de Galve (Teruel). *Estudios geológicos* 60.3-6: 179-202.

Sabath K. 1991. Upper Cretaceous amniotic eggs from the Gobi Desert. Acta Palaeontologica Polonica 36(2): 151-192.

Salgado L, Coria RA, Ribeiro CM, Garrido A, Rogers R, Simon ME, Arcucci AB, Rogers KC, Carabajal AP, Apesteguia S, Fernandez M, Garcia RA, Talevi M. 2007. Upper Cretaceous Dinosaur Nesting Sites of Rio Negro, Northern Patagonia, Argentina. Cretaceous Research 28: 392-404.

Sato T, Cheng YN, Wu XC, Zelenitsky DK, Hsiao YF. 2005. A pair of shelled eggs inside a female dinosaur. Science 308: 375.

Schmitt JG, Moran ME. 1982. Stratigraphy of the Cretaceous Wayan Formation, Caribou Mountains, southeastern Idaho thrust belt. Contributions to Geology, University of Wyoming 21(1): 55-71.

Seymour RS. 1979. Dinosaur eggs: gas conductance through the shell, water loss during incubation and clutch size. Paleobiology 5(1): 1-11.

Thompson MB. 1985. Functional significance of the opaque white patch in eggs of *Emydura macquarii*. Biology of Australian frogs and reptiles: 387-395. Eds G Grigg, R Shine, H Ehmann. Royal Zoological Society, New South Wales, Sydney.

Thulborn RA. 1992. Nest of the Dinosaur Protoceratops. Lethaia 25: 145-149.

Ullman PV, Varricchio D, Knell MJ. 2012. Taphonomy and taxonomy of a vertebrate microsite in the mid-Cretaceous (Albian-Cenomanian) Blackleaf Formation, southwest Montana. Historical Biology 24(30: 311-328.

VanStraelen V. 1925. The Microstructure of the Dinosaurian Eggshells from the Cretaceous Beds of Mongolia. American Museum Noviates No. 173.

Varricchio DJ, Jackson F, Borkowski JJ, Horner JR. 1997. Nest and egg clutches of the dinosaur *Troodon formosus* and the evolution of avian reproductive traits. Nature 385: 247-250.

Varricchio DJ, Martin AJ, Katsura Y. 2007. First trace and body fossil evidence of a burrowing, denning dinosaur. Proceedings of the Royal Society B 247: 1361-1368.

Varricchio DJ, Moore JR, Erickson GM, Norell MA, Jackson FD, Borkowski JJ. 2008. Avian paternal care had dinosaur origin. Science 322: 1826-1828.

Varricchio DJ, Jackson FD, Jackson RA, Zelenitsky DK. 2013. Porosity and water vapor conductance of two *Troodon formosus* eggs: an assessment of incubation strategy in a maniraptoran dinosaur. Paleobiology 39(2): 278-296.

Wang DY, Zhou SQ. 1995. The Discovery of New Typical Dinosaur Egg Fossils in Xixia Basin. Henan Geology 13: 262-267.

Wang D, Feng J, Zhu S, Wu M, Fu G, He P, Qiao G, Pang F, Li G, Li B, Li J, Wang B, Zhang G, Qin Z. 2008. Dinosaur Eggs and Skeletons from Henan Province in China. Beijing: Geological Publishing House: 1-320 (in Chinese).

Wang Q, Zhao Z, Wang X, Jiang Y, Zhang S. 2010. A new oogenus of Macroelongatoolithid eggs from the upper Cretaceous Chichengshan Formation of the Tiantai Basin, Zheziang province and a revision of the Macroelongatoolithids. Acta Palaeontologica Sinica 49: 73-86.

Wang, Q, Wang XL, Zhao ZK, Jiang YG. 2010. A new oogenus of Elongatoolithidae from the Upper Cretaceous Chichengshan Formation of Tiantai basin, Zhejiang Province, Unknown journal.

Wang Q, Zhao Z, Wang X, Li N, Zou S. 2013. A new form of Elongatoolithidae, *Undulatoolithus pengi* oogen. et oosp. nov. from Pingxiang, Jiangxi, China. Zootaxa 3746 (1): 194-200.

Watabe M. 2004. New dinosaur ovifauna from the Upper Cretaceous vertebrate fossil locality, Abdrant Nuru, Central part of the Gobi desert, Mongolia, Hayashibara Museum of Natural Sciences Research Bulletin, 2: 15-27.

Weishampel DB, Meers MB, Akersten WA, McCrady AD. 2002. New Early Cretaceous dinosaur remains, including possible ceratopsians, from the Wayan Formation of eastern Idaho. Idaho Museum of Natural History Occasional Paper 37: 5-17.

Weishampel DB, Barrett PM, Coria RA, Loeuff JL, Xu X, Zhao X, Sahni A, Gomani EM, Noto CR. 2004. Dinosaur Distribution. The Dinosauria: 517- 606. University of California Press.

Weishampel DB, Fastovsky DE, Watabe M, Varricchio D, Jackson D, Tsogtbaatar K, Barsbold R. 2008. New oviraptorid embryos from Bugin-tsav, Nemegt Formation (Upper Cretaceous), Mongolia, with insights into their habit and growth. Journal of Vertebrate Paleontology 28(4):1110-1119.

Whyte M, Zhenyu Z, Zhanyang L. 2000. The dinosaur eggs of the Xixia basin, China, First International Symposium on Dinosaur Eggs and Babies, Extended Abstracts, 177-182.

Xu X, Tan Q, Wang J, Zhao X, Tan L. 2007. A gigantic bird-like dinosaur from the Late Cretaceous of China. Nature 447: 844-847.

Young C. 1954. Fossil Reptilian Eggs from Laiyang, Shantung, China. Acta Paleontologica Sinica II (4): 371-388.

Young C. 1965. Fossil Eggs from Nanhsiung, Kwangtung, and Kanchou, Kiangsi. Vertebrata Palasiatica, 9: 141-170.

Yu Y, Jing X, Wu X, Zhang Z. 2010. The epochs of dinosaurs and fossil eggs from Zhejiang Province. Geology in China 37(1): 94-100.

Yu F, Wang L, Du L, Zou X, Wang G, Zhang H. 2012. Distribution of dinosaurs and their egg fossils in the Cretaceous basins, Zhejiang Province. Journal of Stratigraphy 36(1): 77-88.

Zartman RE, Dyman TS, Tysdal RG, Pearson RC. 1995. U-Pb ages of volcanogenic zircon from porcellanite beds in the Vaughn Member of the mid-Cretaceous Blackleaf Formation, southwest Montana. US Geological Survey Bulletin B 2113: B1-B15.

Zelenitsky DK, Carpenter K, Currie PJ. 2000. First record of Elongatoolithid theropod eggshell from North America: the Asian oogenus *Macroelongatoolithus* from the lower Cretaceous of Utah. Journal of Vertebrate Paleontology 20(1): 130-138.

Zelenitsky DK, Hirsch KF. 1997. Fossil eggs: identification and classification. Dinofest: International Proceedings.

Zelenitsky DK. 2000. Dinosaur eggs from Asia and North America. Paleontological Society of Korea Special Publication No 4: 13-26.

Zelenitsky DK. 2004. Description and phylogenetic implications of extant and fossil oological remains [dissertation]. [Calgary (AB)]: University of Calgary.

Zeng D, Zhang J. 1979. On the Dinosaurian Eggs from the Western Dongting Basin, Hunan. Vertebrata PalAsiatica 17(2): 131-136.

Zhao H, Zhao Z. 1998. Dinosaur Eggs From Xichuan Basin, Henan Province. Vertebrata Palasiatica 36(4): 282-296.

Zhao H, Zhao Z. 1999. A New Form of Elongatoolithid Dinosaur Eggs from the Lower Cretaceous Shahai Formation of Heishan, Liaoning Province. Vertebrata Palasiatica, 37(4): 278-284.

Zhao Z. 1975. The microstructure of the dinosaurian eggshells of Nanxiong Basin, Guangdong Province. Vertebrata PalAsiatica 13: 105-117 (in Chinese).

Zhao Z. 1979. Progress in the Research of Dinosaur Eggs. Mesozoic and Cenozoic Red Beds of South China, Selected Papers from the "Cretaceous-Tertiary Workshop". Edited by Institute of Vertebrate Paleontology, Paleoanthropology and Nanjing Institute of Paleontology. Science Press: 330-340.

Zhao Z. 1994. Dinosaur Eggs in China: On the Structure and Evolution of Eggshells. Dinosaur Eggs and Babies. Cambridge University Press.

Zhao Z. 2000. Nesting behavior of dinosaurs as interpreted from the Chinese Cretaceous dinosaur eggs. International Dinosaur Symposium for Kosong County in Korea.

Zhao Z, Jiang Y. 1974. Microscopic studies on the dinosaurian egg-shells from Laiyang, Shantung Province. Scientia Sinica 17(1): 73-83.

Zhang Y, Li K. 1998. The dinosaur egg fossils in China and their ecostratigraphy. Lithofacies Palaeogeography 18(2): 362-369.

Zhou Z. 1993. A study of dinosaur eggs from Henan Province. Henan Geology 11(1): 44-51.

Zhou S, Li Z, Feng Z, Wang D. 1999. Oolithia of dinosaurs distributed in the Xixia basin of Henan province and its buried features. Geoscience 13(3):298-300.

Zhou S, Feng Z, Zhang G. 2001. Oolithias assemblages in Henan Province and its age significances. Geoscience 15(4): 362-369 (in Chinese).

Zhang Z. 1979. Progress in the Research of Dinosaur Eggs. From: Mesozoic and Cenozoic Red Beds of South China. Selected Papers from the Cretaceous-Tertiary Workshop, Nanxiong, Guangdong Province. Nanjing Institute of Paleontology Science Press: 330-340.